Journal of the Geological Survey of Brazil vol 2, no 1, 37-73, April 2019

Journal of the Geological Survey of Brazil

A review of the geodynamic setting of the Volcanic Domain in the Juruena Magmatic Arc, southwestern Amazon Craton, Brazil, based on geochemical, U-Pb and Sm-Nd data

Tiago B. Duarte[1], Roberto P. Xavier[2], Joseneusa B. Rodrigues[3]

[1]Geological Survey of Brazil (CPRM), Setor Marista, 148, CEP 74170-110, Goiânia-GO, Brazil
[2]Institute of Geosciences, State University of Campinas (UNICAMP), Rua João Pandiá Calógenas 51, CEP 13083-870, Campinas-SP, Brazil
[3]Geological Survey of Brazil (CPRM), SBN, Quadra 2, Bloco H, 1° Andar, CEP 70040-904, Brasília-DF, Brazil

Abstract

In SW Amazon Craton, along the boundary between the Ventuari-Tapajós (1.9 to 1.8 Ga) and the Rio Negro-Juruena (1.8 to 1.55 Ga) provinces, an association of volcanic rocks and related epizonal granitic plutons crop out as a volcanic belt with more than 600 km long. This set of rocks, here called the Volcanic Domain (VD), has been the target of several studies due to its metallogenic importance as well as to the understanding of the geodynamic evolution of the Southwestern Amazon Craton, and various geodynamic models are considered for this plutono-volcanism at about 1.8 Ga, including taphrogenesis, accretionary margin volcanic belt, and late- to post-orogenic extensional magmatism.

In this work, based on whole rock geochemistry, and in U-Pb and Sm-Nd isotopic results we propose a geodynamic model that admit shifts in the tectonic regime through time and unifies the second and third interpretations above. We interpret the intermediate to acid, A-type, oxidized granitic and volcanic rocks from the Colíder Group and the Paranaíta Intrusive Suite as products of continental arc magmatism, whereas the acid, A-type reduced granitic and volcanic rocks resulted from late-stage extensional back-arc and forearc processes being respectively associated with the Teles-Pires Intrusive Suite and Roosevelt Group magmatism.

The continental arc interpretation for the VD is supported by the following lines of evidence: (1) spatial arrangement of the VD in the shape of a volcanic belt; (2) the large volume of volcaniclastic deposits and related epizonal granitic intrusions; (3) variable chemical signatures ranging from subalkaline mafic compositions to high-K calc-alkaline, A-type oxidized granites, showing REE and trace element patterns similar to those of subcontinental lithospheric mantle sources enriched by subduction-zone fluids, and subordinate involvement of continental crust; (4) crystallization and Sm-Nd T_{DM} model ages, respectively, ranging between 1820 and 1780 Ma, and from 2.40 to 1.84 Ga, with $\varepsilon_{Nd(t)}$ values of -3.9 to +2.5, yielding an overlap in U-Pb and Sm-Nd ages of rocks from the Juruena Magmatic Arc; (5) the occurrence of epithermal-porphyry Au systems in the Alta Floresta Gold Province with ages compatible with those of the VD magmatic period.

Article Information

Publication type: Research paper
Submitted: 26 October 2018
Accepted: 13 March 2019
Online pub. 5 April 2019
Editor: Evandro Klein

Keywords:
Volcanism
Juruena Magmatic Arc
Geochemistry
U-Pb geochronology
Sm-Nd
Paleoproterozoic

*Corresponding author
Tiago B. Duarte
E-mail address:
tiago.duarte@cprm.gov.br

1. Introduction

Previous works that focused on the geotectonic evolution of Proterozoic provinces in the southwestern Amazon Craton have consolidated a broad geodynamic model based on the successive accretion of magmatic arcs since 2.0 Ga until the end of the Mesoproterozoic (Cordani et al. 1979; Cordani and Neves 1982; Teixeira et al. 1989; Santos et al. 2000; Tassinari and Macambira 1999; and 2004; Cordani and Teixeira 2007; Santos et al. 2008). These successive events of oceanic crust subduction and continental accretion were driven by soft collision processes, as evidenced by Cordani and Teixeira (2007), and culminated in the assembly of the supercontinents Columbia or NUNA (Hoffman 1997; Rogers and Santosh 2002), and Rodinia (Greenville orogeny) at 1.8 and 1.0 Ga, respectively (Cordani et al. 2009).

Tassinari (1996), Sato and Tassinari (1997), and Tassinari and Macambira (1999), based on mobilistic theories and Rb-Sr (whole rock) isotopic data, have suggested an Archean dynamic evolutionary model that includes the agglutination of crustal fragments and juvenile accretion processes. These authors proposed then the organization of the Amazon Craton into structural and geochronological provinces (Fig. 1).

In accretionary arc environments dominated by soft collision-induced crustal thickening, major continental uplift, as seen in large mountain ranges such as the Himalayas, and the exhumation of deep crustal layers are minimized, allowing volcanic covers and epizonal rocks to be preserved (Cordani and Teixeira 2007; Juliani et al. 2005).

The rocks of the Ventuari-Tapajós Province yield crystallization ages between 1.9 and 1.8 Ga; whereas crystallization ages for the rocks of the Rio Negro-Juruena

ISSN: 2595-1939
https://doi.org/10.29396/jgsb.2019.v2.n1.4
Open access at jgsb.cprm.gov.br

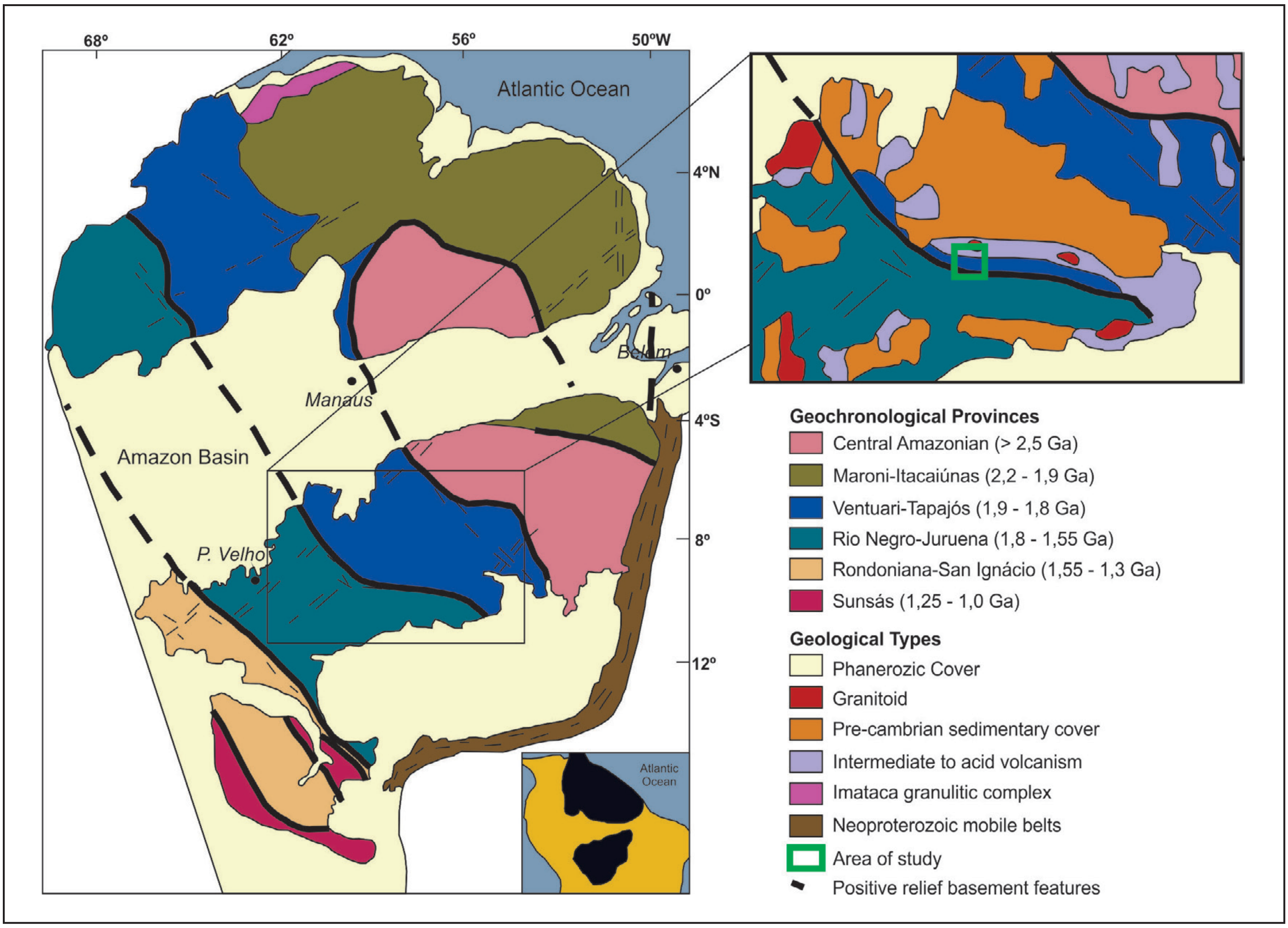

FIGURE 1 – Distribution of the Geotectonic/Geochronological Provinces in the Amazon Craton and location of the study area in the detailed map. modified from Tassinari and Macambira (1999) with a detailed map of the SW portion of the Craton.

Province range from 1.8 to 1.55 Ga. A NW-SE oriented belt about 600 Km long and composed of well-preserved Paleoproterozoic volcanic rocks and plutonic counterparts is located in an intermediate position between the two provinces (Fig. 1) and defines the Juruena Magmatic Arc Volcanic Domain (Duarte et al. 2012).

Despite the number of published works, a unifying geodynamic evolutionary model for the Volcanic Domain has not been consolidated yet. The key point is whether the Volcanic Domain is related to accretionary processes that shaped the Juruena Magmatic Arc or to extensional post-orogenic to anorogenic settings related to the Rio Negro-Juruena or Tapajós-Parima geotectonic evolution.

At the moment three distinctive geodynamic models are considered for this plutono-volcanism. The first model admits that the Volcanic Domain magmatism, called Teles-Pires (including group, magmatism, plutono-volcanism and other designations depending the author), is the result of process that characterizes the Columbia or NUNA taphrogenesis around 1.8 Ga. (Tassinari and Macambira 1999; Pinho et al. 2003; Cordani and Teixeira 2007; Cordani et al. 2009; Barros et al. 2009).

The second model recognizes the Volcanic Domain as an accretionary margin volcanic belt developed on the Ventuari-Tapajós Province at 1.8 Ga, which worked as an active continental margin, resulting in the formation of the Juruena Magmatic Arc (Santos et al. 2000; Souza et al. 2005; Santos et al. 2008; Duarte et al. 2012). Alternatively to the interpretations above, Barros et al. (2009), Alves et al. (2013), and Silva et al. (2014) admit that the Volcanic Domain is a late- to post-orogenic extensional magmatism developed within the Juruena Magmatic Arc.

This work carried out in the western sector of the Volcanic Domain (Fig. 2) brings together recent geological mapping, petrological, lithogeochemical and new important isotopic results of U-Pb (zircon) and whole-rock Sm-Nd data. The main goal is to understand the geodynamic processes and time intervals over which the Volcanic Domain was formed, to establish theoretical foundations based on the discussion of geological factors that allow us to apply them to the context of the Amazon Craton provinces (Rio Negro-Juruena and Ventuari-Tapajós), aiming at providing a more accurate division for these provinces within the study area.

2. Geology and evolution of the Juruena Magmatic Arc

Based on recent geochronological data, and on the current tectonic evolutionary model, the orogeny that gave rise to the Juruena Magmatic Arc (Fig. 2) started at 1820 Ma. Compressive stresses from SW to NE transported an oceanic crust (Bacaeri-Mogno Complex) toward the already stable Tapajós-Parima Province (cratonic margin) leading to plate subduction and consumption (Santos et al. 2000; Souza et al. 2005; Duarte et al. 2012).

The interaction of mantle and crustal sources in this accretionary environment generated hybrid magmas, which is supported by rocks with ε_{Nd} values ranging from slightly negative to positive (Santos et al. 2000; Pinho et al. 2003; Souza et al. 2005; Cordani and Teixeira 2007; Barros et al. 2009; Ribeiro and Duarte 2010). In the study area, rocks related to the earliest stages of subduction are distributed in a volcanic belt which is composed of hypabyssal granites from the Paranaíta Intrusive Suite (1820 to 1769 Ma) and volcanic/volcaniclastic rocks from the Colíder Group (1803 to 1766 Ma) (JICA/MMAJ 2000, 2001; Ribeiro and Duarte 2010; Duarte et al. 2012). Despite the strong ductile deformation, this volcanic domain is well preserved and called Teles-Pires Group undeformed domain and characterized by Pinho et al. (2003) and Barros et al. (2009).

To the east of the survey area, in the Peixoto de Azevedo and Alta Floresta regions (Fig. 2), volcanic rocks associated with granites yielding ages from 1810 to 1750 Ma are also recognized, including the Pium Granite (Alves et al. 2013), the Terra Nova Granite (Prado et al. 2013), and the Peixoto Granite (Silva et al. 2014). These rocks have an A-type signature (Whalen et al. 1987), consistent with those of back-arc settings in a post-collisional to anorogenic period of the Juruena Magmatic Arc, and attributed to the Teles-Pires magmatism (Silva et al. 1980; Pinho et al. 2003; Lacerda Filho 2004; Silva and Abram 2008).

In the study area, the Volcanic Domain occurs in tectonic contact along a transpressional WNW-ESE trending sinistral shear zone with medium to high-grade metamorphic rocks of the Juruena Complex (Ribeiro and Duarte 2010; Duarte et al. 2012), or with the Teles-Pires Group Deformed Domain (Barros et al. 2009). It contains predominantly plutonic rocks with ages ranging from 1787 to 1764 Ma, as well as the Bacaeri-Mogno Complex (Sm-Nd isochron age of 2.24 Ga, and $\varepsilon_{Nd(t)}$ of +2.5), which is interpreted as oceanic crust remnant (Souza et al. 2005). This domain comprises the Vitória Plutonic Suite (1787 to 1765 Ma), the São Pedro (1796 to 1730 Ma) and São Romão (1780 to 1770 Ma) granites,

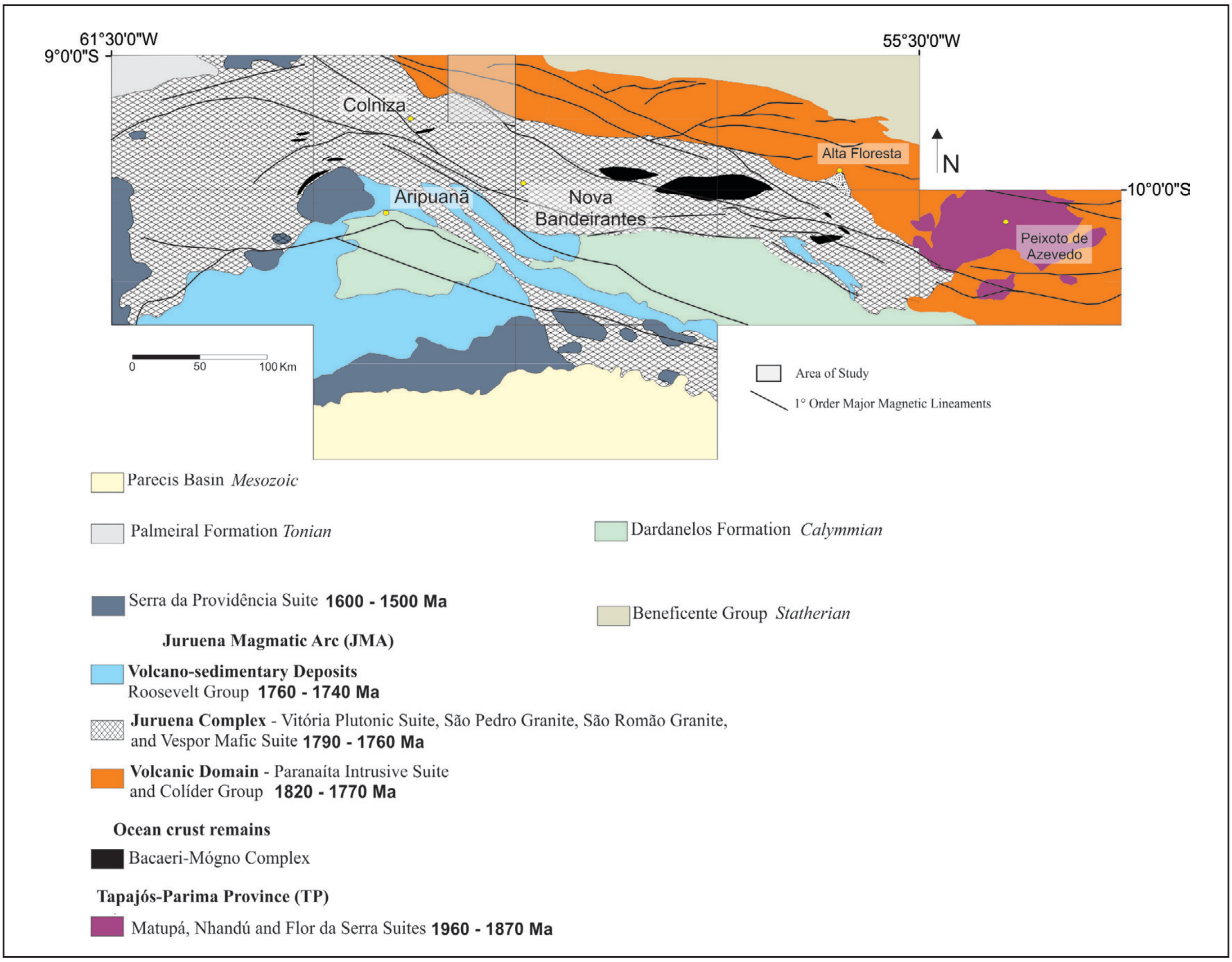

FIGURE 2 – Geotectonic map of part of the SW Amazon Craton highlighting the lithostratigraphic units that composes the Juruena Magmatic Arc, basement fragments of Tapajós-Parima Province at east, anorogenic granites from Serra da Providência Suite and sedimentary basins (modified from Ribeiro and Duarte 2010).

and the Vespor Mafic Suite (1773 to 1764 Ma). Dispersed volcanic rocks in the Juruena Complex, apparently filling retroarc basins, are attributed to the Roosevelt Group (1760 to 1740 Ma) (Fig. 2).

The geological episode that left its high-grade deformation imprint on the Juruena Magmatic Arc was the collisional Quatro Cachoeiras orogeny (Rizzotto et al. 2004; Santos et al. 2008). In the southwest of the area, closer to the suture zone, this orogeny is revealed through metamorphic ages around 1640 Ma obtained on zircon rims of samples from the Jamari Complex (state of Rondônia), as well as by the presence of granulite-facies rocks. The orogeny was followed by post-collisional granitogenesis during the Mesoproterozoic, which nowadays is represented by the Serra da Providência Suite (1605 to 1505 Ma) (Tassinari et al. 1984).

Other events recorded by the regional stratigraphy are represented by graben-like basins, which are related to the Sunsás-Aguapeí orogeny, filled with sediments of the Beneficente Group, and the Piranhas dike swarms emplaced in the early Paleozoic (Santos et al. 2002; Duarte et al. 2012).

3. Volcanic Domain and Juruena Complex: field aspects and petrographic results

The Colíder Group is mostly composed of pyroclastic deposits and subordinate lavas with mainly acid to intermediate composition. The Paranaíta Intrusive Suite is composed of mesozonal to epizonal granites. Apparently, these rocks crop out in places where the pyroclastic deposits were eroded and as apophyses. Even though the Volcanic Domain has not shown evidence of regional metamorphism, it is affected by cataclastic shear bands striking E-W to NW-SE generating schistosity and microfratures.

3.1 Colíder Group

The Colíder Group rocks were grouped based on textural and compositional aspects into: (1) dacite, rhyodacite and rhyolite; (2) mafic; and (3) volcaniclastic. Dacite, rhyodacite, and rhyolite are aphanitic, fine-grained, phaneritic, or micro-porphyritic rocks with quartz and plagioclase phenocrysts. The groundmass shows microcrystalline and micropoikilitic devitrification textures, and commonly micrographic intergrowth and granophyric textures. Phenocrysts are quartz, plagioclase, alkali feldspar, biotite, and hornblende. The observed samples commonly present microfractures and associated hydrothermal alteration with various degrees of metasomatism. These microfractures are filled with an association of sericite + epidote + quartz ± pyrite ± chalcopyrite or calcite ± pyrite ± chalcopyrite. In addition, a more pervasive, intergranular hydrothermal alteration is composed of ultra-fine sericite and limonite, with disseminated sulfides. This pervasive and regional hydrothermal alteration gives the rocks a characteristic reddish color.

The mafic rocks are greenish, fine-grained diabase, andesite, and phaneritic amphibolite. The diabase has ophitic to sub-ophitic texture with a groundmass composed of tabular plagioclase and augite. The plagioclase is often pseudomorphosed, partial or totally altered to clay minerals and saussurite. The augite is also pseudomorphosed and altered to uralite, biotite, chlorite, and calcite. Disseminated sub-millimeter sized magnetite and titanomagnetite are found as accessory minerals, but they may occur in concentrations up to 10%. Andesite has cryptocrystalline to microcrystalline devitrified groundmass and amygdala filled with quartz, chlorite, epidote, and calcite. The rocks are affected by fissure-filling hydrothermal alteration along microfractures filled with epidote, chlorite, calcite, pyrite, and chalcopyrite, and by a pervasive alteration with sericite, chlorite and disseminated Fe-Cu sulfides.

The volcaniclastic rocks are pyroclastic flows and fall deposits classified as welded ignimbrites and welded tuffs that characterize thick stratified and massive volcanogenic deposits. These rocks exhibit a discrete foliation with compacted and stretched pumices and clasts (eutaxitic texture) and complex flow folds as well as lithophysae textures in the strongly welded tuffs and ignimbrites. The eutaxitic and vitriclastic textures are well evidenced by a discontinuous foliation resulted from stretched and flattened devitrified shards, fiammes, pumices, lithic fragments, embayed quartz, and angular feldspar fragments alternating with devitrified ash bands. Hydrothermal processes, similar to those described for the other volcanic rocks, also affect this set of rocks. Pervasive sericitization replaced most aphanitic groundmass mineralogy and feldspar crystal fragments. Epidote and chlorite are less common and occur replacing hornblende and biotite crystal fragments and mafic lithoclasts. Microfractures are filled with an association of sericite + quartz + calcite + sulfide (pyrite and chalcopyrite). Calcite-filled fractures cut across the microfractures representing a late stage hydrothermal alteration.

3.2 Paranaíta Intrusive Suite

The Paranaíta Intrusive Suite is composed mostly of porphyritic granodiorite to monzogranite and granophyre with rocks showing hypidiomorphic-granular, porphyritic to glomeroporphyritic, granophyric and micrographic textures. Phenocrysts are of plagioclase and perthitic microcline in a granular or intergrown groundmass of quartz, feldspar (plagioclase and microcline), biotite, and hornblende. Magnetite, apatite, fluorite, zircon, and titanomagnetite occur as accessory minerals. In some samples, crystals of quartz show undulose extinction and sutured grain boundaries that are indicative of the incipient deformation. Plagioclase is commonly replaced by clay minerals, sericite, and calcite, whereas hornblende and biotite are replaced by chlorite.

A distinct feature of these rocks is the red coloration caused by a pervasive regional hydrothermal alteration to sericite and limonite. Abundant microfractures and some mineral cleavages (feldspar and hornblende) are filled with an association of quartz + sericite + epidote + sulfides (pyrite and chalcopyrite), and calcite.

3.3 Juruena Complex

The Juruena Complex (Ribeiro and Duarte 2010), also known as Deformed Domain (Pinho et al. 2003), occurs in tectonic contact with the Volcanic Domain along a mylonitized corridor approximately 10 km wide as a result of conjugate transpressional sinistral shear zones. This set of faults apparently caused the exhumation of the Juruena Complex rocks to shallower crustal levels (Ribeiro and Duarte 2010).

The lithostratigraphic units that form the Juruena Complex in the study area are the Vitória Plutonic Suite, and the São Pedro Granite. These units have zircon U-Pb crystallization ages and depleted mantle Sm-Nd model ages around 1775 Ma and 2.0 Ga, respectively, and slightly negative and positive ε_{Nd} values (Duarte et al. 2012). They also share major, and trace element signatures, including rare earth elements (REE) that, combined with radiometric isotopic data, indicate a common petrogenetic origin (Ribeiro and Duarte 2010).

3.3.1 Vitória Plutonic Suite

The Vitória Plutonic Suite comprises intermediate to acid calc-alkaline (Ribeiro and Duarte 2010) plutonic rocks including metadiorites, metaquartz-diorites, metatonalites, and metagranodiorites. The rocks are spatially arranged as sigmoidal-shaped bodies deformed under a ductile structural regime driven by a complex set of steeply-dipping (~70° to 90°) oblique shear zones, striking E-W with inflections to NE-SW and NW-SE (Pinho et al. 2003; Souza et al. 2005; Ribeiro and Duarte 2010; Duarte et al. 2012).

Macroscopic features mostly observed in these rocks are of protomylonite texture and gneissic layering. In addition, incomplete magma mixing and mingling features are common, such as elongate dioritic enclaves. Under the microscope, we observed oriented textures indicative of ductile deformation, including predominantly mylonitic, lepidoblastic, nematoblastic and porphyroclastic. In less deformed samples, granular and porphyritic textures are preserved. The mineralogy consists of quartz, plagioclase, hornblende, biotite, and microcline. Accessory minerals are apatite, epidote, magnetite, titanite, rutile, zircon and allanite.

3.3.2 São Pedro Granite

The São Pedro Granite is composed of metamonzogranite and metasyenogranite. Similarly to rocks of the Vitória Plutonic Suite, these rocks have an ellipsoidal shape and complex and diffuse contacts that resulted from ductile deformation and gradational contacts with other units.

In hand specimens, the granites have foliated protomylonitic and porphyroclastic textures, with quartz ribbons and oriented mafic minerals. The less deformed rocks are medium- to coarse-grained, and have hypidiomorphic-granular to porphyritic textures. Under the microscope, we observed granolepidoblastic and porphyroclastic to mylonitic textures, exhibiting undulose extinction and subgrains in quartz tracks and sub-grains. The porphyroclasts are of deformed perthitic K-feldspar and plagioclase embedded in a groundmass consisting of lamellar quartz, biotite, and oriented hornblende crystals. The primary mineral assemblage is quartz, plagioclase, K-feldspar, biotite, and hornblende; accessory minerals are magnetite, titanite, rutile, garnet, apatite, allanite, and zircon.

4. Previous U-Pb (zircon) crystallization ages

In the vicinity of the study area, various works applied zircon U-Pb geochronological analyses to support lithostratigraphic and geodynamic evolutionary hypotheses and interpretations for the SW Amazon Craton (Santos et al. 2000; JICA/MMAJ 2000, 2001; Neder et al. 2002; Pinho et al. 2003; Souza et al. 2005; Silva and Abram 2008; Ribeiro and Duarte 2010; Alves et al. 2013; Serrato et al. 2014 and Santos et al. 2019). The results available for units of the Volcanic Domain and the Juruena Complex are shown in Table 1.

5. Analytical procedures

5.1 Geochemistry

The selected rock samples were crushed in an agate disc mill to a 150-mesh at the laboratory facility of the CPRM - Geological Survey of Brazil, and analyzed by the SGS-Geosol laboratory. The powdered samples were then mixed with lithium metaborate and tetraborate, and melted through induction furnace at 1832° Fahrenheit. The resulting glassy tablets were dissolved in a 5% HNO3 solution containing a laboratory internal standard, and mixed until complete dissolution. The major oxide elements were analyzed by x-ray fluorescence (XRF); in turn, the REE and trace elements were analyzed by inductively coupled plasma-mass spectrometry (ICP-MS), and FeO via gravimetric method. Rare Earth Elements (REE) values are normalized to chondrite (Nakamura 1974). $Eu/Eu^* = Eu_N/(Sm_N \times Gd_N)^{(1/2)}$, magnesium number #mg = molar and $FeO_t = FeO + Fe_2O_3$. Major elements are in wt. %, and trace elements in ppm (detection limit, D. L.). Analytical results were plotted on classification and tectono-magmatic discrimination diagrams using the GCDKit v.3.0 software (Janousek et al. 2006).

5.2 Geochronology and isotope geology

5.2.1 U-Pb LA-ICPMS

The procedure for concentrating zircon crystals followed the steps of sample crushing and then selecting the fractions thinner than 500 µm that were panned to recover a heavy-mineral concentrate. Next, the concentrate was passed through the Frantz isodynamic separator, and finally zircon grains were handpicked under a binocular microscope. The grains were mounted in cold epoxy resin, ground and polished to reveal their internal surfaces. The mounts were cleaned with 3% nitric acid, as well as cleaned ultrasonically with Nanopure® water, and acetone for the extraction of any moist residue. Analyses were conducted using a Multicollector Inductively Coupled Plasma Mass Spectrometer MC-ICP-MS Neptune (Thermo-Finnigan) coupled with the Nd:YAG (λ = 213 nm) Laser Ablation System (New Wave Research, USA), at the Brasília University, Brazil. The analytical procedure was described by Bühn et al. (2009) and consists of ablation of crystals with spots 25 to 40 µm of diameter using a laser of 9 to 13 Hz, and fluence of 0.19 to 1.02 J/cm2. The powdered material is carried by He and Ar at flow rates of ~ 0.40 L/min, and ~ 0.90 L/min, respectively. All sample analyses were performed using the international standard GJ-1 for standard-sample bracketing, and the TEMORA or internal standard PAD-1 for accuracy. Data acquisition occurred in 40 cycles of 1 second with a reading sequence of 1 blank, 1 standard, 4 samples, 1 blank, and 1 standard. The mass intensities of ^{202}Hg, $^{204}(Pb+Hg)$, ^{206}Pb, ^{207}Pb, ^{208}Pb and ^{238}U were determined for each reading. The raw data were reduced using an Excel worksheet of the laboratory, including blank corrections, standard deviation and common lead. All ratio uncertainties are at the 1-σ level. Age calculations were carried out using Isoplot 3.00 (Ludwig 2009).

TABLE 1 – U-Pb (zircon) isotopic dating results and crystallization ages for the Volcanic Domain and Juruena Complex (Vitória Plutonic Suite and São Pedro Granite) (dataset from bibliography).

Colíder Group						
Sample(Key)	**Longitude**	**Latitude**	**Rock**	**Age (Ma)**	**Error**	**Analytical Method**
DFR-041 (12)	-54.78	-9.82	rhyolite	1810	9	U-Pb ICP-MS-LA
Fi-05 (1)	-59.12	-9.00	mafic tuff	1797	5	U-Pb ID TIMS
GM-008 (2)	-53.97	-10.52	rhyolite	1792	8	U-Pb ICP-MS-LA
DFR-14 (13)	-54.82	-9.86	ignimbrite	1792	14	U-Pb ICP-MS-LA
F2001(11)	-56.65	-9.51	rhyolite	1786	17	U-Pb TIMS
MA-004 (3)	-57.05	-9.35	rhyolite porphyry	1785	6.3	U-Pb ICP-MS-LA
GM-080 (4)	-55.04	-10.88	monzogranite	1781	8	U-Pb SHRIMP
B-04 (1)	-59.06	-8.96	basalt	1776	3	U-Pb ID TIMS
WB-08 (1)	-59.07	-8.97	ignimbrite	1774	2	U-Pb ID TIMS
B-01 (1)	-59.02	-8.96	rhyolite	1770	8	U-Pb ID TIMS
Paranaíta Intrusive Suite						
Sample	**Longitude**	**Latitude**	**Rock**	**Age (Ma)**	**Error**	**Analytical Method**
F2005(11)	-57.37	-9.41	granite	1819	6	U-Pb ID TIMS
MA-12A(3)	-55.94	-9.82	monzogranite	1808	14	U-Pb ICP-MS-LA
F2002(11)	-56.66	-9.45	granodiorite	1803	16	U-Pb ID TIMS
P29(1)	-59.12	-9.15	monzogranite	1803	3	U-Pb ID TIMS
F2003(11)	-56.60	-9.51	monzogranite	1801	8	U-Pb ID TIMS
TD-151(5)	-59.30	-9.03	porphyry granite	1797	14	U-Pb ICP-MS-LA
CT-03(13)	-54.83	-9.92	porphyry granite	1794	7	U-Pb ICP-MS-LA
CC-21(6)	-56.18	-9.87	porphyry granite	1793	6	U-Pb ID TIMS
Sample 25(7)	-58.57	-9.14	microgranite	1792	6	SHRIMP
Sample 21(7)	-58.57	-9.14	monzogranite	1790	6	SHRIMP
FR2(10)	-55.05	-10.24	granodiorite	1781	10	SHRIMP
Vitória Plutonic Suite						
Sample	**Longitude**	**Latitude**	**Rock**	**Age (Ma)**	**Error**	**Analytical Method**
PS-306 (5)	-61.32	-9.45	metagranodiorite	1787	14	U-Pb LA-ICP-MS
PS-042 (4)	-57.78	-9.79	metatonalite	1785	8	SHRIMP
MC-027A (5)	-59.13	-9.42	metatonalite	1783	14	U-Pb LA-ICP-MS
P-21 (1)	-59.13	-9.37	metagranodiorite	1765	4	U-Pb TMIS
São Pedro Granite						
Sample	**Longitude**	**Latitude**	**Rock**	**Age (Ma)**	**Error**	**Analytical Method**
CC-138 (4)	-62.89	-13.15	orthogneiss	1786	17	SHRIMP
CC-158 (4)	-56.65	-9.92	orthogneiss	1784	17	SHRIMP
WA-151 (9)	-57.74	-10.95	orthogneiss	1780	12	U-Pb LA-ICP-MS
A4 (1)	-59.37	-9.27	orthogneiss	1775	13	U-Pb TMIS
A3 (1)	-59.35	-9.29	orthogneiss	1774	4	U-Pb TMIS
A8 (1)	-59.29	-9.39	orthogneiss	1766	5	U-Pb TMIS
P-25 (1)	-59.12	-9.35	orthogneiss	1763	6	U-Pb TMIS
2 (8)	-59.54	-10.08	orthogneiss	1755	5	SHRIMP

Key to references: (1) Pinho et al. 2003; (2) Alves et al. 2012; (3) Silva and Abram (2008); (4) Souza et al. (2005); (5) Ribeiro and Duarte (2010); (6) Santos et al. (2000); (7) Serrato et al. (2014); (8) Neder et al. (2002); (9) Souza and Abreu (2007); (10) Silva et al. 2014; (11) JICA/MMAJ (2000) (2001); (12) Santos et al. (2019); (13) Silva et al. (2015);Results are ordered from the oldest to the youngest age. All coordinates are in decimal degrees and configured in WGS84 datum.

5.2.2 Sm-Nd

The Sm-Nd isotopic analyses followed the methodology described by Gióia and Pimentel (2000). According to this procedure, approximately 50 mg of powdered sample is spiked with a ^{149}Sm-^{150}Nd tracer solution. The sample is then dissolved into Savillex® capsules through successive HF, HNO_3, and HCl attacks. The Sm and Nd concentrations are determined using cationic exchange columns made of Teflon, and filled with LN-Spec resin. The Sm and Nd salts are deposited in rhenium filaments containing nitric acid followed by evaporation. Isotopic ratios were measured in a static mode using a multi-collector mass spectrometer, model Finnigan MAT 262 at the Brasília University, Brazil. Uncertainties in the ^{147}Sm/^{144}Nd and ^{143}Na/^{144}Nd ratios are less than ± 0.55 (2σ) and ± 0.0055 (2σ), respectively, based on repeated analyses of the international standards BHVO-1 and BCR-1. ^{143}Nd/^{144}Nd ratios are normalized to ^{146}Nd/^{144}Nd= 0.7219. T_{DM} values were calculated using the DePaolo (1981) model for the depleted mantle.

6. Geochemistry of the Volcanic Domain

The geochemical datasheet from the Volcanic Domain samples are presented in the Appendix A. The samples were grouped into Colíder Group volcaniclastic and basic to acid effusive volcanic rocks, and into Paranaíta Intrusive Suite granites based on textural aspects. After this step, the samples were geochemically classified using the De la Roche et al. (1980) R1-R2 diagram (Fig. 3).

Both the Colíder Group and the Paranaíta Intrusive Suite show calc-alkaline to mostly high-K calc-alkaline affinity (Fig. 4a), and span the entire compositional range from basalt to rhyolite. The intermediate to basic rocks are metaluminous, and the felsic rocks are peraluminous and metaluminous (Fig. 4b).

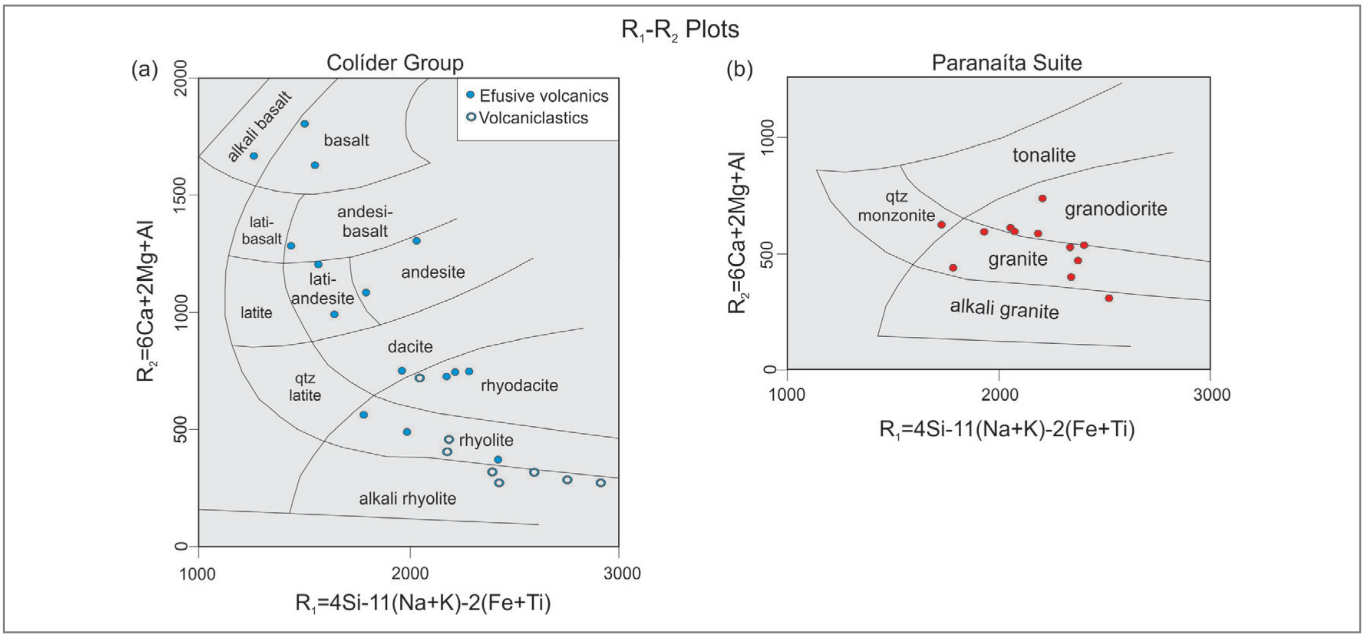

FIGURE 3 – De la Roche et al. (1980) R1-R2 diagrams used for the classification of rock samples from the Colíder Group volcanics (a) and Paranaíta Suite (b).

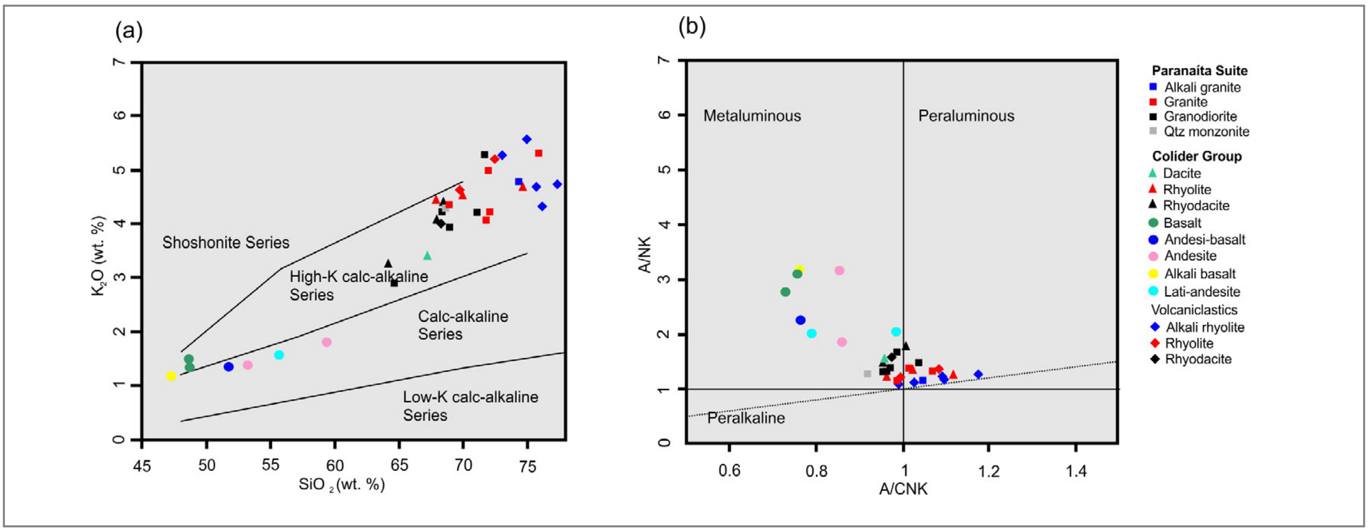

FIGURE 4 – SiO_2 versus K_2O diagram of Peccerillo and Taylor (1976); and (b) Alumina saturation index Al_2O_3/Na_2O+K2O (A/NK) versus $Al_2O_3/CaO+Na_2O+K_2O$ (A/CNK) diagram of Maniar and Piccoli (1989).

Considering the rocks of the Volcanic Domain as products of the same magmatic source, all data were plotted on Harker diagrams (Fig. 5a to f). Most major elements exhibit negative correlations with SiO_2 suggesting the role of fractional crystallization during magmatic evolution resulting in the crystallization of the following common phases: (Al_2O_3, CaO) plagioclase; (MgO) pyroxene, hornblende and biotite; (TiO_2) sphene; (Fe_2O_3) magnetite. As expected, K_2O is the only major element positively correlated with SiO_2 due to the high-K calc-alkaline affinity of these rocks.

Spider diagrams for REE from both the Colíder Group and Paranaíta Intrusive Suite have similar patterns (Fig. 6a and Fig. 6b). They show light REE enrichment relative to heavy REE (La_n/Yb_n 7.01 to 20.34) and have well defined to weakly negative Eu anomalies related to plagioclase concentration (Eu/Eu* 0.15 to 0.86).

Chondrite-normalized REE patterns of the acid rocks (Fig. 6d and Fig. 6e) show fractionation of light REE relative to heavy REE and well-defined Nb, P and Ti negative anomalies, and a Pb positive anomaly. Chondrite-normalized REE patterns

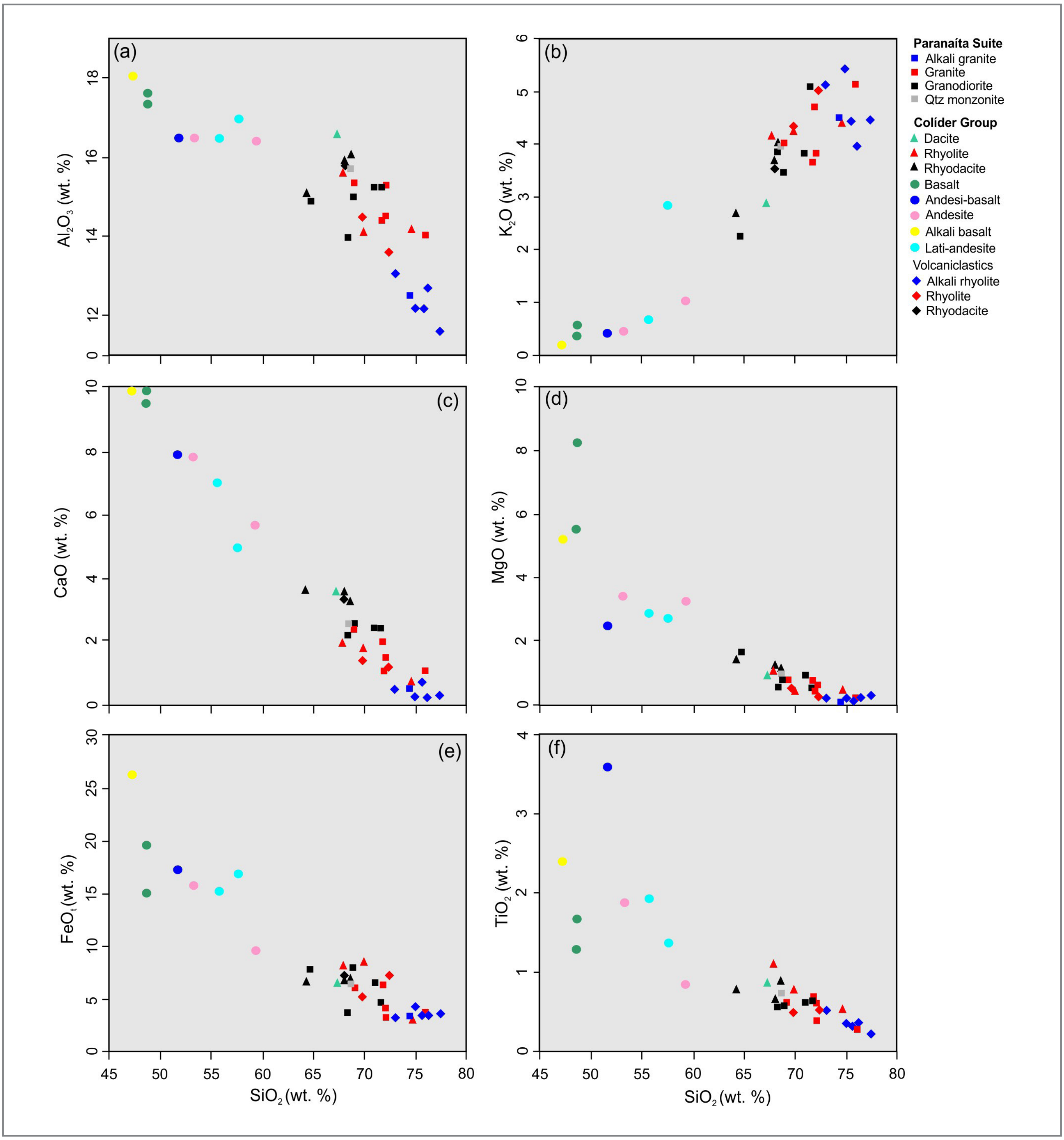

FIGURE 5 – Major- and trace-element Harker's variation diagrams of rocks from the Colíder Group and Paranaíta Intrusive Suite.

(Fig. 6c) of the basic rocks from the Colíder Group show a very slight fractionation of light REE relative to heavy REE, and a little pronounced compositional gap between basalts and andesites that are more differentiated. The primitive mantle normalized spidergram (Fig. 6f) also exhibit differences between these rocks mainly regarding the distribution pattern of high field strength elements (HFSE). Conversely, both are enriched in large ion lithophile elements (LILE) relative to HFSE, and show well-defined Nb and Ti negative anomalies similar to those of spidergrams for acid rocks.

In order to discriminate the tectonic setting of the Volcanic Domain, the samples were plotted in the Ta/Yb versus Th/Yb diagram (Fig. 7) which has shown to be useful for allowing distinguishing subduction-related types from mantle-derived types (Pearce 1982). The results plot in the active continental margin area and show a distribution similar to that observed for the rocks of the Central Andes.

The Dall´Agnol and Oliveira (2007) diagrams in Fig. 8 allow the distinction between Type A and calc-alkaline (Active Continental Margin) granites as well as between reduced and

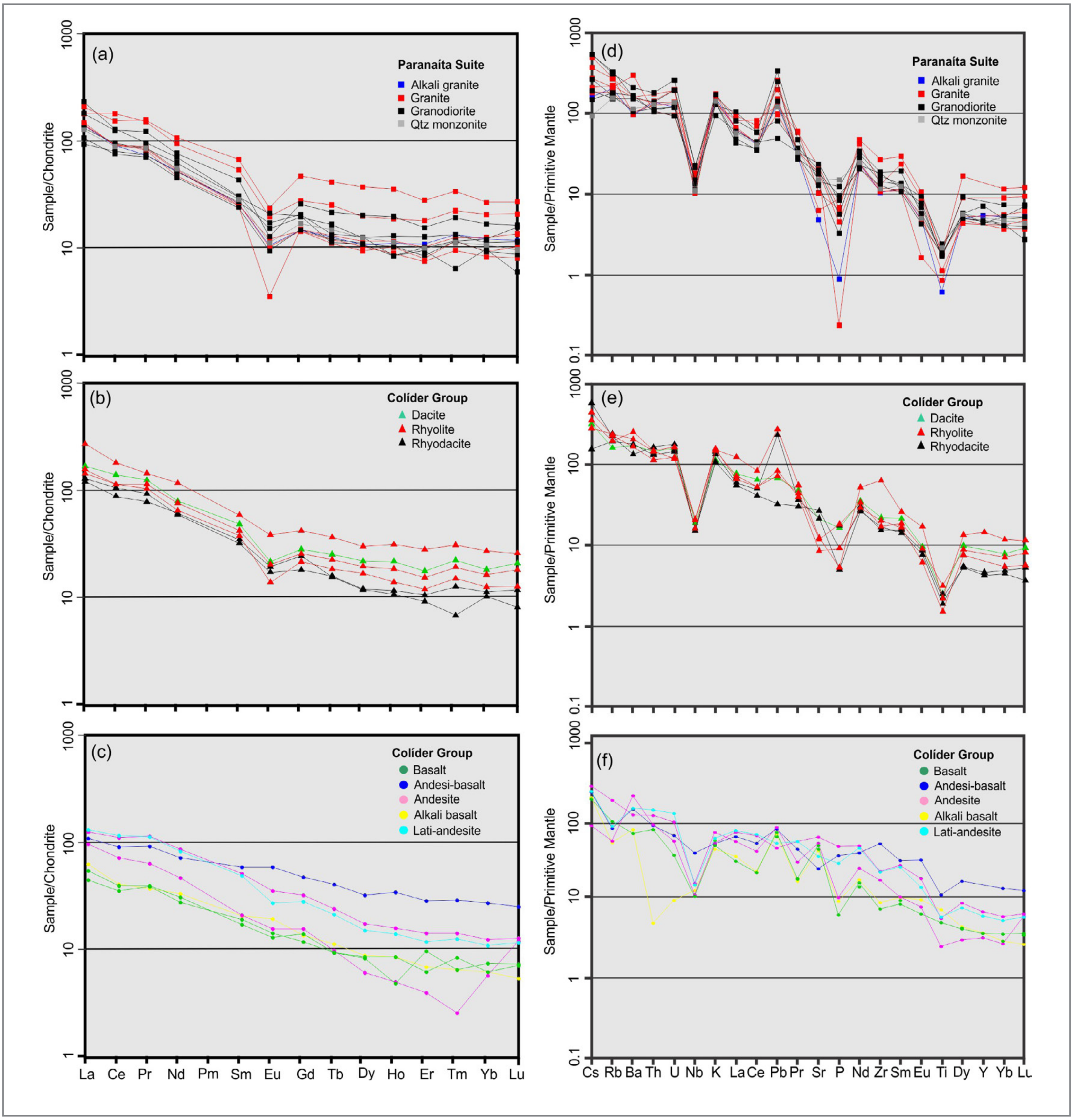

FIGURE 6 – Chondrite-normalized rare earth elements (REE) diagram (Nakamura 1974) of acid rocks from the Paranaíta Intrusive Suite (a), Colíder Group (b) and of the basic rocks from the Colíder Group (c); Primitive mantle-normalized trace element (LILE and HFSE) spidergram (Sun and McDonough 1989) for the Paranaíta Intrusive Suite (d), Colíder Group (e) and Colíder Group basic rocks (f).

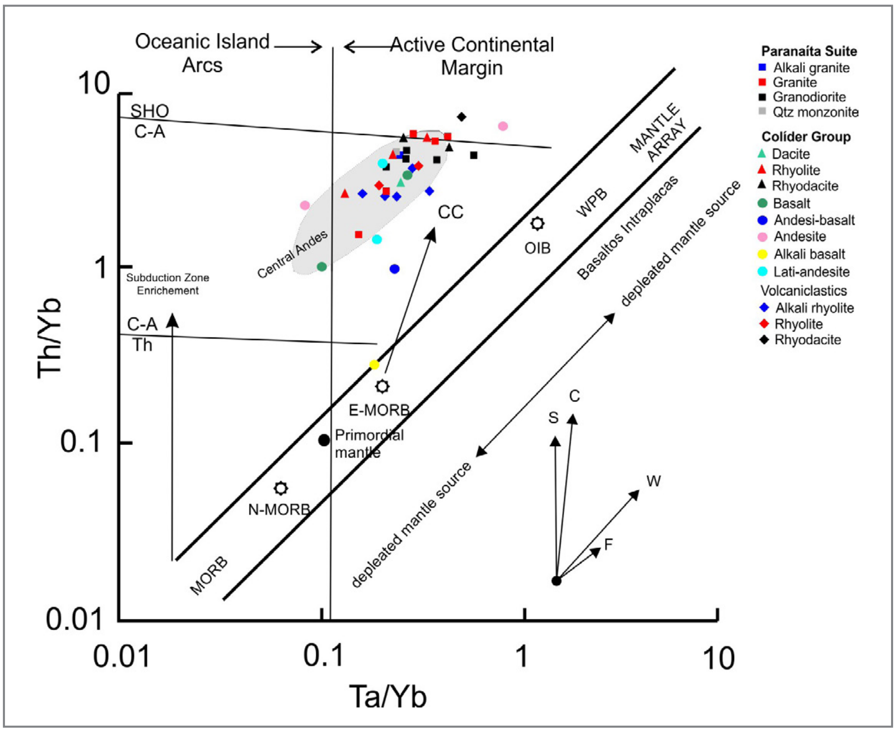

FIGURE 7 – Th/Yb versus Ta/Yb tectonic-magmatic discrimination diagram (Pearce et al. 1984) for the samples of the Volcanic Domain. Uncontaminated intracontinental plate basalts should plot in the WPB region. Vectors indicate subduction-related components (S), within-plate enrichment (W), crustal contamination (C) and fractional crystallization (F). CC - crustal contamination. Th - Tholeiitic field, C-A calc-alkaline field, SHO - shoshonitic field. N-MORB, E-MORB and OIB values from Sun and McDonough (1989).

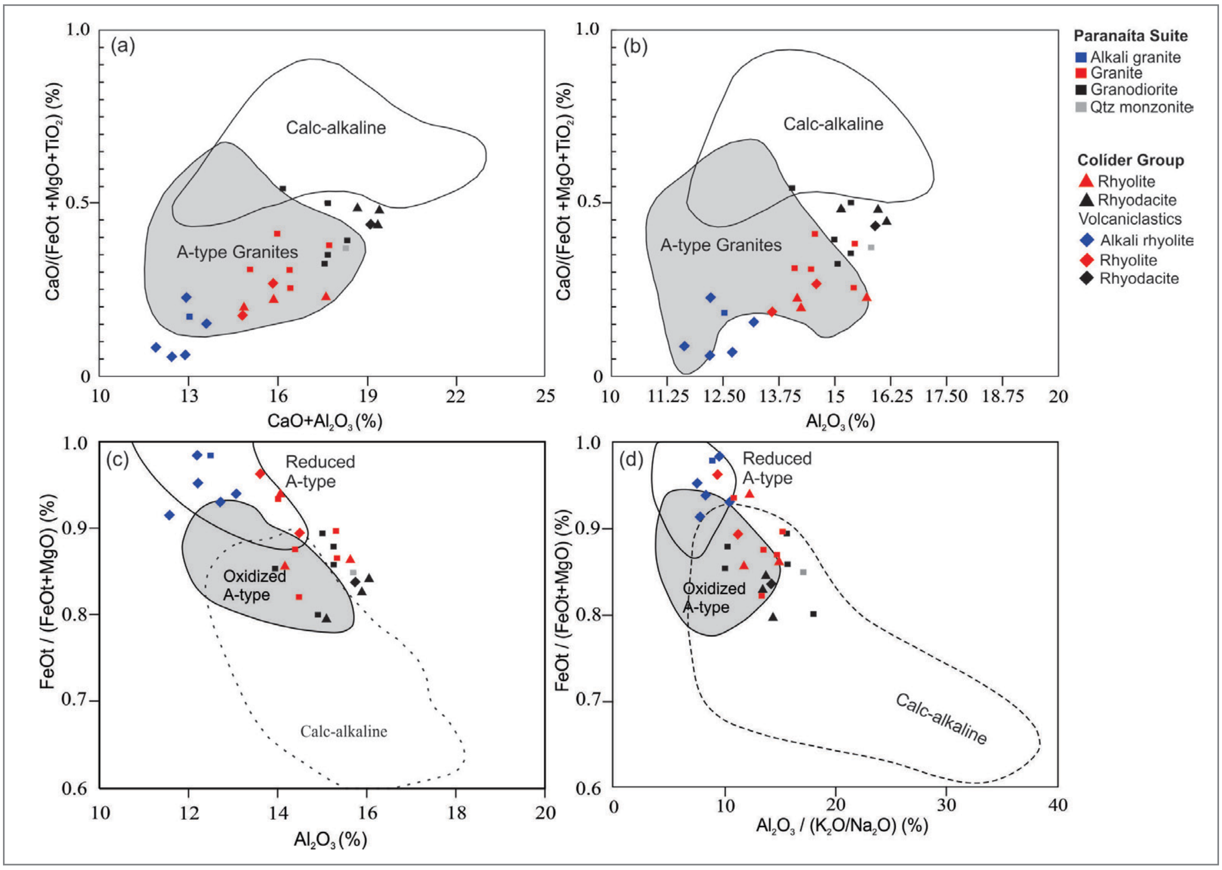

FIGURE 8 – Granite classification diagrams using major element concentrations for the acid rocks from the Volcanic Domain Dall`Agnol and Oliveira (2007). In (a) and (b) diagrams with the compositional fields of A-type and calc-alkaline granites. In (c) and (d) diagrams with the compositional fields of A-type reduced, oxidized and calc-alkaline granites.

oxidized granites. All samples plot in the Type A field (Fig. 8a and b), although some samples of alkali granite, granodiorite, rhyodacite, granite and quartz monzonite plot outside the delimited fields. In addition, in Fig. 8 c and d, it is possible to observe that the majority of the samples plot in or adjacent to the oxidized A-type fields (in a region of interface between the calc-alkaline field), with exception of the more differentiated samples (alkali rhyolites and granites with high Fe*) which plotted in the reduced A-type granites field.

7. Geochronology

This work reports seven zircon U-Pb geochronological analyses and four whole-rock Sm-Nd analyses from the Volcanic Domain. Sample locations are presented in Table 2, and the isotopic results are shown in the Appendix B.

7.1. U-Pb zircon results

7.1.1 Paranaíta Intrusive Suite

Sample GR-001 (micromonzogranite). Cathodoluminescence (CL) images of zircon grains reveal simple oscillatory zoning and rarely re-equilibration zones (Fig. 9a). Two typical morphologies are observed. The predominant types have stubby and equant morphologies, {100} and {110}, with a length/width ratio of 1.5:1, and (y) axis size between 300 and 400 µm. The subordinate population is needle-shaped, {101}, with a length/width ratio of 5:1, and (y) axis size between 400 and 500 µm. Twenty-seven spots were made throughout the cores and rims of twenty-four zircons that differ from each other in their habits but still yielded a single $^{207}Pb/^{206}Pb$ age group ranging from 1815 to 1780 Ma. Except for pits Z7, Z11, Z18, and Z24 that show data dispersion, the other analyses were used to calculate an upper intercept age of 1793.4 ± 7.2 Ma (MSWD =1.4). An alternative calculation using the most concordant data yielded a concordia age of 1780.3 ± 4.5 Ma (MSWD =2.3) (Fig. 9b). The two ages overlap within analytical uncertainty, and both can be used to express the crystallization age of the analyzed granite.

Sample GR-001A is a porphyritic granite that occurs in contact with the microgranite GR-001. The zircons extracted from this sample are inclusion-rich and cracked. Backscattered electron (BSE) imaging of zircons reveals fine-scale and well-defined oscillatory zonation patterns; zircon overgrowth is not observed (Fig. 10a). The crystal morphology is typical of plutonic rocks cooled slowly, types {100} and {110}, with a length/width ratio of 2:1 and (y) axis size between 150 and 300 µm. Twenty-four analyses were made on twenty-four zircons. The regression of all analyses gives an upper intercept age of 1807.2 ± 8.2 Ma (MSWD = 1.3) (Fig. 10b), which is interpreted as the crystallization age for this sample.

Samples TD-T-050S and TD-T-050AM. These samples are of a porphyry granite and a micromonzogranite similar to the samples GR-001A and GR-001, respectively. The zircons from TD-T-050S are idiomorphic, cracked, resembling external deformation processes such as mylonitization (Wayne and Sinha 1988), and have a few mineral inclusions. The internal structure revealed by BSE imaging (Fig. 11a) is marked by fine-scale oscillatory and rare sector zoning. The morphologies are similar to those of zircons from plutonic rocks (stubby and equant), type {100}, with a length/width ratio of 1.5:1, and (y) axis between 150 and 250 µm. Among the twenty-four analyses, two were discarded due to high errors (Z22) and scattered behavior (Z12) (Table 13). The other results yielded $^{207}Pb/^{206}Pb$ ages ranging between 1844 and 1761 Ma, with a mean $^{207}Pb/^{206}Pb$ age of 1810 +7/-18 Ma (94.3% conf.), and an upper intercept age of 1801 ± 12 (MSWD = 1.6) (Fig. 11b). The upper intercept age is interpreted as the crystallization age.

In the sample TD-T-050AM the zircon crystals are idiomorphic to sub-idiomorphic with a simple combination of short prisms and bipyramidal terminations. They are commonly fractured and contain inclusions. It is possible to identify mainly fine-scale oscillatory zonation and rare radial fractures in BSE image (Fig. 12a). Even though this sample shows petrographic texture typical of subvolcanic rocks; needle-shaped zircons are not identified. Instead, the zircon morphology is more similar to that of plutonic granites (stubby and equant), such as the {100} type, with a length/width ratio of 1.5:5.1, and (y) axis between 50 and 100 µm. Twenty-four analyses were obtained and one was discarded due to high analytical errors (Z12). The other spots show consistent results yielding an upper intercept age of 1815 ± 10 Ma (MSWD =0.95). An alternative calculation using the most concordant data yielded a concordia age of 1812 ±5.2 Ma (MSWD =0.049) (Fig. 12b). The two ages overlap within analytical uncertainty and both can be used to express the crystallization age of the analyzed granite.

TABLE 2 – Information about the analyzed samples. Geographic coordinates in decimal degrees (WGS84).

Sample	Latitude	Longitude	Lithology	Unit	Analytical Method
TD-095	-9.0430	-58.8644	Rhyodacite	Colíder Group	U-PB LA-ICP-MS
TD-T-063K	-9.1652	-58.5575	Volcanoclastic	Colíder Group	U-PB LA-ICP-MS and Sm-Nd
TD-107	-9.2646	-59.0704	Amphibolite	Colíder Group	U-PB LA-ICP-MS and Sm-Nd
GR-001	-9.1394	-58.5659	Microgranite	Paranaíta Suite	U-PB LA-ICP-MS
GR-001A	-9.1394	-58.5659	Porphyry granite	Paranaíta Suite	U-PB LA-ICP-MS
TD-T-050S	-9.1394	-58.5659	Porphyry granite	Paranaíta Suite	U-PB LA-ICP-MS and Sm-Nd
TD-T-050AM	-9.1394	-58.5659	Microgranite	Paranaíta Suite	U-PB LA-ICP-MS and Sm-Nd

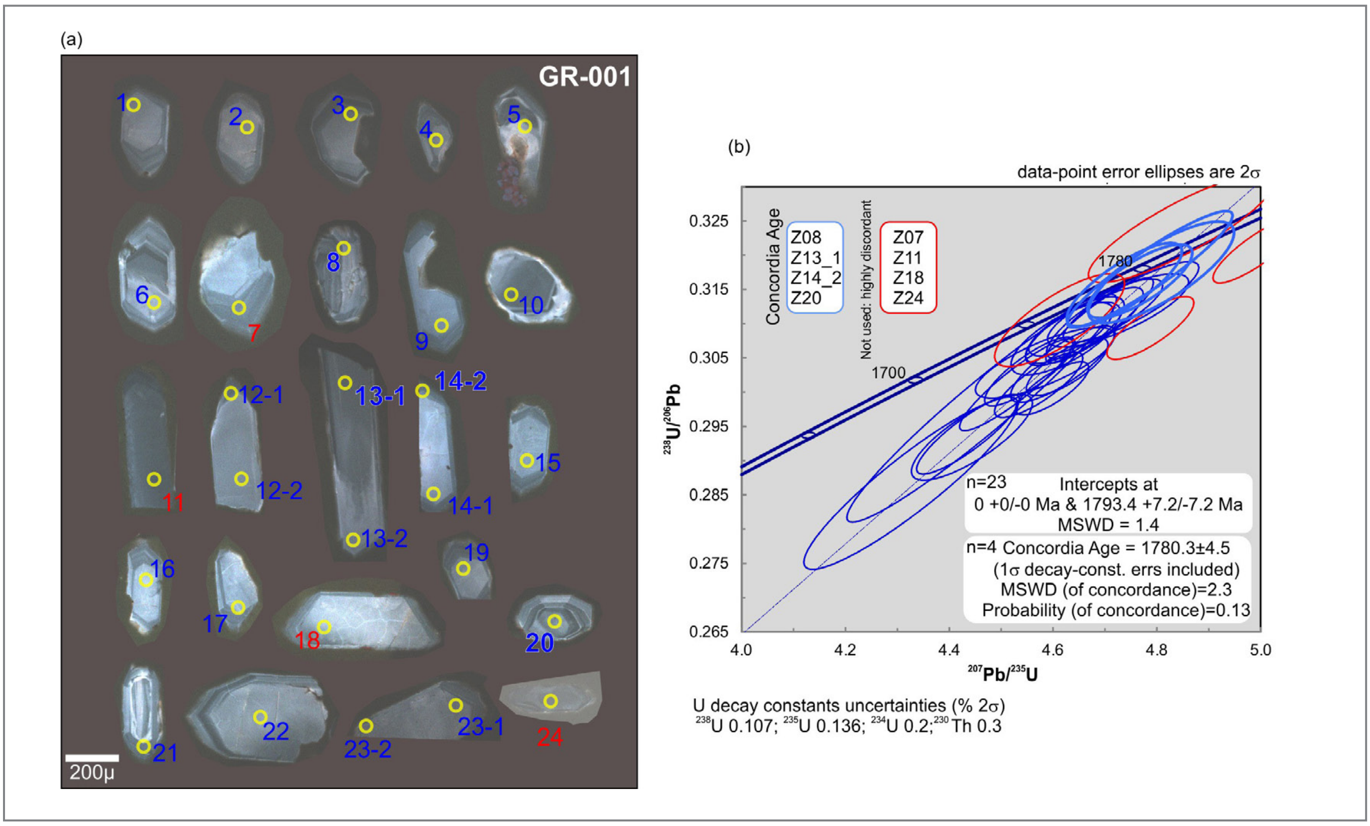

FIGURE 9 – (a) Cathodoluminescence image of zircons of a microgranite from the Paranaíta Intrusive Suite (sample GR-001) showing morphological features and location of pits; (b) U-Pb upper intercept age in the concordia diagram and the ^{207}Pb/ ^{206}Pb age of the two crystals aging around 1840 Ma. The blue color represent the spots results used in the upper intercept calculation, conversely, the red color represent those not used.

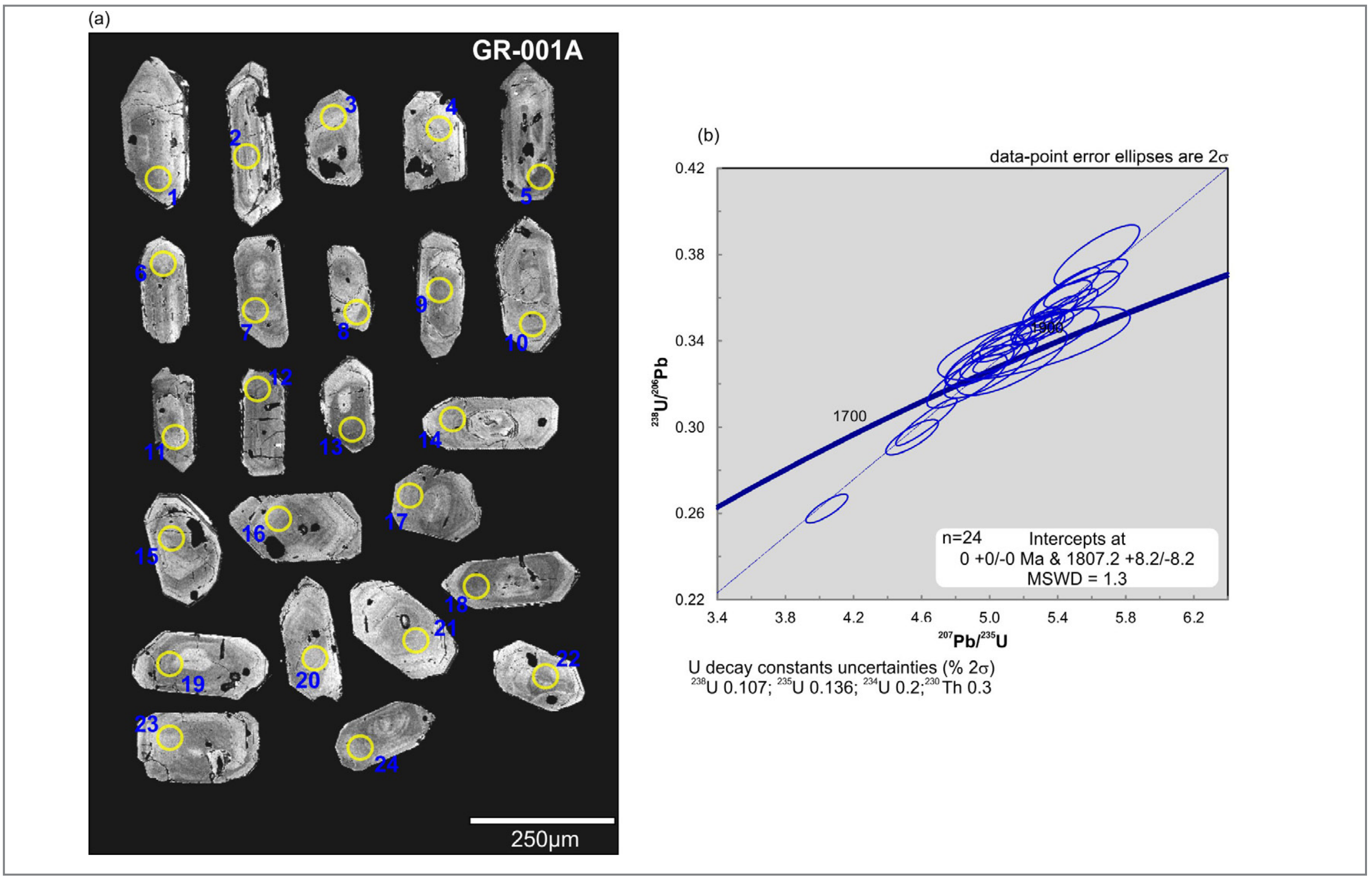

FIGURE 10 – (a) BSE image of zircons of a porphyritic granite from the Paranaíta Intrusive Suite (sample GR-001A) showing their morphological features, location and ID of pits; (b) U-Pb concordia diagram for GR-001A.

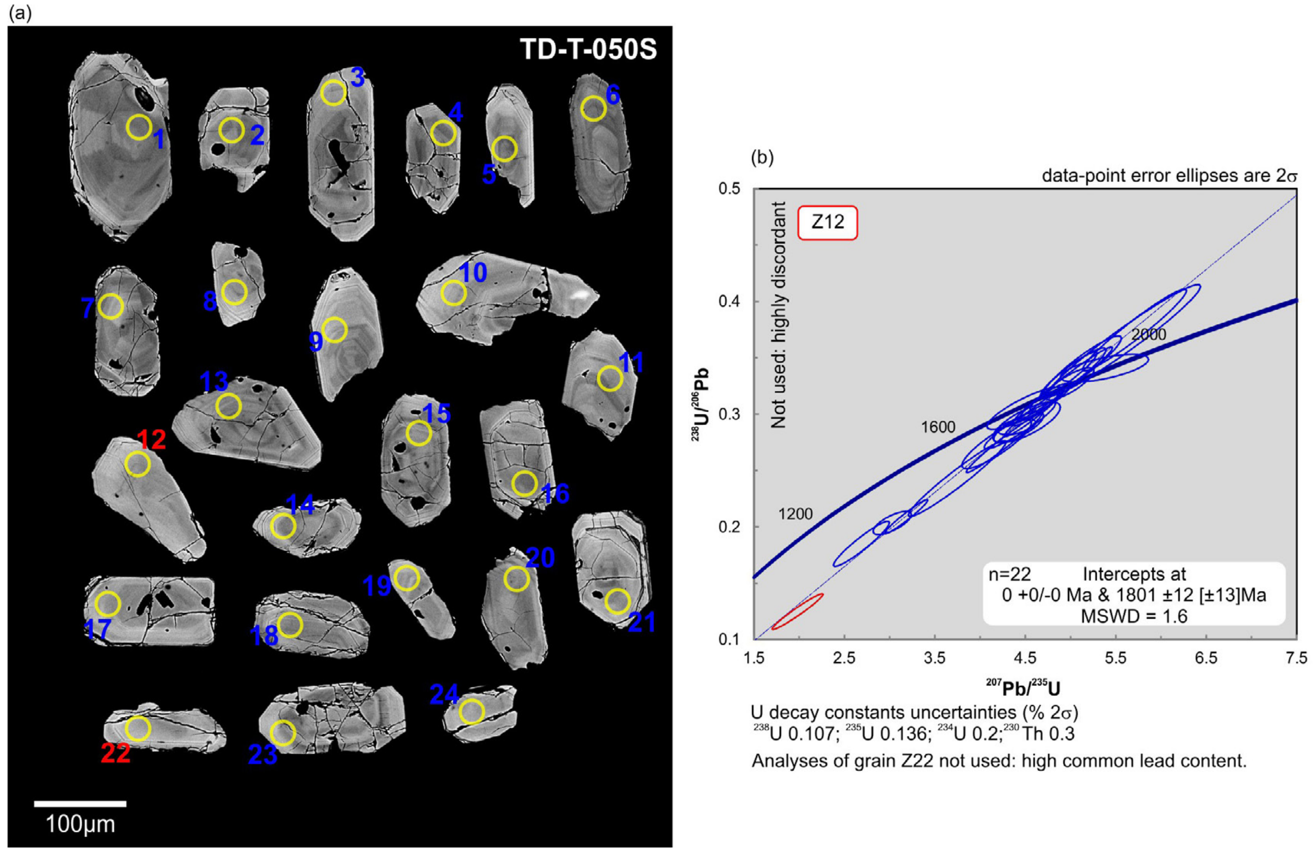

FIGURE 11 – (a) BSE image of zircons of a porphyritic granite from the Paranaíta Intrusive Suite (sample GR-001A) showing their morphological features, location and ID of pits; (b) U-Pb concordia diagram for GR-001A.

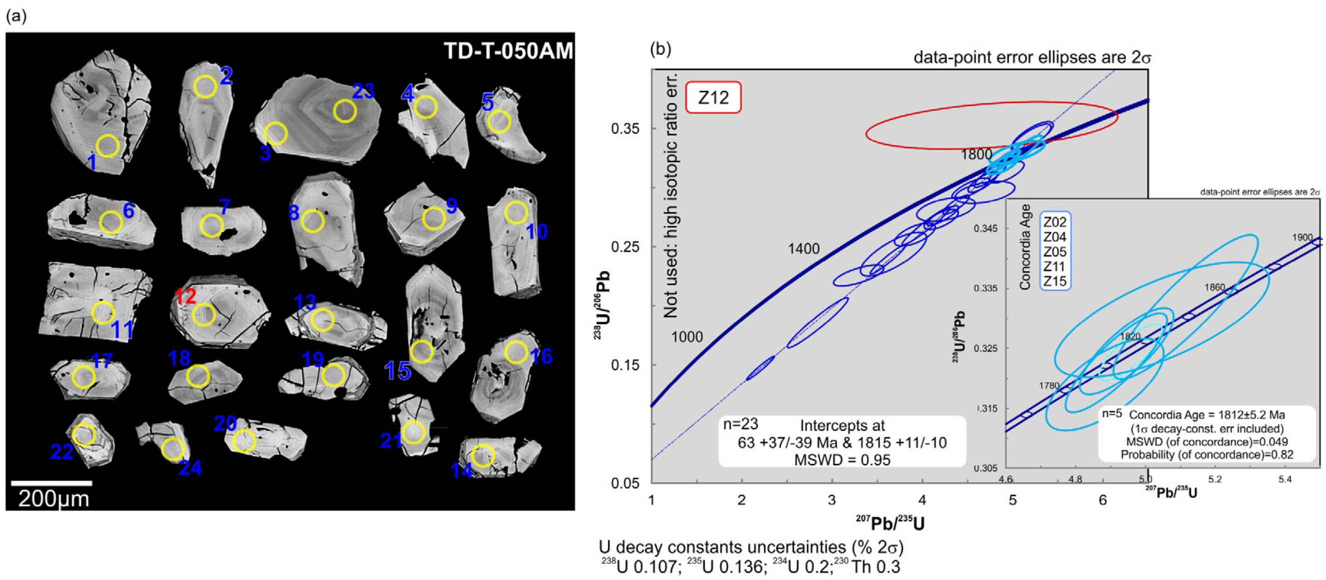

FIGURE 12 – (a) BSE image of zircons of a microgranite from the Paranaíta Intrusive Suite (sample TD-T-050AM) revealing the morphological features, location and ID of pits; and (b) U-Pb concordia diagram and the upper intercept age calculated. The blue color represent the spots results used in the upper intercept calculation, conversely, the red color represent those not used.

7.1.2. Colíder Group

The sample TD-T-063K is an ignimbrite composed of devitrified pumices, lithoclasts and glass shards. The zircons are short with a combination of prismatic and bipyramidal terminations, their morphology is equidimensional, types {100} and {211}, having a length/width ratio of 1.5:1, and (y) axis between 150 and 200 µm. BSE imaging (Fig. 13a) reveals large-scale oscillatory zoning. Semi-circular indentations are commonly observed in zircon rims as a result of magmatic resorption and are characteristic of pyroclastic rocks (Corfu et al. 2003). Among twenty-four U-Pb isotopic analyses, twenty-three gave good quality of results and one discarded due to high analytical error (Z4). The results were used to calculate an upper intercept age of 1823 ±33 Ma (MSWD = 0.74). An alternative calculation using the most concordant data yielded a concordia age of 1812 ±12 Ma (MSWD =1.6) (Fig. 13b), which is interpreted as the crystallization age of this rock.

Sample TD-095 is a porphyritic rhyodacite showing granophyric texture. The bipyramidal zircons with short-prismatic shape are homogeneous, inclusion-rich and abundantly fractured. The morphology is equidimensional, nearly rounded types {100} and {211}, with a length/width ratio of 1.5:1, and (y) axis between 100 and 150 µm. The BSE image (Fig. 14a) reveals discrete and well-defined oscillatory zoning. Despite the more fractured condition, these zircons are similar to those of sample TD-T-063K, which exhibits magmatic resorption features. Among the twenty-four analyses, five of them with high-analytical errors were discarded (Z5, Z8, Z10, Z12, and Z19). The regression of seventeen analyses gave an upper intercept age of 1813 ± 12 Ma (MSWD = 0.99). Alternatively, the five most concordant results were used to calculate a concordia age of 1809 ±6.5 (MSWD =1.6) (Fig. 14b). The two ages overlap within analytical uncertainty and both can be used to express the crystallization age of the analyzed sample. Analyses of zircons Z2 and Z15 were also not used in the calculation. They resulted in the oldest $^{207}Pb/^{206}Pb$ ages in all analyzed samples; 1924 and 1966 Ma, respectively, and are probably inherited.

Sample TD-107 is an amphibolite from the Colíder Group. The zircons are small, fractured and contain inclusions. Their (y) axis are between 50 and 120 µm with a morphology that is equidimensional and rounded, types {100}, {211} and {101}, with a length/width ratio of 2:1 and 1:1. BSE image (Fig. 15a) reveals discrete oscillatory zoning. The less fractured crystals exhibit a homogeneous internal structure and darker extremities, resembling compositional variations instead of overgrowth. Parallel fractures observed in these zircons may be related to deformation due to rapid decompression during volcanic eruptions (Rudnick and Williams 1987), and concentric diffusion bands are also common. Probably due to the fracturing and alteration, six out of twenty-four spots analyzed were discarded because of the high analytical error and common lead content (Z3, Z12, Z14, Z17, Z18, and Z19). The remaining zircons were then used to calculate three distinct upper intercept ages, based on different $^{207}Pb/^{206}Pb$ age populations. The regression of the seven oldest $^{207}Pb/^{206}Pb$ relative ages resulted in an upper intercept age of 1852 ± 15 Ma (MSWD =0.72). This age

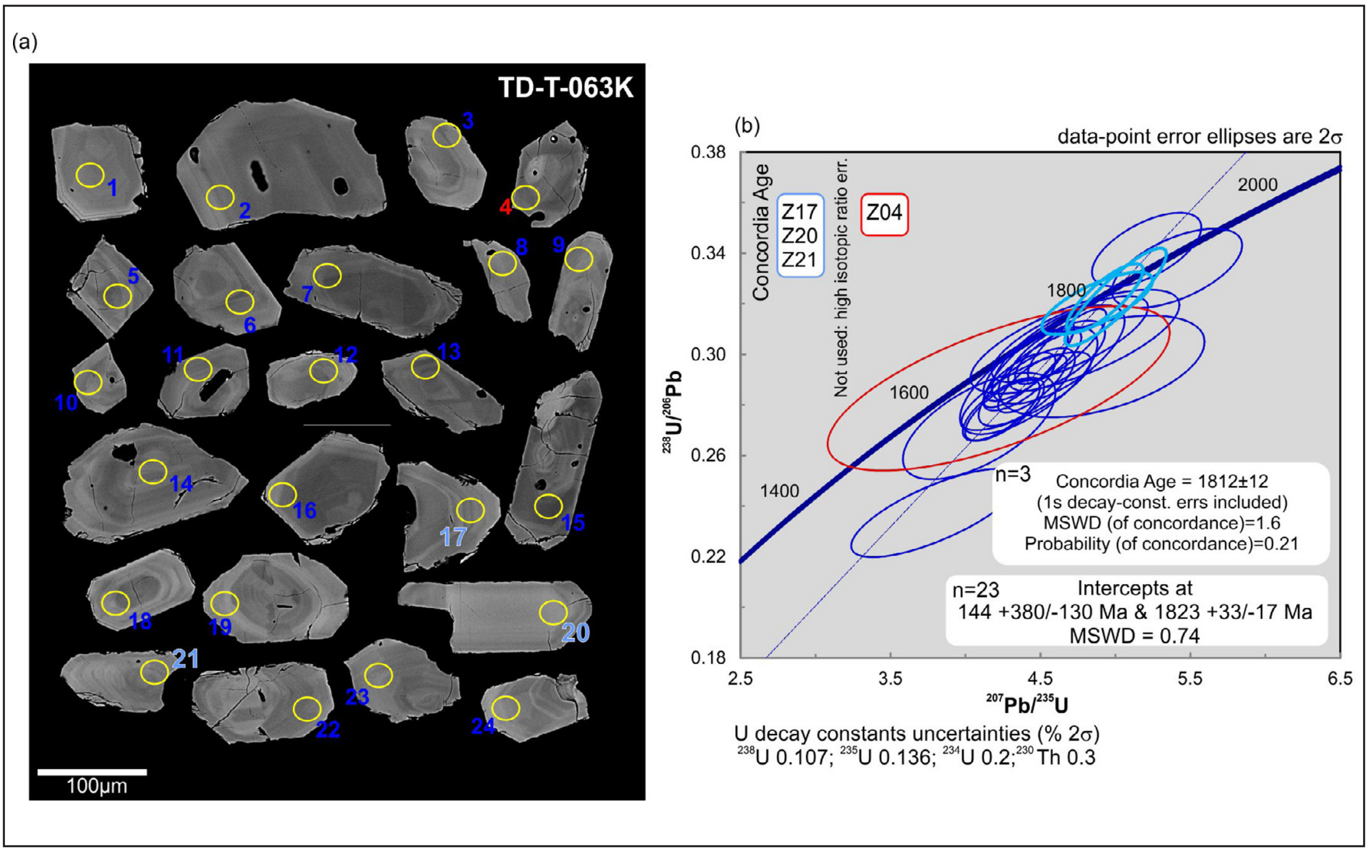

FIGURE 13 – (a) BSE image of zircons of a volcaniclastic from the Colíder Group (sample TD-T-063K) showing their morphological features, location and ID of pits; and (b) U-Pb upper intercept age in the concordia diagram. The blue color represent the spots results used in the upper intercept and concordia age calculation, conversely, the red color represent those not used.

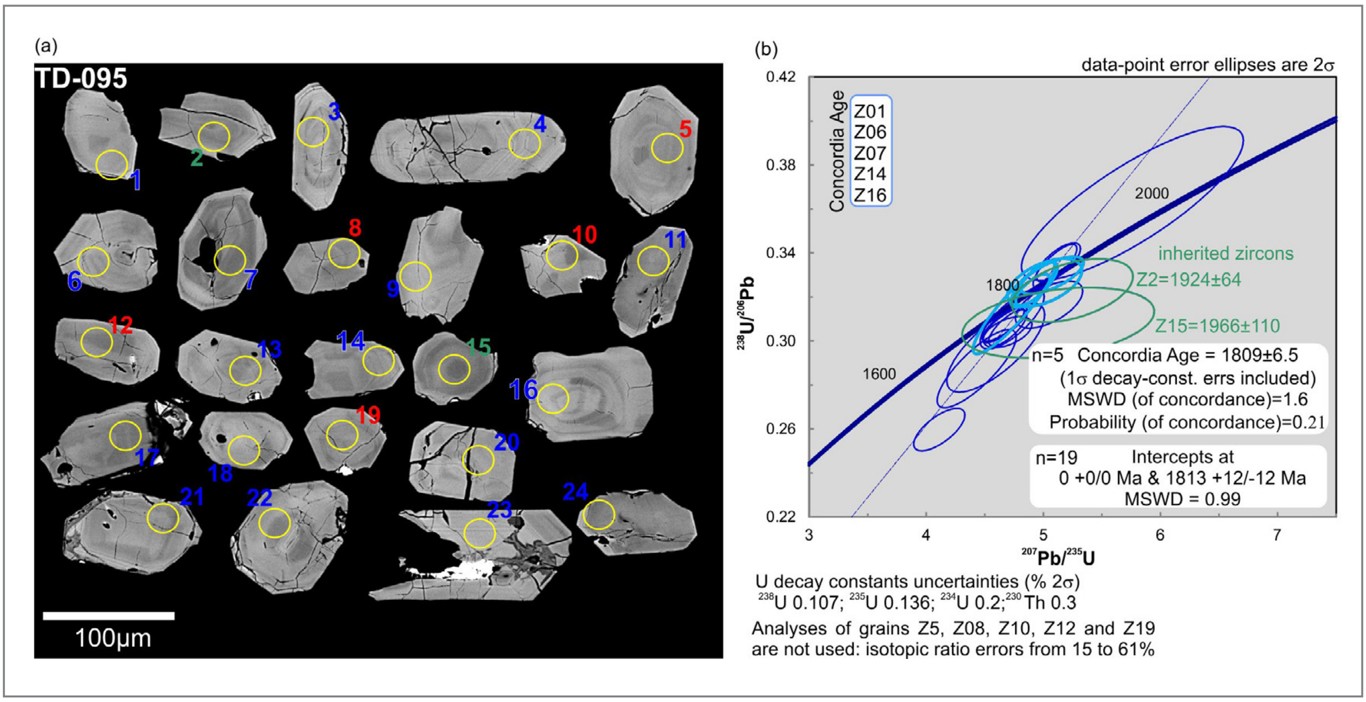

FIGURE 14 – (a) BSE image of zircons of a rhyodacite (sample TD-095) from the Colíder Group showing their morphological features, location and ID of pits; and (b) U-Pb concordia diagram and the upper intercept age calculated including the ages related to inherited zircons.

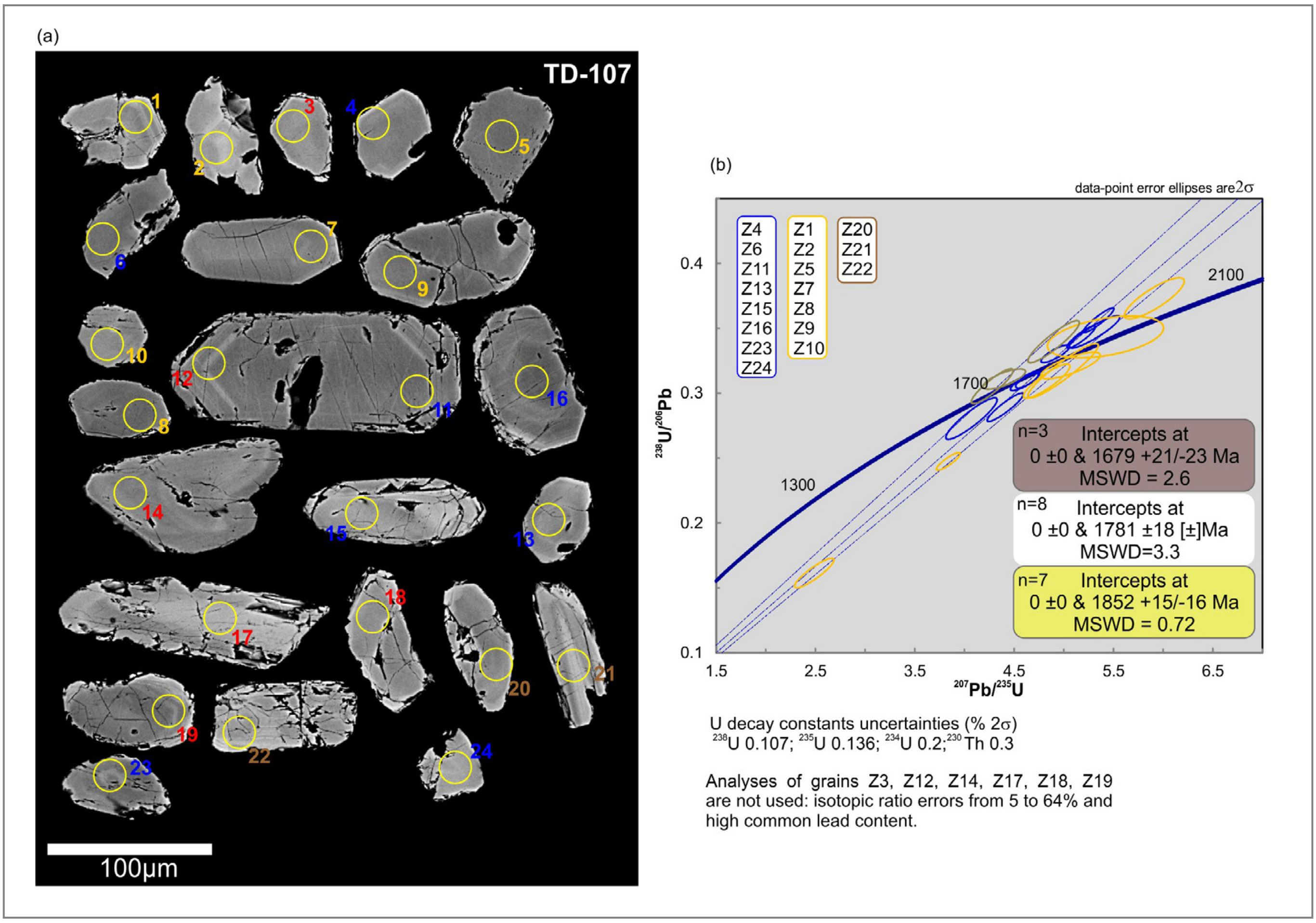

FIGURE 15 – (a) BSE image of zircons of an amphibolite (sample TD-107) from the Colíder Group showing the morphological features, location and ID of pits; and (b) U-Pb concordia diagram and the upper intercept age calculated. The spots marked in blue, brown and yellow were used in the calculations of the middle, younger and older upper intercept ages respectively. The spots marked with red number were not used in the calculations.

is related to inherited zircons. The second upper intercept age was obtained by the regression of eight $^{207}Pb/^{206}Pb$ ages around 1800 Ma, ordinarily obtained in the Colíder Group rocks. This regression resulted in an upper intercept age of 1781 ± 18 Ma (MSWD =3.3), which is considered as the crystallization age of this rock. The third and younger age was obtained by the regression of only three $^{207}Pb/^{206}Pb$ relative ages, around 1650 Ma, which resulted in an upper intercept age of 1679 ± 21 Ma (MSWD =2.6) (Fig. 15b) that could be the result of a geological event that induced Pb loss.

7.2 Sm-Nd results

Table 3 gathers the whole-rock Sm-Nd analyses as well as depleted mantle model ages, T_{DM}, and ε_{Nd} calculations for rocks of the Colíder Group and Paranaíta Intrusive Suite. The T_{DM} age for the acid rocks from the Colíder Group (TD-T-063K) is 1.9 Ga with a positive ε_{Nd} value of +2.05. The sample TD-R-107, representative of the basic to intermediate magmatism of the Colíder Group, yielded a T_{DM} age of 2.2 Ga and ε_{Nd} value of +0.4, which is also consistent with the Sm-Nd isotopic signature of the Volcanic Domain magmatism.

The sample TD-T-050S from the Paranaíta Suite yielded the oldest T_{DM} age of 2.4 Ga, and also a unique negative ε_{Nd} value in this dataset. Conversely, another sample from the Paranaíta Intrusive Suite (TD-T-050AM) yielded a younger T_{DM} age and a slightly positive ε_{Nd} value (2.0 Ga and +0.68), respectively.

The diagram of ε_{Nd} evolution versus time (Fig. 16) was elaborated to enable the comparison between the present Sm-Nd results with the available Sm-Nd data results from the literature for the Volcanic Domain and Juruena Complex (Table 4).

The dataset gathered in Tables 3 and 4 and plotted in Figure 16 shows a broad interval of T_{DM} ages ranging from 2.40 to 1.84 Ga and the $\varepsilon_{Nd(t)}$ (t=1.8 Ga) calculated for these samples vary from negative (-0.20 to -3.90) to positive (0.10 to 2.50) values. Note that the negative and positive $\varepsilon_{Nd(t)}$ values are directly related to the oldest (2.4 to 2.1 Ga) and younger (2.0 a 1.9 Ga) T_{DM} ages. The younger T_{DM} ages with positive $\varepsilon_{Nd(t)}$ values of the Colíder Group are related to the basic rocks.

The pattern of T_{DM} ages and $\varepsilon_{Nd(t)}$ values of the Juruena Complex (darker envelope) is very similar to that of the Volcanic Domain. The T_{DM} age interval is of 370 Ma for 13 rock samples, between 2.30 and 1.93 Ga with a mean age of 2.07 Ga, and $\varepsilon_{Nd(t)}$ values with (t=1.78 Ga) vary from positive (0.26 to 2.10) to negative (-0.25 to -2.57).

A direct relationship between older and younger T_{DM} ages related to negative and positive $\varepsilon_{Nd(t)}$ values respectively is observed for the Volcanic Domain. Similarly, identical intervals of T_{DM} ages and $\varepsilon_{Nd(t)}$ values are found among the results for the Juruena Complex as follows: older interval (2.3 to 2.1 Ga with $\varepsilon_{Nd(t)}$ -0.25 to -2.57), and younger interval (2.0 to 1.9 Ga with $\varepsilon_{Nd(t)}$ 0.26 to 2.10).

8. Discussion

8.1 The relation among the Paranaíta-Colíder association with other volcano-plutonic units (Teles-Pires Intrusive Suite and Roosevelt Group).

In the southwestern Amazon Craton, the 1.8 Ga undeformed volcanic rocks and associated granites (Volcanic Domain) have been understood geologically in three different ways, as well, many distinct names have been proposed for the units.

For some authors (Neder et al. 2002; Pinho et al. 2003; Cordani and Teixeira 2007 and 2009), the Volcanic Domain is the result of an intra-plate magmatism related to extensional structures developed at the SW border of the Ventuari-Tapajós Province, as well as related to the breakup of the supercontinent Columbia (or NUNA). These authors consider this volcano-plutonism as part of the Teles-Pires magmatism, and yield crystallization ages for these rocks ranging from 1800 to 1776 Ma (Pinho et al. 2003; Cordani and Teixeira 2007; Barros et al. 2009). Other authors (Santos et al. 2000 and 2008; Souza et al. 2005; Ribeiro and Duarte 2010; Duarte et al. 2012; Scandolara et al. 2014) have understood the coeval (1.8 Ga) plutonic-volcanic event (Volcanic Domain) as a subduction-related continental arc magmatism of the Juruena Magmatic Arc, and attributed to the volcanic and plutonic rocks to the Colíder Group and to the Paranaíta Intrusive Suite, respectively (Fig. 17).

More recently, Barros et al. (2009), Alves et al. (2013) and Silva et al. (2014) have interpreted similar rocks as related to a late- to post-tectonic extensional back-arc environment in relation to the Juruena Magmatic Arc evolution. Alves et al. (2013) dated A-type volcanic rocks at 1792 Ma and associated granites at 1775 Ma (Pium Granite) assigning these rocks to the Teles-Pires magmatism.

Another example of widespread volcanism in the Juruena Magmatic Arc is the volcano-sedimentary sequence of the Roosevelt Group and the associated Aripuanã Granite (Neder et al. 2002; Santos et al. 2000; Rizzotto et al. 2002; Biondi et al. 2013). These rocks exhibit crystallization ages between 1762 and 1740 Ma (Fig. 17). Even though these rocks are 30 to 40 Ma younger than the Teles-Pires magmatism,

TABLE 3 – Whole rock Sm-Nd analyses of the Volcanic Domain.

Sample	Rock	Sm(ppm)	Nd(ppm)	$^{147}Sm/^{144}Nd$	$^{143}Nd/^{144}Nd$ (± error 10^{-6})	$\varepsilon_{Nd (0)}$	$\varepsilon_{Nd (t)}$	T_{DM} (Ga)	t(Ga)
TD-T-063K	Volcaniclastic	4.787	30.316	0.0954	0.511541+/-14	-21.4	2.05	1.9	1.8
TD-T-050AM	Microgranite	3.834	21.847	0.1061	0.511592+/-16	-20.4	0.68	2.0	1.8
TD-R-107	Amphibolite	4.691	19.579	0.1448	0.512042+/-22	-11.64	0.4	2.2	1.8
TD-T-050S	Porphyry granite	4.567	23.888	0.1156	0.511518+/-17	-21.85	-3.09	2.4	1.8

Notes: Samples are displayed in order from youngest to oldest ages. All data recalculated using CHUR isotopic ratios: $^{147}Sm/^{144}Nd$=0.19665; $^{144}Nd/^{143}Nd$=0.512655; MORB isotopic ratios: $^{147}Sm/^{144}Nd$=0.21353; $^{144}Nd/^{143}Nd$=0.513168. Depleted mantle model (De Paolo 1981). (t) Crystallization ages are in Ga.

TABLE 4 – Whole rock Sm-Nd results from the bibliography used in the construction of the Nd-isotope evolution diagram presented in Figure 16.

	Sample	Longitude	Latitude	Rock	Sm(ppm)	Nd(ppm)	$^{147}Sm/^{144}Nd$	$^{143}Nd/^{144}Nd(\pm 10^{-6})$	$\varepsilon_{Nd\,(0)}$	$\varepsilon_{Nd\,(t)}$	T_{DM} (Ga)
Volcanic Domain	**Colíder Group (t = 1.8 Ga)**										
	MC-017 (1)	-59.10	-9.12	dacite	7.241	40.92	0.107	0.511679	-18.72	1.79	1.94
	B-04.060 (2)	-59.03	-8.96	basalt	0.63	4.47	0.12993	0.511924	-13.9	1.3	2.00
	FG-2.162 (2)	-59.10	-8.93	basalt	0.5	3.62	0.13617	0.512007	-12.3	1.5	2.02
	Fi-05.080 (2)	-59.12	-9.00	basalt	0.1	0.84	0.12293	0.511783	-16.7	0.1	2.10
	Fi-02.027 (2)	-59.12	-9.00	rhyolite	0.64	5.4	0.1174	0.511701	-18.3	-0.2	2.11
	GM-R-69A (3)	-55.47	-10.83	andesite	7	38.4	0.1109	0.51161	-20.1	-0.2	2.12
	WB--08 (2)	-59.07	-8.07	ignimbrite	0.76	6.82	0.10966	0.511574	-20.8	-0.9	2.14
	B-03.150 (2)	-59.03	-8.96	rhyolite	0.07	8.82	0.11976	0.511706	-18.2	-0.7	2.16
	MA-012B (3)	-55.94	-9.82	dacite	4.7	29.8	0.0955	0.51134	-25.4	-1.9	2.19
	GM-R-118 (3)	-54.74	-10.25	rhyolite	3.3	19.2	0.1021	0.51138	-24.5	-2.6	2.26
	Paranaíta Intrusive Suite (t = 1.8 Ga)										
	CC-R-156 (3)	-56.57	-9.52	monzogranite	9.8	56.5	0.1051	0.51168	-18.7	2.5	1.90
	MC-120 (1)	-58.91	-9.19	monzogranite	5.713	35.428	0.0975	0.511513	-21.94	0.97	1.99
	MC-140 (1)	-58.52	-9.78	monzogranite	6.849	38.387	0.1078	0.511641	-19.44	1.09	2.01
	FBP-90.5 (2)	-59.11	-8.95	granite	0.9	8.5	0.10618	0.511593	-20.4	0.2	2.04
	FBP-150 (2)	-59.11	-8.95	granite	0.82	7.93	0.10245	0.511465	-22.9	-1.4	2.15
	MA-012B (3)	-55.94	-9.82	dacite	4.7	29.8	0.0955	0.51134	-25.4	-1.9	2.19
Juruena Complex	**São Pedro Granite (t = 1.8 Ga)**										
	MA-07 (3)	-56.43	-10.37	metamonzo-granite	8.7	45.4	0.1155	0.51179	-16.5	2.05	1.93
	A-4 (2)	-59.37	-9.27	metamonzo-granite	1.18	10.01	0.11499	0.511776	-16.78	1.90	1.94
	AF-R-82A (3)	-56.98	-10.16	metamonzo-granite	7.3	36	0.1224	0.51187	-14.94	2.04	1.94
	P-29 (2)	-59.12	-9.15	metamonzo-granite	0.64	6.61	0.09489	0.511441	-23.31	-0.06	2.04
	A-8 (2)	-59.29	-9.39	metamonzo-granite	1.03	8.39	0.12125	0.511766	-16.97	0.26	2.09
	TD-137 (1)	-58.91	-9.11	metamonzo-granite	5.902	33.613	0.1061	0.511527	-21.63	-0.94	2.14
	A-7 (2)	-59.36	-9.39	metamonzo-granite	0.93	8.2	0.11152	0.511589	-20.42	-0.97	2.16
	P-20 (2)	-59.13	-9.38	metasienogranite	2.47	20.84	0.11626	0.511563	-20.93	-2.57	2.30
	Vitória Plutonic Suite (t = 1.8 Ga)										
	P-19 (2)	-59.15	-9.42	metatonalite	1.43	11.26	0.12451	0.511898	-14.39617975	2.10	1.94
	PS-042 (4)	-57.79	-9.89	tonalite gneiss	11.6	79.1	0.0884	0.5114	-24.11067502	0.63	1.99
	AF-47C (3)	-56.19	-10.35	norite	5.1	19.2	0.1622	0.51232	-6.164217886	1.72	2.12
	P-18 (2)	-59.14	-9.39	metagranodiorite	0.72	5.58	0.1268	0.511805	-16.21033248	-0.25	2.16
	A3 (2)	-59.35	-9.29	tonalite gneiss	1.8	14.94	0.11843	0.511614	-19.93617304	-2.07	2.28

Notes: (1) Ribeiro and Duarte (2010) (2) Pinho et al. 2003; (3) Silva and Abram (2008); (4) Souza et al. (2005). The $\varepsilon_{Nd(t)}$ values were recalculated for t=1.8 Ga. All coordinates in decimal degrees and WGS84 datum.

and occur outside of the Volcanic Domain trend, Pinho et al. (2003) and Cordani and Teixeira (2007) correlate these rocks to the Teles-Pires magmatism. However, other works that take into consideration the crystallization ages and occurrence pattern of the Roosevelt Group have interpreted this unit to be developed in a retro-arc setting in relation to the Juruena Magmatic Arc Evolution. In addition to the younger crystallization age range, Neder et al. (2002) and Biondi et al. (2013) also have described Pb-Zn-Cu volcanic-hosted massive sulfide deposits for the Roosevelt Group that are very distinct from the Au epithermal-porphyry systems found within the Volcanic Domain.

The cross-section presented in Figure 18 shows the arrangement of the Juruena Magmatic Arc geology according to a continental magmatic arc tectonic evolution. In this model, the precursor magmas are related to subduction processes and hydrous melting of the SCLM plus the assimilation and reworking (AFC processes) of a Ventuari-Tapajós crust. The products

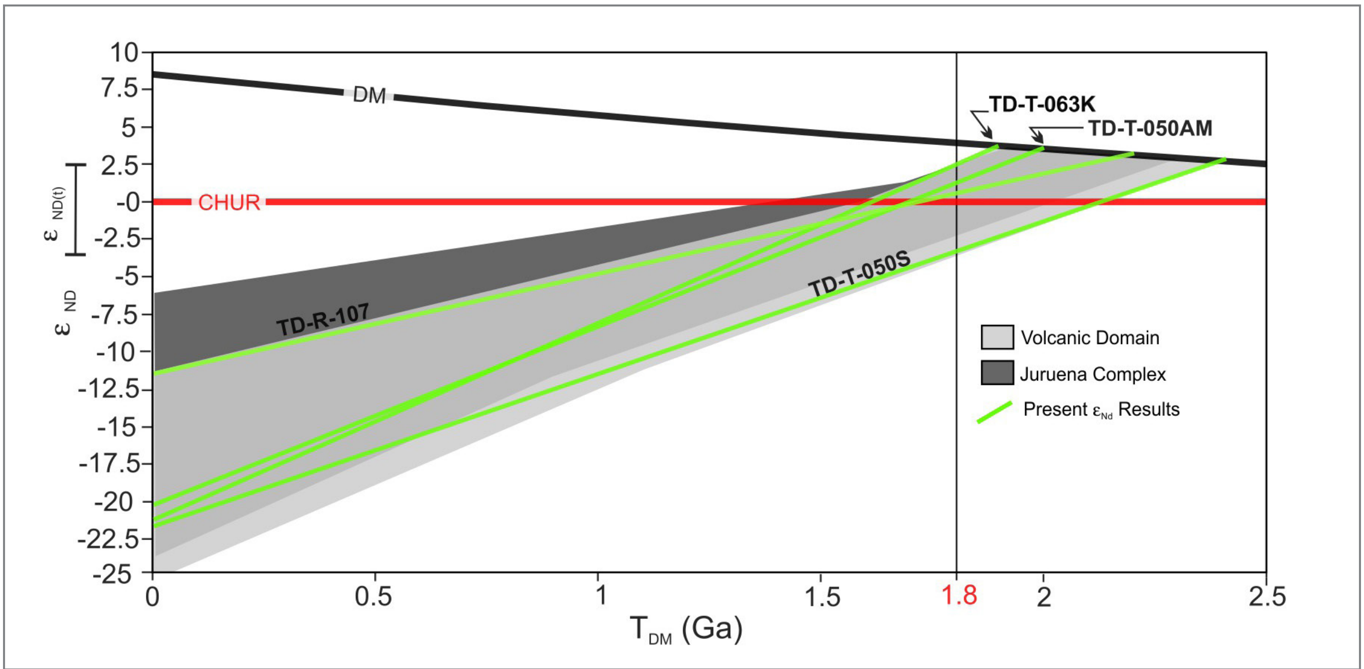

FIGURE 16– Nd-isotope evolution diagram of the Volcanic Domain and Juruena Complex. The solid green lines are from the present whole rock Sm-Nd analyses results. The grey areas envelope the bibliography whole rock eNd results from Volcanic Domain and Juruena Complex. The $\varepsilon_{Nd(t)}$ values were recalculated for t=1.8 Ga. Depleted Mantle (DM); Chondritic Uniform Reservoir (CHUR). Depleted mantle model (De Paolo 1981). Chondrite present day values $^{147}Sm/^{144}Nd$=0.1967 and $^{143}Nd/^{144}Nd$=0.512636. ^{147}Sm Decay constant=6.54x10-12.

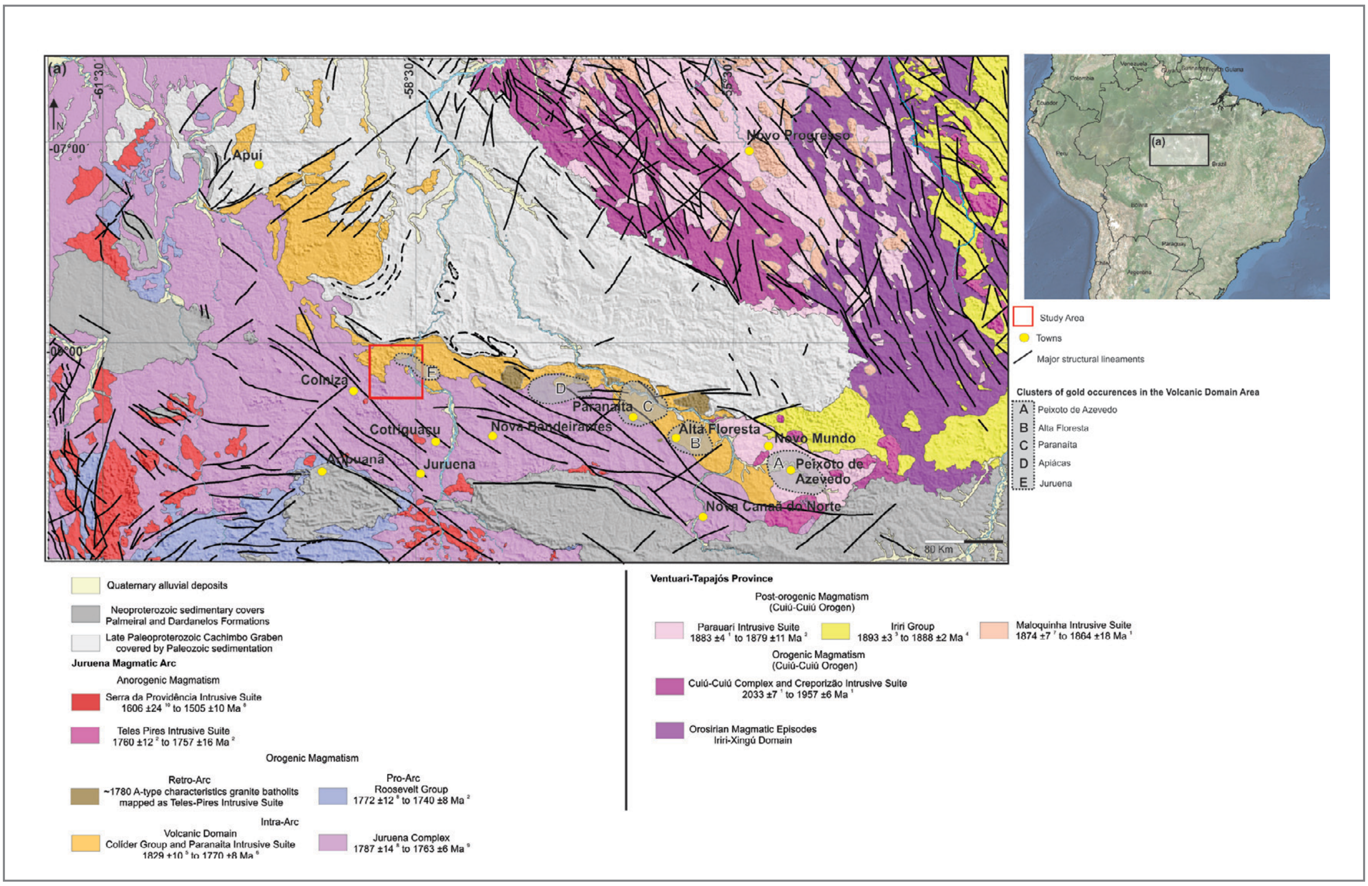

FIGURE 17 – Geotectonic and simplified geological map of part of the SW Amazon Craton. Letters A to E are showing the occurrence of gold clusters of the Alta Floresta Gold Province in the Volcanic Domain. The geology and major structural features were modified from the geological map of Brazil, 1:1.000.000 scale (Bizzi 2003). U-Pb crystallization ages reference: 1 Santos et al. (2001); 2 Santos et al. (2000); 3 Vasquez et al. (1999); 4 Dall'Agnol et al. (1999); 5 Present data; 6 Pinho et al. (2003); 7 Vasquez et al. (2008); 8 Ribeiro and Duarte (2010); 9 Neder et al. (2002); 10 Bettencourt et al. (1999); 11 Rizzotto (2002).

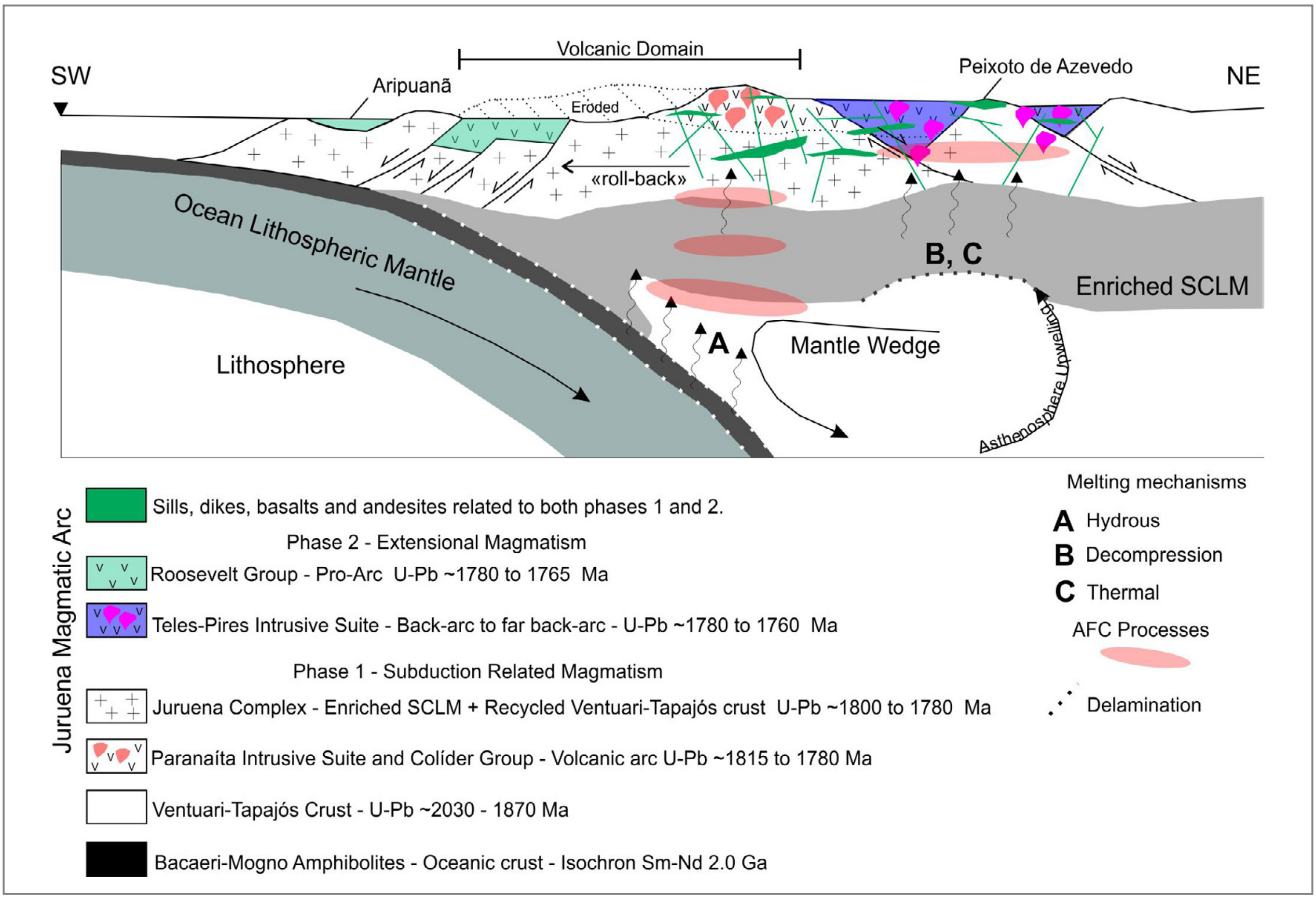

FIGURE 18 – Cross section scheme of tectonic evolution of the Juruena Magmatic Arc showing the arrangement of the discussed geological units within a proposal of magmatism in two phases related to subduction and extensional character.

are the basic to intermediate rocks as well as the oxidized A-type granitic rocks from the Volcanic Domain, including its volcanic counterparts. In addition, the deeper emplaced calc-alkaline rocks of the Juruena Complex were also generated (Phase 1). The same figure illustrates the relationship between the Volcanic Domain with the other volcanic-plutonic units (Roosevelt Group and Teles-Pires Suite), which developed in a more mature period of the arc (<1780 Ma), reflecting changes in the tectonic regime with the establishment of forearc and back-arc type tectonic environments (Phase 2).

Santos et al. 2019 also recognize two magmatic events in the Colíder Group based on slightly different geochemical signatures and U-Pb geochronology. The first one around 1.80 Ga (lower succession), dominantly magnesian, and the second one around 1.76 Ga (upper succession), dominantly ferroan and with more pronounced Eu, Sr and P negative anomalies.

8.2. Geodynamic setting of the Volcanic Domain based on the geochemistry

Although the use of granites as geodynamic indicators in some cases has shown to be inappropriate, careful combination of the methodology proposed by Barbarin (1999) with geochronological data usually succeeds in solving geotectonic issues.

High-K calc-alkaline magma series along with an alumina saturation index, which varies from metaluminous to peraluminous, suggests a mixed crustal-mantle source for the magmatism of the Volcanic Domain prevailing the crustal component (Barbarin 1999). Even though some monzogranites and granodiorites from the Paranaíta Intrusive Suite have amphibole, these rocks are potassium-rich and, therefore, classified as K-rich calc-alkaline granitoids (KCG). The volcanic rocks from the Colíder Group (mainly rhyodacite), the less differentiated varieties (regarding SiO_2 contents), with lower K_2O and higher CaO, MgO and Fe_2O_3 contents also belong to the high-K calc-alkaline series.

The REE spectrum with enrichment in light REE relative to heavy REE and negative Eu anomalies are similar to that of high fractioned high-K calc-alkaline magmas. The Harker's diagrams and trace element patterns show well-defined Nb, P and Ti negative anomalies, suggesting a magmatic evolution dominated by fractional crystallization of plagioclase, minerals containing Mg-Fe (pyroxene, hornblende and biotite), apatite and Ti-magnetite (Fig. 5 and 6), and implying contamination of the source by subduction of continental crust (Wilson 1989). Samples from the Volcanic Domain plot in the active continental margin field in tectonic-magmatic discrimination diagram (Fig. 7) (Pearce et al. 1984), a behavior that is similar to that observed for the Central Andes.

Conversely, in the major elements diagrams the acid rocks samples plot in the A-type oxidized and reduced field (Fig. 8). Thus, the hypothesis of more differentiated A-type reduced granitic rocks from the Volcanic Domain as result of extensional tectonics in the Juruena Magmatic Arc is plausible.

Also, taking into account the discussion above, it is not possible to confirm a major presence of amphibole-bearing calc-alkaline granitoids (ACG) in the Volcanic Domain that is supposed to prevail in continental magmatic arc subduction-related settings. A hypothesis is that most of these intermediate rocks are probably covered by the volcaniclastic deposits.

However, it is necessary to understand the Volcanic Domain in the context of the Juruena Magmatic Arc evolution. The Vitória Plutonic Suite and the Vespor Suite (Scandolara et al. 2014), which contain typical arc-related rocks such as calc-alkaline metagabbros, metadiorites, metatonalites, and metagranodiorites, best fit what is expected to be found in continental arc settings in association with KCG granitoids. Highly metamorphosed sediments and remnants of oceanic crust belonging to the Bacaeri-Mogno Complex accreted to the arc are also identified and reinforce the hypothesis that the Volcanic Domain in the Juruena Complex is related to a continental arc.

8.3 The volcano-plutonic association of the Volcanic Domain as part of the Juruena Magmatic Arc

The integration of the Volcanic Domain to the Juruena Complex discussed above in the context of the Juruena Magmatic Arc is based on depleted mantle model ages, ε_{Nd} values and zircon U-Pb crystallization ages.

Among twenty analyses carried out on samples from the Volcanic Domain, T_{DM} ages range from 2.40 to 1.84 Ga, and the calculated ε_{Nd}(t=1.8) values for the same samples vary between negative (-0.20 to -3.90) and positive (+0.10 to +2.50). The results from the T_{DM} dataset of the Juruena Complex are very similar, with T_{DM} ages ranging between 2.30 and 1.93 Ga, and ε_{Nd}(t=1.78) values also ranging between negative (-0.25 to -2.57) and positive (+0.26 to +2.10).

These two T_{DM} age intervals with distinct ε_{Nd} values indicate heterogeneous magma sources. Although apparently, the older T_{DM} ages from 2.3 to 2.1 Ga, and negative $\varepsilon_{Nd(t)}$ values (around -1.5) are compatible with a continental crust source, they could represent a more fractioned source. Conversely, the younger source with T_{DM} ages varying between 2.0 and 1.9 Ga, and positive $\varepsilon_{Nd(t)}$ values (around +1.0) suggests a less differentiated and juvenile source.

The older source has T_{DM} ages compatible with the crystallization ages from the Orosirian magmatic episodes of the Erepecuru-Trombetas and Irirí-Xingu Domain (Leal et al. 2018); in turn, the younger (more juvenile) source have T_{DM} ages similar to the crystallization ages of the Ventuari-Tapajós Province formation stage (Cuiú-Cuiú - island arc; Creporizão - continental arc; Tropas - island arc/continental arc) (Santos et al. 2004).

The zircon U-Pb crystallization ages obtained in this work for the Volcanic Domain are comparatively homogeneous showing the following results: Paranaíta Intrusive Suite (from 1815 ± 10 to 1780 ± 5 Ma), and Colíder Group (from 1813 ± 12 to 1781 ± 18 Ma). The overlap of these ages indicates that the volcanism and the plutonism are coeval (Fig. 19).

Another observation is the presence of inherited or pre-magmatic zircons in the Volcanic Domain samples TD-095 and TD-107 were ^{207}Pb/^{206}Pb relative ages around 1950 Ma and 1870 Ma respectively are present in the results. These ages around 1950 Ma and 1870 are common within the rocks from Creporizão or Nhandú and Maloquinha or Matupá Intrusive Suites from the Ventuari-Tapajós Province and so are probably related to that basement inlier.

Miller et al. (2003) describe such inheritance-poor granitoids as “hot” (crystallization above 800 °C) rocks, which are generated by current well-known magmatic processes (dehydration-melting in the crust; fractionation of mantle melts, with or without crustal contamination), including the transport of crystal-poor and highly eruptible magma. On the other hand, “cold” inheritance-rich granitic intrusions (crystallization below 800 °C) are usually crust-derived, as well as crystal-rich and unlikely to erupt.

The younger upper intercept age of 1679 ± 20 obtained for the sample TD-107 (amphibolite) is an issue to be studied in this undeformed rock that does not show metamorphic overgrowths in the zircons crystals. Thus, this age may be only related to some sort of Pb loss during this time. However, it is valid to mention that to the west of the area, metamorphic ages around 1640 Ma (zircon overgrowth rims) were obtained in rocks of highly deformed granulite facies from Jamari Complex and thus they are related to the collisional orogeny Quatro Cachoeiras (Rizzotto et al. 2004; Santos et al. 2008). Also Pinho et al. (2003) and Lacerda Filho (2004) obtained within the Juruena Complex (Vitória Suite tonalite gneiss), very close to the study area, zircon Pb-Pb and U-Pb ages around 1660 Ma that were interpreted as related to the collisional orogeny mentioned above.

Another alternative is that these younger zircon apparent ages could represent the crystallization time, although ages around 1700 Ma (even K-Ar or Ar-Ar) are absent in the Ventuari-Tapajós and Rio Negro-Juruena Provinces.

Volcanic and plutonic rocks often occur in similar geodynamic settings. Examples include the Andes (De Silva et al. 2006), the San Juan volcanic field in Colorado (Lipman 2007) and the Colorado River region to the south of Nevada and Arizona (Metcalf 2004) were the volcano-plutonic association is directly observed in places where the volcanic cover has been eroded, thus exposing the upper parts of cogenetic intrusions (Bachmann et al. 2007).

A Paleoproterozoic example described in the Ventuari-Tapajós Province (Santos et al. 2004) includes the Iriri intermediate to acid volcanic sequence that is associated with late-orogenic to post-collisional granitic intrusions. Juliani et al. (2005) have identified high-sulfidation epithermal gold deposits in the same region related to large caldera complexes and epizonal porphyry intrusion domes, an analogous framework to that observed in the Volcanic Domain.

The interpretation of late-orogenic to post-collisional tectonic settings, proposed by Barros et al. (2009), Alves et al. (2013) and Silva et al. (2014), also supports the Volcanic Domain as high-K calc-alkaline magmatism. However, in order to consider this hypothesis, the oldest crystallization ages obtained for the Juruena Magmatic Arc must be discarded. Indeed, this implies that the Volcanic Domain is not related to the Juruena Complex and therefore, the Volcanic Domain should be classified as a Terrane.

The hypothesis of Volcanic Domain be a Terrane is impracticable due to field relationships, lithogeochemical similarities, Sm-Nd data, and U-Pb dataset, which point to the integration of the Volcanic Domain with the Juruena Complex. As shown in Fig. 20, the crystallization ages of the Juruena Complex, which is interpreted to be a calc-alkaline syn-orogenic continental arc magmatism (1787 ± 14 to 1755 Ma), are overlapping with those from the Volcanic Domain.

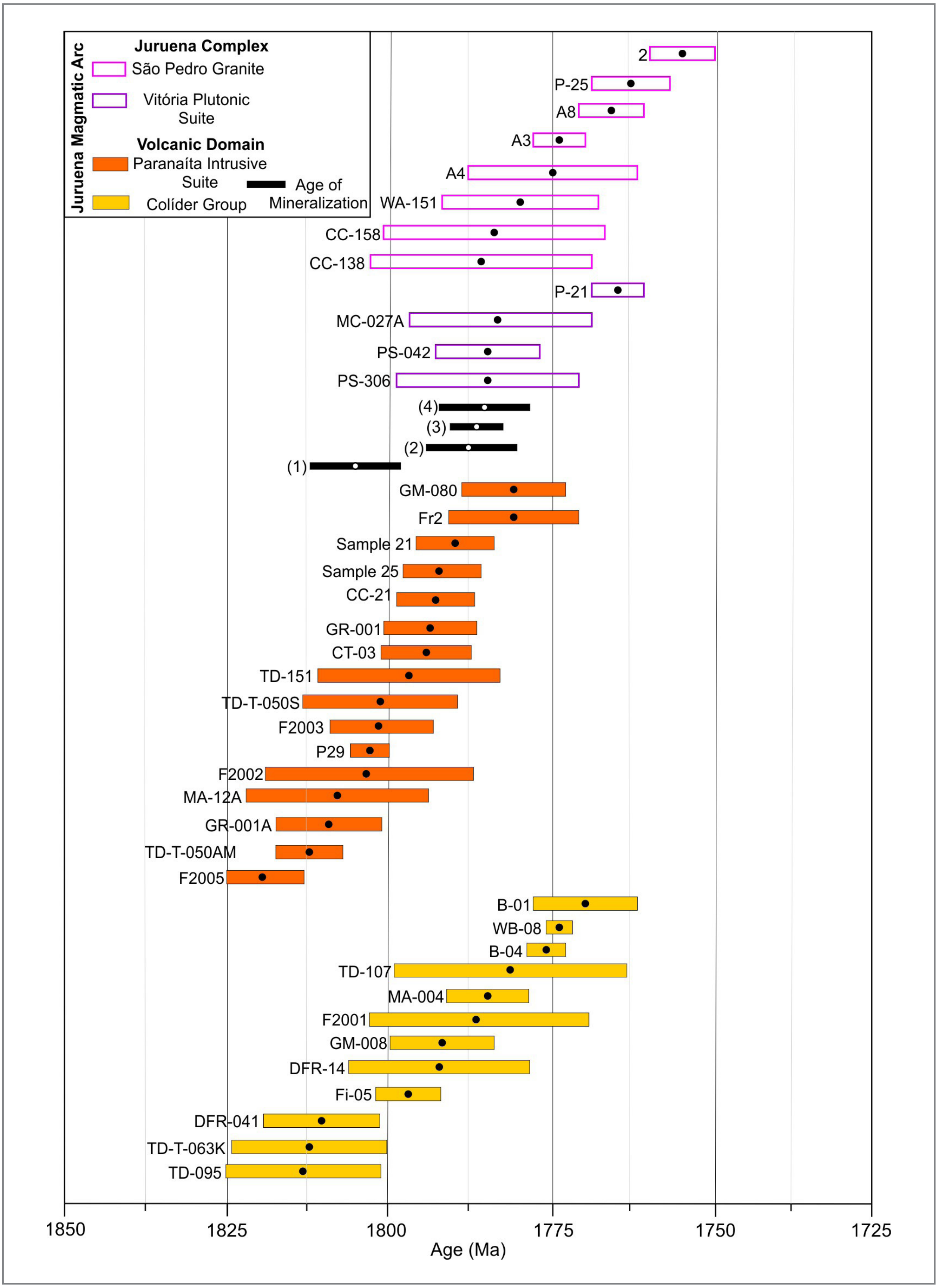

FIGURE 19 – Summary of the geochronological U-Pb (zircon) data from lithostratigraphic units of the Juruena Magmatic Arc that crop out in the study area (Volcanic Domain - Colíder Group and Paranaíta Intrusive Suite; Juruena Complex - Vitória Plutonic Suite and São Pedro Granite) and ages obtained from mineralized plutons. (1) Re-Os (molybdenite) Serrato et al. 2014; (2) Re-Os (molybdenite); (3) Re-Os (pyrite); (4) Re-Os (molybdenite) Xavier et al. (2013). Complete information about samples are present in Tables 1 and 2.

8.4. Mafic Magmatism in the southwestern Amazon Craton and geodynamic implications for the Columbia (or NUNA) Supercontinent

The mafic rocks cropping out in the study area are correlated to the Colíder Group magmatism. An amphibolite sample analyzed via U-Pb (zircon) and Sm-Nd yielded a crystallization age of 1781 ±18 Ma and a T_{DM} age of 2.2 Ga with $\varepsilon_{Nd(t=1.8)}$ value of + 0.4. Pinho et al. (2003) also obtained U-Pb (zircon) ages within that age interval for two mafic samples collected from around the survey area: 1797 ± 5 Ma (mafic tuff), and 1776 ± 3 Ma (basalt).

Santos et al. (2002) established five mafic magmatic events for the Ventuari-Tapajós Province by using a considerable dataset of U-Pb (baddeleyite and zircon) analyses from mafic rocks cropping out to the north of the area. The oldest stocks and dikes with ages around 1893 Ma are called Ingarana and they are related to orogeny. The other dikes, all related to distinct extensional anorogenic periods, show ages around 1780 Ma, 1180 Ma, and 500 Ma. These are called Crepori, Cachoeira Seca, and Piranhas, respectively, while a younger set of dikes, with ages in the interval between 260 Ma to 120 Ma, are named Periquito. Among all dikes analyzed, the Crepori has been of great importance to this study with ages correlating with the mafic magmatism of the Colíder Group. Santos et al. (2002) observed that ages around 1780 Ma are linked to mafic intrusions in the Amazon and La Plata Cratons. Examples include the Avanavero magmatism in northern Amazon Craton (1778 ± 12 Ma) (Reis et al. 2013), and Tumatumari in Guiana (1786 ± 5 Ma) (Norcross et al. 2000) and Piedra Alta Terranes (1785 ± 4 Ma) (Hall et al. 2001; Teixeira et al. 2010) in the La Plata Craton. Santos et al. (2002) stated that these intrusions define an N-S alignment that corresponds to the western border of the Columbia (NUNA) supercontinent and its breakup (Rogers 1996), taking into account that worldwide large volumes of mafic magmatism at the end of the Paleoproterozoic are related to this supercontinent disassembly.

Scandolara et al. (2014) studied the Vespor Suite, the mafic lithostratigraphic unit in the Juruena Complex, based on lithogeochemistry and geochronology. The samples, which yielded U-Pb ages of 1773 ± 15 Ma (gabbronorite) and 1764 ± 14 Ma (gabbro), belong to the tholeiitic magma series, and have chemical signature typical of continental arc settings; the magma derived from a source that is a mixture of metasomatic oceanic crust and crustal components. Based on these results, Scandolara et al. (2014) interpreted the SW border of the Amazon Craton (Juruena Magmatic Arc) to be developed along an oceanic trench with subduction of oceanic crust under a passive continental margin (Central Amazonian and Ventuari-Tapajós Provinces) at the beginning of the Paleoproterozoic.

Several continental arcs of 1.8-1.7 Ga are recognized worldwide (Rogers and Santosh 2002 and 2004; Zhang et al. 2012) and they are considered as products of continental arc amalgamations over the Paleoproterozoic (2.0 to 1.8 Ga) that culminated in the assembly of the Columbia supercontinent (or NUNA) (Hoffman 1989; Roger and Santosh 2002, 2004; Zhao et al. 2004). Scandolara et al. (2014) based on the proposed continental arc geodynamic setting for the Juruena Magmatic Arc, with ages between 1.8 and 1.74 Ga, suggested that the period of Columbia (NUNA) amalgamation must be revised and extended until around 1.74 Ga.

Bispo-Santos et al. (2012) have also proposed that the period of Columbia amalgamation should be extended for this sector and the taphrogenesis period revised with basis on paleomagnetic data and biotite Ar-Ar ages (1420 Ma) from a set of mafic dikes (Nova Guarita Intrusive Mafics) at the Peixoto de Azevedo Region, extreme east of the Volcanic Domain.

9. Conclusions

The Colíder Group and the Paranaíta Intrusive Suite form a plutonic-volcanic association whose eruptions from ~1815 to 1780 Ma gave rise to the Juruena Magmatic Arc Volcanic Domain.

The predominance of rocks with high-K calc-alkaline A-type (oxidized and reduced) chemical signatures suggests that the magmatism in the Volcanic Domain is from distal geodynamic settings in relation to a stable continental platform (Ventuari-Tapajós Province). As a result, it has been usually associated with the (1) Columbia supercontinent (NUNA) disassembly at 1.8 Ga, or (2) Juruena Magmatic Arc late- to post-orogenic stages. However, both models show contradictions:

(1) Assuming the Columbia Supercontinent (or NUNA) taphrogenesis, it would be expected to identify rocks with crystallization ages of the displaced block (Ventuari-Tapajós) to the west/southwest of the Volcanic Domain. In addition, recent works based on geochronology and paleomagnetism of the dike swarms shows that in the Amazon Craton the Columbia supercontinent (NUNA) disassembly was after 1.8 Ga.

(2) The crystallization ages obtained for the Volcanic Domain include the older ages of the Juruena Magmatic Arc and, therefore, part of these rocks cannot be related to the late-orogenic or post-collisional magmatism stage in relation to this arc.

Based on the data presented here, it is more adequate to consider the basalts, andesites and less differentiated oxidized A-type granitic rocks of the Volcanic Domain as part of the Juruena Magmatic Arc volcanic belt and to correlate the more differentiated and reduced A-type rocks to the back-arc Teles-Pires magmatism or forearc Roosevelt magmatism. This set of granitic rocks alone, with A-type signatures, is showing variations in the tectonic regime throughout the time interval of 1815 to 1780 Ma instead of a specific geodynamic setting.

The maintenance of a continental arc-related interpretation for part of the Volcanic Domain magmatism is based upon its spatial arrangement, the volume of acid volcaniclastic deposits and associated epizonal granite intrusions, T_{DM} age intervals and ε_{Nd} values similar to the rocks from the Juruena Magmatic Arc (Juruena Complex and Volcanic Domain), presence of oceanic crust remnants from the Bacaeri-Mógno Complex and by the syn-plutonic epithermal-porphyry gold systems along the Alta Floresta Gold Province. Also, the REE and trace-element chemical signatures of basic to acid rocks from the Volcanic Domain are also indicative of the continental arc related geodynamic setting, because they show the influence of an enriched SCLM source in subduction zone fluids and crustal contamination.

In addition, the older source with T_{DM} ages between 2.3 and 2.1 Ga and negative ε_{Nd} values (~ -1.5), and a younger, more juvenile source, with T_{DM} ages between 2.0 and 1.9 Ga and positive ε_{Nd} values (~ +1.0) are indicative of a mixed magmatic source with contribution of crustal materials (subducted sediments) and mantle, resulting in these distinct Sm-Nd isotopic signatures.

Acknowledgments

The authors acknowledge CPRM - Geological Survey of Brazil and the Technical- Scientific Chamber of this federal public institution for allowing us to use data from the Brazilian Programme for Strategic Evaluation of Mineral Potential, and the financial support for this project.

The Institute of Geosciences at the State University of Campinas (IG-UNICAMP), the postgraduate program at the institute where the study was conducted and the examination board composed of Dr. Evandro Luiz Klein and Dr. Maria José Maluf Mesquita.

We also thank and appreciated the careful review performed by Dr. Marcia Aparecida Sant'Ana Barros and the anonymous reviewer from the Journal of the Geological Survey of Brazil.

References

Alves C. L., Sabóia A. M., Scandolara J. E., Ribeiro P. S. E., Martins E. G. 2013. Magmatismo Tipo A-2 Colíder-Pium no SE do Cráton Amazônico, Província Rondônia-Juruena - MT: litoquímica e geocronologia. In: Wankler F. L., Holanda E. C., Vasquez M. L. (ed.). Contribuições à geologia da Amazônia, 8. Belém, SBG Núcleo Norte, 26-44.

Bachmann O., Charlier B. L. A., Lowenstern J. B. 2007. Zircon crystallization and recycling in the magma chamber of the rhyolitic Kos Plateau Tuff (Aegean arc). Geology, 35(1), 73-76. https://doi.org/10.1130/G23151A.1

Barbarin B. 1999. A review of the relationships between granitoid types, their origins and their geodynamic environments. Lithos, 46(3), 605-626. https://doi.org/10.1016/S0024-4937(98)00085-1

Barros M. A. D. S. A., Júnior F. C., Nardi L. V. S., Lima E. F. 2009. Paleoproterozoic bimodal post-collisional magmatism in the southwestern Amazonian Craton, Mato Grosso, Brazil: geochemistry and isotopic evidence. Journal of South American Earth Sciences, 27(1), 11-23. https://doi.org/10.1016/j.jsames.2008.11.003

Bettencourt J. S., Leite W. B., Ruiz A. S., Matos R., Payolla B. L., Tosdal R. M. 2010. The Rondonian-San Ignacio Province in the SW Amazonian Craton: an overview. Journal of South American Earth Sciences, 29(1), 28-46. https://doi.org/10.1016/j.jsames.2009.08.006

Biondi J. C., Santos R. V., Cury L. F. 2013. The Paleoproterozoic Aripuanã Zn-Pb-Ag (Au, Cu) Volcanogenic Massive Sulfide Deposit, Mato Grosso, Brazil: geology, geochemistry of alteration, carbon and oxygen isotope modeling, and implications for genesis. Economic Geology, 108(4), 781-811. http://dx.doi.org/10.2113/econgeo.108.4.781

Bispo-Santos F., D'Agrella-Filho M. S., Trindade R. I., Elming S. Å., Janikian L., Vasconcelos P. M., Barros M. A. 2012. Tectonic implications of the 1419Ma Nova Guarita mafic intrusives paleomagnetic pole (Amazonian Craton) on the longevity of Nuna. Precambrian Research, 196-197, 1-22. https://doi.org/10.1016/j.precamres.2011.10.022

Bizzi L. A., Schobbenhaus C., Vidotti R. M., Gonçalves, J. H. 2003. Geologia, tectônica e recursos minerais do brasil: texto, mapas e SIG. Brasília, CPRM, 642p. Avaiable on line at http://rigeo.cprm.gov.br/jspui/handle/doc/1212 / (accessed on 08 March 2019).

Bonin, B. 1990. From orogenic to anorogenic settings: evolution of granitoid suites after a major orogenesis. Geological Journal, 25(3-4), 261-270. https://doi.org/10.1002/gj.3350250309

Bühn B., Pimentel M.M., Martini M., Dantas E.L. 2009. High spatial resolution analysis of Pb and U isotopes for geochronology by laser ablation multi-collector inductively coupled plasma mass spectrometry (LA-MC-ICP-MS). Anais da Academia Brasileira de Ciências, 81(1), 1-16. http://dx.doi.org/10.1590/S0001-37652009000100011

Cordani U. G., Tassinari C. C. G., Teixeira W., Basei M. A. S., Kawashita K. 1979. Evolução tectônica da Amazônia com base nos dados geocronológicos. In: Congreso Geológico Chileno, 2, J137-J148.

Cordani U. G., Neves B. B. 1982. The geologic evolution of South America during the Archean and Early Proterozoic. Revista Brasileira de Geociências, 12(1-3), 78-88.

Cordani U. G., Teixeira W. 2007. Proterozoic accretionary belts in the Amazonian Craton. In: Hatcher, Jr R. D., Carlson M. P., McBride J. H., Catalán, J. R. M. 4-D Framework of Continental Crust, 297-320. https://doi.org/10.1130/2007.1200(14)

Cordani U. G., Teixeira W., D'Agrella-Filho M. S., Trindade R. I. 2009. The position of the Amazonian Craton in supercontinents. Gondwana Research, 15(3-4), 396-407. https://doi.org/10.1016/j.gr.2008.12.005

Corfu F., Hanchar J. M., Hoskin P. W., Kinny P. 2003. Atlas of zircon textures. Reviews in mineralogy and geochemistry, 53(1), 469-500. https://doi.org/10.2113/0530469

De La Roche H., Leterrier J. T., Grandclaude P., Marchal M. 1980. A classification of volcanic and plutonic rocks using R1R2-diagram and major-element analyses—its relationships with current nomenclature. Chemical Geology, 29(1-4), 183-210. https://doi.org/10.1016/0009-2541(80)90020-0

De Silva S., Zandt G., Trumbull R., Viramonte J. G., Salas G., Jiménez N. 2006. Large ignimbrite eruptions and volcano-tectonic depressions in the Central Andes: a thermomechanical perspective. London, Geological Society, Special Publications, 269(1), 47-63. https://doi.org/10.1144/GSL.SP.2006.269.01.04

DePaolo D.J. 1981. A neodymium and strontium isotopic study of Mesozoic calc-alkaline granitic batholiths of Sierra Nevada and Peninsular Ranges, California. Journal of Geophysical Research, 86, 10470-10488. https://doi.org/10.1029/JB086iB11p10470

Dall'Agnol, R, Oliveira, D. C. 2007. Oxidized, magnetite-series, rapakivi-type granites of Carajás, Brazil: implications for classification and petrogenesis of A-type granites. Lithos, 3(3-4), 215-233. https://doi.org/10.1016/j.lithos.2006.03.065

Duarte T.B., Rodrigues J.B., Ribeiro P.S.E., Scandolara J.E. 2012. Tectonic evolution of the Juruena magmatic arc between the Aripuanã and Juruena rivers: northwest Mato Grosso State, Brazil. Revista Brasileira de Geociências, 42(4), 824-840. DOI: 10.25249/0375-7536.2012424824840

Gióia S.M.C.L., Pimentel M.M. 2000. The Sm-Nd isotopic method in the geochronology laboratory of the University of Brasília. Anais da Academia Brasileira de Ciências, 72(2), 219-245. http://dx.doi.org/10.1590/S0001-37652000000200009

Hall H. C., Campal N., Davis D. W., Bossi J. 2001. Magnetic studies and U–Pb geochronology of the Uruguayan dyke swarm, Rio de la Plata craton, Uruguay: paleomagnetic and economic implications. Journal of South American Earth Sciences, 14(4), 349-361. https://doi.org/10.1016/S0895-9811(01)00031-1

Hoffman P. F. 1989. Speculations on Laurentia's first gigayear (2.0 to 1.0 Ga). Geology, 17(2), 135-138. https://doi.org/10.1130/0091-7613(1989)017<0135:SOLSFG>2.3.CO;2

Hoffman P. F. 1997. Tectonic genealogy of North America. In: Van Der Pluijm B. A., Marshak Stephen. Earth structure: an introduction to structural geology and tectonics. New York, McGraw-Hill, 459-464.

Janousek V., Farrow C. M., Eerban V. 2006. Interpretation of whole-rock geochemical data in igneous geochemistry: introducing Geochemical Data Toolkit (GCDkit). Journal of Petrology, 47(6), 1255-1259. https://doi.org/10.1093/petrology/egl013

Japan International Cooperation Agency JICA. 2000. Report on the mineral exploration in the Alta Floresta area, Federative Republic of Brazil: final report. Metal Mining Agency of Japan – MMAJ, Tokyo, 137 p.

Japan International Cooperation Agency JICA. 2001. Report on the mineral exploration in the Alta Floresta area, Federative Republic of Brazil: phase III. Metal Mining Agency of Japan – MMAJ, Tokyo, 307p.

Juliani C., Rye R. O., Nunes C. M., Snee L. W., Silva R. H. C., Monteiro L. V., Neto A. A. 2005. Paleoproterozoic high-sulfidation mineralization in the Tapajós gold province, Amazonian Craton, Brazil: geology, mineralogy, alunite argon age, and stable-isotope constraints. Chemical Geology, 215(1), 95-125. https://doi.org/10.1016/j.chemgeo.2004.06.035

Lacerda Filho J. D., Abreu Filho W., Valente C. R., Oliveira C. D., Albuquerque M. C. D. 2004. Geologia e recursos minerais do estado de Mato Grosso. Cuiabá, CPRM. Programa Integração, Atualização e Difusão de Dados de Geologia do Brasil. Convênio CPRM/SICME-MT, MME.

Leal R. E., Lafon J. M., Rosa-Costa L. T., Dantas E. L. 2018. Orosirian magmatic episodes in the erepecuru-trombetas domain (southeastern Guyana shield): implications for the crustal evolution of the Amazonian craton. Journal of South American Earth Sciences, 85, 278-297. https://doi.org/10.1016/j.jsames.2018.04.011

Lipman P. W. 2007. Incremental assembly and prolonged consolidation of Cordilleran magma chambers: evidence from the Southern Rocky Mountain volcanic field. Geosphere, 3(1), 42-70. https://doi.org/10.1130/GES00061.1

Ludwig K.R. 2009. Isoplot 3.00 - a geochronological toolkit for Microsoft Excel. Berkeley Geochronology Center, Special Publication, 4.

Maniar P. D., Piccoli P. M. 1989. Tectonic discrimination of granitoids. GSA Bulletin, 101(5), 635-643. https://doi.org/10.1130/0016-7606(1989)101<0635:TDOG>2.3.CO;2

Metcalf R. V. 2004. Volcanic-plutonic links, plutons as magma chambers and crust-mantle interaction: a lithospheric scale view of magma systems. Geological Society of America Special Papers, 389, 357-374. https://doi.org/10.1017/S0263593300001127

Miller C. F., McDowell S. M., Mapes R. W. 2003. Hot and cold granites? Implications of zircon saturation temperatures and preservation of inheritance. Geology, 31(6), 529-532. https://doi.org/10.1130/0091-7613(2003)031<0529:HACGIO>2.0.CO;2

Neder R. D., Leite J. A. D., Figueiredo B. R., McNaughton N. J. 2002. 1.76 Ga volcano-plutonism in the southwestern Amazonian craton, Aripuanã-MT, Brazil: tectono-stratigraphic implications from SHRIMP U–Pb zircon data and rock geochemistry. Precambrian Research, 119(1-4), 171-187. https://doi.org/10.1016/S0301-9268(02)00122-5

Norcross C., Davis D. W., Spooner E. T., Rust A. 2000. U-Pb and Pb-Pb age constraints on Paleoproterozoic magmatism, deformation and gold mineralization in the Omai area, Guyana Shield. Precambrian Research, 102(1-2), 69-86. https://doi.org/10.1016/S0301-9268(99)00102-3

Pearce J. A. 1982. Trace element characteristics of lavas from destructive plate boundaries. In: Thorpe R.S. (ed.). Orogenic andesites and related rocks. Chichester, England, John Wiley and Sons, 528-548.

Pearce J. A., Harris N. B., Tindle A. G. 1984. Trace element discrimination diagrams for the tectonic interpretation of granitic rocks. Journal of Petrology, 25(4), 956-983. https://doi.org/10.1093/petrology/25.4.956

Peccerillo A., Taylor S. R. 1976. Geochemistry of eocene calc-alkaline volcanic rocks from the Kastamonu area, northern Turkey. Contributions to Mineralogy and Petrology, 58(1), 63-81. https://doi.org/10.1007/BF00384745

Pinho M. A., Chemale Jr F., Van Schmus W. R., Pinho F. E. 2003. U–Pb and Sm–Nd evidence for 1.76–1.77 Ga magmatism in the Moriru region, Mato Grosso, Brazil: implications for province boundaries in the SW Amazon Craton. Precambrian Research, 126(1-2), 1-25. https://doi.org/10.1016/S0301-9268(03)00126-8

Prado S. E., Barros M. A. S., Pinho F. E. C., Pierosan R. 2013. Granito Terra Nova - petrologia e geocronologia: um granito tipo-A da Província Aurífera Alta Floresta - Cráton Amazônico. Brazilian Journal of Geology, 43 (1),101-116. http://dx.doi.org/10.5327/Z2317-48892013000100009

Reis N. J., Teixeira W., Hamilton M. A., Bispo-Santos F., Almeida M. E., D'Agrella-Filho M. S. 2013. Avanavero mafic magmatism, a late Paleoproterozoic LIP in the Guiana Shield, Amazonian Craton: U–Pb ID-TIMS baddeleyite, geochemical and paleomagnetic evidence. Lithos, 174, 175-195. https://doi.org/10.1016/j.lithos.2012.10.014

Ribeiro P.S.E., Duarte T.B. 2010. Geologia e recursos minerais das folhas Rio Guariba e Rio Aripuanã. Projeto Noroeste-Nordeste de Mato Grosso. Programa Geologia do Brasil. Goiânia, CPRM, 248 p.

Rizzotto G. J., Quadros M. L. E. S., Silva L. C., Armstrong R., Almeida M. 2002. O granito Aripuanã: datação U-Pb (SHRIMP) e implicações metalogenéticas. In: Congresso Brasileiro de Geologia, 41, 469p.

Rizzotto G.J., Quadros M.L.E.S., Bahia R.B.C, Ferreira R.B.C, Lopes R.C, Cordeiro A.V. 2004. Folha SC.21- Juruena. In: Schobbenhaus C., Gonçalves J.H., Santos J.O.S., Abram M.B., Leão Neto R., Matos G.M.M., Vidotti R.M., Ramos M.A.B., Jesus J.D.A (ed.). Carta geológica do Brasil ao milionésimo. Sistema de informações Geográficas-SIG. Programa Geologia do Brasil. Brasília, CPRM. 1 CD-ROM.

Rogers J. J. W. 1996. A history of continents in the past three billion years.The Journal of Geology, 104(1), 91-107. http://dx.doi.org/10.1086/629803

Rogers J. J. W., Santosh M. 2002. Configuration of Columbia, a Mesoproterozoic supercontinent. Gondwana Research, 5(1), 5-22. https://doi.org/10.1016/S1342-937X(05)70883-2

Rogers J. J.W., Santosh M. 2004. Continents and supercontinents. Gondwana Research, 7(2), 653. https://doi.org/10.1016/S1342-937X(05)70827-3

Rudnick R. L., Williams I. S. 1987. Dating the lower crust by ion microprobe. Earth and Planetary Science Letters, 85(1-3), 145-161. https://doi.org/10.1016/0012-821X(87)90028-8

Santos J. O. S., Hartmann L. A., Gaudette H. E., Groves D. I., Mcnaughton N. J., Fletcher I. R. 2000. A new understanding of the provinces of the Amazon Craton based on integration of field mapping and U-Pb and Sm-Nd geochronology. Gondwana Research, 3(4), 453-488. https://doi.org/10.1016/S1342-937X(05)70755-3

Santos J. O. S., Groves D. I., Hartmann L. A., Moura M. A., McNaughton N. J. 2001. Gold deposits of the Tapajós and Alta Floresta Domains, Tapajós–Parima orogenic belt, Amazon Craton, Brazil. Mineralium Deposita, 36(3-4), 278-299. https://doi.org/10.1007/s001260100172

Santos J. O. S., Hartmann L. A., McNaughton N. J., Fletcher I. R. 2002. Timing of mafic magmatism in the Tapajós Province (Brazil) and implications for the evolution of the Amazon craton: evidence from baddeleyite and zircon U–Pb SHRIMP geochronology. Journal of South American Earth Sciences, 15(4), 409-429. https://doi.org/10.1016/S0895-9811(02)00061-5

Santos J. O. S., Van Breemen O. B., Groves D. I., Hartmann L. A., Almeida M. E., McNaughton N. J., Fletcher I. R. 2004. Timing and evolution of multiple Paleoproterozoic magmatic arcs in the Tapajós Domain, Amazon Craton: constraints from SHRIMP and TIMS zircon, baddeleyite and titanite U–Pb geochronology. Precambrian Research, 131(1), 73-109. https://doi.org/10.1016/j.precamres.2004.01.002

Santos J. O. S., Rizzotto G. J., Potter P. E., McNaughton N. J., Matos R. S., Hartmann L. A., Quadros M. E. S. 2008. Age and autochthonous evolution of the Sunsás Orogen in West Amazon Craton based on mapping and U–Pb geochronology. Precambrian Research, 165(3), 120-152. https://doi.org/10.1016/j.precamres.2008.06.009

Santos F.S., Pierosan R., Barros M.A.D.S.A., Geraldes M.C., de Lima M.F. 2019. Petrology of the Colíder Group volcanic successions in the northernmost Mato Grosso, Brazil: a contribution to the knowledge of the felsic volcanism of the Alta Floresta Gold Province. Journal of South American Earth Sciences, 89, 10-29. https://doi.org/10.1016/j.jsames.2018.10.007

Sato K., Tassinari C.C.G. 1997. Principais eventos de acreção continental no Cráton Amazônico baseados em idade-modelo Sm-Nd, calculada em evoluções de estágio único e estágio duplo. In: Costa M.L., Angélica R.S. (ed). Contribuições à Geologia da Amazônia. Belém, SBG Núcleo Norte, 91-142.

Scandolara J. E., Ribeiro P. S., Frasca A. A., Fuck R. A., Rodrigues J. B. 2014. Geochemistry and geochronology of mafic rocks from the Vespor suite in the Juruena arc, Roosevelt-Juruena terrain, Brazil: Implications for Proterozoic crustal growth and geodynamic setting of the SW Amazonian craton. Journal of South American Earth Sciences, 53, 20-49. https://doi.org/10.1016/j.jsames.2014.04.001

Serrato A.A.S. 2014. Geocronologia do sistema hidrotermal do depósito aurífero de Juruena, Província Aurífera de Alta Floresta (MT), Brasil. MSc Dissertation, Instituto de Geociências, Universidade Estadual de Campinas, 81p.

Silva G. H., Leal J. W. L., Montalvao R. D., Bezerra P. E. L., Pimenta O. D. S., Tassinari C. C. G., Fernandes C. A. C. 1980. Folha SC. 21 Juruena; geologia, geomorfologia, pedologia, vegetação e uso potencial da terra. Rio de Janeiro, DNPM.

Silva M.G., Abram M.B. 2008. Projeto metalogenia da província Aurífera Juruena-Teles Pires, Mato Grosso. Informe de Recursos Minerais, Série Ouro, 16. Goiânia, CPRM. 212p.

Silva F. R., Barros M.A.S.A., Pierosan R., Pinho F. E. C., Rocha M. L. B. P., Vasconcelos B. R., Rocha J. 2014. Geoquímica e geocronologia U-Pb (SHRIMP) de granitos de região de Peixoto de Azevedo - Província Aurífera de Alta Floresta, Mato Grosso. Brazilian Journal of Geology, 44(3). http://dx.doi.org/10.5327/Z2317-4889201400030007

Silva F. R., Barros M. A. S., Moura M. A., Pierosan R., Santos J. O. S., Oliveira D. R. P. 2015. Petrografia, química mineral e geocronologia U-Pb dos granitos da região de Guarantã do Norte, MT: evidências de mistura de magmas. In: Simpósio de Geologia do Centro Oeste, 14.

Souza J. O., Frasca A. A. S., Oliveira C. C. 2005. Geologia e recursos minerais da folha Alta Floresta (relatório integrado): folhas SC.21-X-C, SC.21-V-D, SC.21-Z-A e SC.21-Z-B: estados de Mato Grosso e do Pará. CPRM, Brasília. Programa Levantamentos Geológicos Básicos do Brasil - PLGB; Projeto Província Mineral de Alta Floresta (PROMIN-Alta Floresta).

Sun S.S., McDonough W. 1989. Chemical and isotopic systematics of oceanic basalts: implications for mantle composition and processes. London, Geological Society, Special Publications, 42(1), 313-345. https://doi.org/10.1144/GSL.SP.1989.042.01.19

Tassinari C.C.G., Siga Jr. O., Teixeira W. 1984. Épocas metalogenéticas relacionadas à granitogênese do Cráton Amazônico. In: Congresso Brasileiro de Geologia, 32, 2963-2977.

Tassinari C. C. G. 1996. O mapa geocronológico do Cráton Amazônico no Brasil: revisão dos dados isotópicos. PhD Thesis, Instituto de

Geociências, Universidade de São Paulo, São Paulo, 139p. DOI: 10.11606/T.44.2013.tde-22082013-163642

Tassinari C.C., Macambira M. J. 1999. Geochronological provinces of the Amazonian Craton. Episodes: Journal of International Geoscience, 22(3), 174-182.

Tassinari C.C.G., Macambira M. J. B. 2004. A evolução tectônica do Cráton Amazônico. In: Mantesso-Neto V., Bartorelli A., Carneiro C. D. R., Brito-Neves B. B. Geologia do continente sul-americano: evolução da obra de Fernando Flávio Marques de Almeida. São Paulo, Editora Beca, 471-485.

Teixeira W., Tassinari C. C. G., Cordani U. G., Kawashita K. 1989. A review of the geochronology of the Amazonian Craton: tectonic implications. Precambrian Research, 42(3-4), 213-227. https://doi.org/10.1016/0301-9268(89)90012-0

Teixeira W., Geraldes M. C., Matos R., Ruiz A. S., Saes G., Vargas-Mattos G. 2010. A review of the tectonic evolution of the Sunsás belt, SW Amazonian Craton. Journal of South American Earth Sciences, 29(1), 47-60. https://doi.org/10.1016/j.jsames.2009.09.007

Vasquez M. L.; Rosa-Costa L. T. 2008. Mapa geológico e de recursos minerais do Estado do Pará. Projeto Geologia e Recursos Minerais do Pará – Sistema de Informações Geográficas: texto-explicativo. Belém, CPRM. Mapa, Escala 1:1.000.000. 1 CD-ROM.

Wayne D. M., Sinha A. K. 1988. Physical and chemical response of zircons to deformation. Contributions to Mineralogy and Petrology, 98(1), 109-121. https://doi.org/10.1007/BF00371915

Whalen J. B., Currie K. L., Chappell B. W. 1987. A-type granites: geochemical characteristics, discrimination and petrogenesis. Contributions to Mineralogy and Petrology, 95(4), 407-419. https://doi.org/10.1007/BF00402202

Wilson B. M. 1989. Igneous petrogenesis a global tectonic approach. . Netherlands, Springer Science and Business Media. https://doi.org/10.1007/978-1-4020-6788-4

Xavier R. P., Assis R. R. A., Creaser R., Barros A. J. 2013. Timing of gold metallogeny in the Alta Floresta Gold Province: evidence from pyrite and molybdenite, re-os isotopic dating. In: Simpósio de Geologia da Amazônia, 13.

Zhang S., Li Z. X., Evans D. A., Wu H., Li H., Dong J. 2012. Pre-Rodinia supercontinent Nuna shaping up: a global synthesis with new paleomagnetic results from North China. Earth and Planetary Science Letters, 353-354, 145-155. https://doi.org/10.1016/j.epsl.2012.07.034

Zhao G., Sun M., Wilde S. A., Li S. 2004. A Paleo-Mesoproterozoic supercontinent: assembly, growth and breakup. Earth-Science Reviews, 67(1), 91-123. https://doi.org/10.1016/j.earscirev.2004.02.003

APPENDIX A1 – Major and trace element contents of acid effusive rocks from the Colíder Group. (cont.)

Sample		TD-R-178	MC-155A	MC-162	TD-R-008	TD-R-235	MC-153	MC-156A
Chemical Class.		**Rhyolite**	**Dacite**	**Rhyolite**	**Rhyodacite**	**Rhyodacite**	**Rhyodacite**	**Rhyolite**
Latitude		**-91.253**	**-93.010**	**-90.276**	**-92.133**	**-92.078**	**-93.861**	**-92.674**
Longitude		**-58,7285**	**-586.123**	**-586.026**	**-586.650**	**-592.097**	**-585.373**	**-586.256**
	D.L.							
SiO_2	0.100	69.900	67.310	67.870	64.240	68.000	68.570	74.620
Al_2O_3	0.100	14.100	16.590	15.640	15.090	15.900	16.060	14.180
Fe_2O_3	0.010	3.890	3.970	4.700	4.230	3.860	4.450	2.120
MgO	0.100	0.460	0.910	1.060	1.410	1.190	1.080	0.440
CaO	0.010	1.760	3.510	1.920	3.570	3.500	3.270	0.670
Na_2O	0.100	3.940	4.420	4.230	3.050	3.390	3.750	3.870
K_2O	0.010	4.570	3.380	4.450	3.230	4.040	4.340	4.700
MnO	0.010	0.120	0.110	0.130	0.090	0.070	0.100	0.080
TiO_2	0.010	0.480	0.540	0.690	0.490	0.410	0.550	0.330
P_2O_5	0.010	0.116	0.360	0.400	0.200	0.109	0.380	0.200
SUM		99.340	101.100	101.090	95.600	100.470	102.550	101.210
FeO	0.140	3.500	1.790	2.480	1.680	2.190	1.770	0.710
FeOt		7.000	5.360	6.710	5.490	5.660	5.770	2.620
K_2O/Na_2O		1.160	0.760	1.050	1.060	1.190	1.160	1.210
Na_2O+K_2O		8.510	7.800	8.680	6.280	7.430	8.090	8.570
A/NK		1.230	1.520	1.330	1.770	1.600	1.480	1.240
A/CNK		0.960	0.960	1.020	1.010	0.970	0.960	1.120
Ba	5.000	1.783.000	1.188.000	1.160.000	1.252.000	942.000	1.232.000	1.432.000
Be	0.100	2.900	2.000	2.200	2.400	1.900	2.900	2.400
Cs	0.050	2.790	2.490	3.500	1.230	4.570	5.110	2.230
Ga	0.100	17.100	18.500	18.800	16.900	16.400	17.900	17.200
Hf	0.050	13.940	6.970	5.770	5.290	5.000	5.920	6.860
Nb	0.050	14.710	13.440	11.530	10.970	10.850	11.670	15.080
Rb	0.200	124.300	102.000	145.000	124.000	140.500	154.000	150.000
Sn	0.300	1.600	4.600	2.800	1.100	0.900	3.800	2.400
Sr	0.500	262.300	449.000	249.000	566.900	455.100	404.000	181.000
Ta	0.050	0.780	1.000	0.830	0.980	0.640	<D.L.	0.940
Th	0.100	12.600	12.400	9.700	11.200	13.900	11.500	12.400
U	0.050	3.430	3.320	2.590	3.070	3.730	3.180	2.470
W	0.100	2.800	<D.L.	<D.L.	1.500	2.100	<D.L.	<D.L.
Zr	0.500	715.500	247.000	193.000	174.400	188.600	225.000	227.000
Ag	0.010	<D.L.	0.030	0.020	0.020	<D.L.	0.080	0.050
Au	0.100	<D.L.	<D.L.	<D.L.	<D.L.	<D.L.	<D.L.	<D.L.
As	1.000	2.000	1.000	2.000	1.000	1.000	2.000	<D.L.
Bi	0.020	0.070	0.080	0.050	<D.L.	0.510	0.050	0.030
Cd	0.010	0.290	0.070	0.070	0.090	0.030	0.040	0.020
Co	0.100	2.500	6.900	5.300	5.600	6.600	7.400	4.700
Cu	0.500	8.600	6.800	5.500	4.700	28.400	14.600	3.500
Hg	0.010	<D.L.	<D.L.	<D.L.	<D.L.	<D.L.	<D.L.	<D.L.
Mo	0.050	2.490	1.030	0.600	0.390	1.510	0.730	0.200
Ni	0.500	2.500	5.600	3.300	2.100	5.200	6.000	5.800
Pb	0.200	19.500	4.800	5.100	2.300	16.500	6.600	5.900
Sb	0.050	0.380	0.120	0.150	0.070	0.450	0.320	0.170
Se	1.000	1.000	<D.L.	<D.L.	<D.L.	<D.L.	<D.L.	<D.L.
Zn	1.000	126.000	48.000	88.000	21.000	40.000	48.000	50.000
Ce	0.100	148.800	115.500	93.700	73.100	87.600	89.800	94.100
Dy	0.050	9.940	7.270	6.500	3.920	4.040	5.570	5.590
Er	0.050	6.100	3.870	3.380	2.030	2.320	2.590	2.610
Eu	0.050	2.860	1.620	1.520	1.450	1.290	0.310	1.040
Gd	0.050	11.160	7.550	6.850	6.510	4.880	5.970	5.790
Ho	0.050	2.120	1.480	1.260	0.730	0.790	0.600	0.950
La	0.100	85.100	53.000	49.300	38.200	40.800	46.700	45.300
Lu	0.050	0.850	0.690	0.600	0.270	0.390	<D.L.	0.420
Nd	0.100	70.500	48.000	46.100	37.000	35.900	41.300	39.200
Pr	0.050	15.400	13.310	12.220	8.420	9.970	10.160	11.060
Sm	0.100	11.500	9.500	8.300	6.800	6.300	7.100	7.400
Tb	0.050	1.660	1.150	1.030	0.710	0.730	0.370	0.840
Tm	0.050	0.900	0.650	0.560	0.200	0.370	0.140	0.440
Yb	0.100	5.800	3.900	3.500	2.200	2.400	2.700	2.700
Eu/Eu*		0.770	0.580	0.620	0.670	0.710	0.150	0.490
LaN/YbN		9.890	9.160	9.500	11.710	11.460	11.660	11.310
Sum_REE		372.690	267.490	234.820	181.540	197.780	213.340	217.440

DL: Detection Limit
Major elements in wt. %; Trace elements in ppm

APPENDIX A2 – Major and trace element contents of volcaniclastic rocks from the Colíder Group. (cont.)

Sample		FD-R-001	FD-R-029	TD-R-115	TD-R-123	TD-R-128	TD-R-195	TD-R-198	TD-R-208
Chemical Class.		A Rhyolite	A Rhyolite	A Rhyolite	A Rhyolite	Rhyolite	A Rhyolite	Rhyolite	Rhyodacite
Latitude		-9.084	-9.108	-9.118	-9.1028	-9.0893	-9.0878	-9.1059	-9.2815
Longitude		-58.926	-58.819	-59.1017	-58.9273	-58.9189	-58.7148	-58.6829	-58.7526
	D.L.								
SiO_2	0.100	73.000	76.200	75.700	75.000	69.800	77.400	72.400	68.100
Al_2O_3	0.100	13.100	12.700	12.200	12.200	14.500	11.600	13.600	15.800
Fe_2O_3	0.010	2.020	2.010	1.730	2.060	2.720	1.680	3.320	4.030
MgO	0.100	0.180	0.220	<D.L.	0.180	0.520	0.280	0.230	1.180
CaO	0.010	0.500	0.230	0.720	0.240	1.390	0.300	1.200	3.350
Na_2O	0.100	3.260	3.490	3.590	3.310	3.550	3.000	3.540	3.530
K_2O	0.010	5.270	4.300	4.680	5.540	4.620	4.720	5.210	3.970
MnO	0.010	0.060	0.060	0.050	0.060	0.080	0.090	0.110	0.070
TiO_2	0.010	0.330	0.230	0.200	0.220	0.310	0.140	0.330	0.410
P_2O_5	0.010	0.047	0.023	0.034	0.024	0.102	<D.L.	0.063	0.113
SUM		97.770	99.460	98.900	98.830	97.590	99.210	100.000	100.550
FeO	0.140	0.900	1.130	1.320	1.720	1.920	1.510	2.990	2.450
FeOt		2.720	2.940	2.880	3.570	4.370	3.020	5.970	6.080
K_2O/Na_2O		1.620	1.230	1.300	1.670	1.300	1.570	1.470	1.120
Na_2O+K_2O		8.530	7.790	8.270	8.850	8.170	7.720	8.750	7.500
A/NK		1.180	1.220	1.110	1.070	1.340	1.150	1.190	1.560
A/CNK		1.090	1.170	0.990	1.030	1.080	1.100	1.000	0.980
#mg		9.900	11.100	2.840	7.820	16.650	13.520	6.100	24.510
Ba	5.000	1438.000	354.000	302.000	400.000	743.000	178.000	1904.000	887.000
Be	0.100	4.400	2.700	3.400	2.100	2.900	2.200	2.800	1.800
Cs	0.050	2.680	1.820	1.180	0.810	3.130	1.360	2.350	4.350
Ga	0.100	16.500	16.900	14.800	15.000	15.700	13.800	15.200	15.700
Hf	0.050	9.370	7.290	6.820	6.220	5.430	4.740	10.660	5.650
Nb	0.050	16.240	15.340	16.360	18.190	10.850	14.010	15.950	12.050
Rb	0.200	180.200	105.500	145.300	150.600	160.100	131.700	121.300	137.100
Sn	0.300	1.100	1.900	1.200	36.300	<D.L.	1.500	2.200	1.600
Sr	0.500	142.400	120.000	75.500	70.500	160.000	32.600	223.500	428.800
Ta	0.050	1.230	1.000	1.270	1.830	0.950	0.740	0.960	1.090
Th	0.100	15.200	11.000	16.600	14.600	11.900	12.500	14.600	16.000
U	0.050	3.830	2.600	5.450	3.720	4.060	4.190	3.580	3.380
W	0.100	4.400	2.600	1.800	3.300	1.600	1.300	3.900	3.400
Zr	0.500	301.200	289.400	182.600	180.900	173.600	170.500	445.900	175.200
Ag	0.010	<D.L.	<D.L.	<D.L.	<D.L.	<D.L.	<D.L.	<D.L.	<D.L.
Au	0.100	<D.L.	<D.L.	<D.L.	<D.L.	<D.L.	<D.L.	<D.L.	<D.L.
As	1.000	5.000	2.000	1.000	<D.L.	<D.L.	<D.L.	<D.L.	<D.L.
Bi	0.020	0.030	0.050	0.130	0.100	0.020	0.070	0.100	0.100
Cd	0.010	1.670	0.100	0.050	0.100	0.030	0.070	0.080	0.030
Co	0.100	0.400	0.700	0.700	1.900	2.500	0.400	1.200	5.800
Cu	0.500	3.300	2.700	2.400	10.500	2.000	3.500	5.900	13.900
Hg	0.010	<D.L.	0.020	0.010	<D.L.	<D.L.	<D.L.	<D.L.	<D.L.
Mo	0.050	0.280	0.680	0.630	1.720	0.310	2.360	8.710	0.710
Ni	0.500	1.500	3.300	3.100	6.700	2.000	2.100	2.900	4.700
Pb	0.200	29.500	7.400	7.500	86.000	5.400	21.400	11.500	2.700
Sb	0.050	0.670	0.760	0.140	0.140	0.110	0.130	0.560	<D.L.
Se	1.000	<D.L.	<D.L.	<D.L.	<D.L.	<D.L.	<D.L.	<D.L.	<D.L.
Zn	1.000	16.000	9.000	14.000	44.000	30.000	28.000	60.000	40.000
Ce	0.100	133.100	90.300	105.200	100.600	85.100	77.900	149.000	80.400
Dy	0.050	10.210	5.210	5.900	7.210	4.610	6.500	8.010	3.590
Er	0.050	6.090	3.540	3.960	5.840	2.990	4.350	5.030	2.070
Eu	0.050	2.710	0.540	0.490	0.640	0.970	0.480	2.150	1.240
Gd	0.050	11.970	4.860	5.880	7.630	4.690	5.770	9.030	4.590
Ho	0.050	2.140	1.080	1.250	1.790	0.970	1.420	1.640	0.720
La	0.100	74.400	43.800	54.200	59.600	42.200	46.800	91.600	37.400
Lu	0.050	0.870	0.620	0.710	0.770	0.440	0.670	0.690	0.370
Nd	0.100	70.300	34.600	43.700	43.800	34.500	34.100	65.000	32.600
Pr	0.050	17.860	9.870	12.320	12.330	9.940	8.040	14.820	8.990
Sm	0.100	13.500	6.400	7.900	7.700	6.600	6.300	10.300	5.600
Tb	0.050	1.780	0.820	0.930	1.100	0.710	0.990	1.340	0.660
Tm	0.050	0.820	0.520	0.560	0.830	0.420	0.680	0.730	0.310
Yb	0.100	5.700	4.100	4.300	5.100	3.000	4.500	4.800	2.100
Eu/Eu*		0.650	0.300	0.220	0.260	0.530	0.240	0.680	0.750
LaN/YbN		8.800	7.200	8.500	7.880	9.480	7.010	12.870	12.010
Sum_REE		351.450	206.260	247.300	254.940	197.140	198.500	364.140	180.640

DL: Detection Limit
Major elements in wt. %; Trace elements in ppm

APPENDIX A3 – Major and trace element contents of samples from the Paranaíta Intrusive Suite. (cont.)

Sample		MC-R-104	MC-R-120	MC-R-141	MC-R-156B	MC-R-158B	MC-R-165
Chemical Class.		**Qtz monzonite**	**Granite**	**Granodiorite**	**Granodiorite**	**Granodiorite**	**Granite**
Latitude		**-9.1471**	**-9.1912**	**-9.8054**	**-9.2637**	**-9.1815**	**-9.1425**
Longitude		**-58.9525**	**-58.9118**	**-58.5228**	**-58.6307**	**-58.6522**	**-58.6975**
	D.L.						
SiO_2	0.100	68.670	68.990	71.050	75.970	71.640	72.010
Al_2O_3	0.100	15.730	15.340	15.270	14.040	15.250	15.320
Fe_2O_3	0.010	4.040	3.720	3.710	2.290	2.910	2.570
MgO	0.100	0.970	0.790	0.910	0.210	0.530	0.400
CaO	0.010	2.540	2.370	2.390	1.050	2.390	1.090
Na_2O	0.100	4.710	4.210	4.270	3.950	3.490	4.940
K_2O	0.010	4.320	4.350	4.200	5.280	5.260	4.930
MnO	0.010	0.080	0.050	0.070	0.100	0.080	0.070
TiO_2	0.010	0.460	0.380	0.390	0.180	0.400	0.380
P_2O_5	0.010	0.330	<D.L.	0.210	0.190	0.270	0.140
SUM		101.850	100.200	102.470	103.260	102.220	101.850
FeO	0.140	1.790	1.720	2.130	0.930	1.210	1.140
FeOt		5.430	5.070	5.470	2.990	3.830	3.450
K_2O/Na_2O		0.920	1.030	0.980	1.340	1.510	1.000
Na_2O+K_2O		9.030	8.560	8.470	9.230	8.750	9.870
A/NK		1.270	1.320	1.320	1.150	1.330	1.140
A/CNK		0.920	0.960	0.960	0.990	0.970	0.990
Ba	5.000	809.000	735.000	747.000	1126.000	1478.000	2103.000
Be	0.100	1.300	1.800	1.400	1.900	3.200	2.800
Cs	0.050	0.740	1.460	2.110	2.990	4.330	2.180
Ga	0.100	13.000	12.900	13.000	14.000	17.200	17.200
Hf	0.050	5.220	4.430	5.560	4.040	6.480	8.350
Nb	0.050	7.790	7.260	8.100	10.070	15.320	13.110
Rb	0.200	100.000	117.000	107.000	175.000	202.000	136.000
Sn	0.300	1.700	1.300	0.900	2.900	3.900	3.500
Sr	0.500	315.000	376.000	378.000	132.000	302.000	217.000
Ta	0.050	0.560	0.520	0.550	1.000	1.400	0.890
Th	0.100	11.000	11.000	9.800	15.000	15.500	9.100
U	0.050	2.890	2.780	2.520	4.100	5.500	2.000
W	0.100	<D.L.	5.300	0.900	<D.L.	12.100	<D.L.
Zr	0.500	129.000	119.000	142.000	120.000	211.000	301.000
Ag	0.010	0.030	0.010	0.060	<D.L.	0.260	0.010
Au	0.100	<D.L.	<D.L.	<D.L.	<D.L.	<D.L.	<D.L.
As	1.000	<D.L.	<D.L.	<D.L.	1.000	1.000	<D.L.
Bi	0.020	0.060	0.050	0.040	0.030	12.370	0.110
Cd	0.010	0.020	<D.L.	0.020	<D.L.	0.050	0.190
Co	0.100	4.900	3.500	3.700	1.900	2.600	1.000
Cu	0.500	10.500	11.600	11.900	4.200	7.000	4.500
Hg	0.010	<D.L.	<D.L.	<D.L.	<D.L.	<D.L.	<D.L.
Mo	0.050	1.810	8.060	8.130	0.650	0.530	3.530
Ni	0.500	2.900	3.200	2.500	3.500	3.000	5.500
Pb	0.200	8.700	7.000	10.300	18.600	24.100	14.300
Sb	0.050	0.150	0.050	0.070	0.080	0.090	0.060
Se	1.000	<D.L.	<D.L.	1.000	<D.L.	<D.L.	<D.L.
Zn	1.000	76.000	33.000	40.000	31.000	25.000	37.000
Ce	0.100	73.400	76.600	62.600	77.500	103.700	125.800
Dy	0.050	4.170	3.500	3.690	3.890	6.720	12.270
Er	0.050	2.200	1.660	1.880	2.250	3.410	6.070
Eu	0.050	0.840	0.770	0.710	0.270	0.960	1.770
Gd	0.050	4.550	3.900	3.990	4.030	6.900	12.470
Ho	0.050	0.780	0.610	0.710	0.790	1.340	2.400
La	0.100	39.600	44.400	33.600	43.900	56.400	65.000
Lu	0.050	0.320	0.270	0.290	0.450	0.540	0.890
Nd	0.100	33.300	32.600	27.700	28.500	46.100	64.300
Pr	0.050	9.130	9.370	7.580	8.870	13.030	16.710
Sm	0.100	5.600	5.100	4.700	4.900	8.500	13.100
Tb	0.050	0.680	0.550	0.560	0.600	0.980	1.870
Tm	0.050	0.330	0.280	0.340	0.370	0.560	0.980
Yb	0.100	2.300	1.800	2.000	2.700	3.600	5.700
Eu/Eu*		0.510	0.530	0.500	0.190	0.380	0.420
LaN/YbN		11.610	16.630	11.330	10.960	10.560	7.690
Sum_REE		177.200	181.410	150.350	179.020	252.740	329.330

DL: Detection Limit
Major elements in wt. %; Trace elements in ppm

APPENDIX A4 – Major and trace element contents of samples from the Paranaíta Intrusive Suite. (cont.)

Sample		TD-053	TD-072	TD-R-139	TD-R-186	TD-R-006	TD-R-036
Chemical Class.		Granite	Granite	Granodiorite	Alkali granite	Granodiorite	Granodiorite
Latitude		-9.1947	-9.1845	-9.2549	-9.17	-9.1814	-9.1785
Longitude		-58.318	-58.4184	-58.8699	-58.83	-58.6525	-58.9467
	D.L.						
SiO_2	0.100	72.100	71.800	68.900	74.500	68.350	64.700
$Al2O_3$	0.100	14.500	14.400	15.000	12.500	13.970	14.910
Fe_2O_3	0.010	1.940	3.420	3.700	1.540	2.380	4.760
MgO	0.100	0.600	0.750	0.790	<D.L.	0.540	1.630
CaO	0.010	1.470	1.980	2.540	0.530	2.190	3.410
Na_2O	0.100	3.860	3.780	4.020	3.530	3.000	3.500
K_2O	0.010	4.200	4.050	3.900	4.750	4.230	2.880
MnO	0.010	0.050	0.110	0.100	0.060	0.070	0.090
TiO_2	0.010	0.240	0.410	0.370	0.130	0.360	0.510
P_2O_5	0.010	0.097	0.147	0.122	0.019	0.070	0.180
SUM		99.057	100.847	99.442	97.559	95.160	96.570
FeO	0.140	1.000	2.170	3.330	1.390	0.990	2.230
FeOt		2.750	5.250	6.660	2.770	3.130	6.510
K_2O/Na_2O		1.090	1.070	0.970	1.350	1.410	0.820
Na_2O+K_2O		8.060	7.830	7.920	8.280	7.230	6.380
A/NK		1.330	1.360	1.380	1.140	1.470	1.680
A/CNK		1.070	1.010	0.970	1.050	1.040	0.990
Ba	5.000	1098.000	689.000	1076.000	677.000	1123.000	1186.000
Be	0.100	3.500	3.700	1.600	1.900	2.500	4.200
Cs	0.050	1.690	4.010	1.530	1.290	4.310	1.190
Ga	0.100	13.900	17.900	14.100	12.800	16.900	18.100
Hf	0.050	3.540	4.320	4.070	3.140	5.240	4.230
Nb	0.050	11.760	11.430	9.560	10.180	16.030	10.720
Rb	0.200	142.900	177.500	98.400	132.500	214.200	115.800
Sn	0.300	2.000	2.600	1.500	<D.L.	3.300	0.900
Sr	0.500	395.700	456.000	423.200	100.500	268.300	500.900
Ta	0.050	0.860	0.950	0.520	0.640	1.550	0.570
Th	0.100	11.700	12.300	9.400	12.000	11.900	9.100
U	0.050	2.950	4.170	2.600	2.530	4.150	1.980
W	0.100	1.600	3.600	0.900	1.700	30.800	1.100
Zr	0.500	131.800	148.200	185.400	117.500	199.500	160.900
Ag	0.010	<D.L.	<D.L.	<D.L.	<D.L.	0.230	<D.L.
Au	0.100	<D.L.	<D.L.	<D.L.	<D.L.	<D.L.	<D.L.
As	1.000	<D.L.	<D.L.	<D.L.	<D.L.	2.000	<D.L.
Bi	0.020	0.040	0.070	0.020	0.040	7.630	-0.020
Cd	0.010	0.010	0.060	0.020	0.030	<D.L.	0.040
Co	0.100	3.100	5.100	4.900	0.500	1.600	7.900
Cu	0.500	8.600	6.300	3.000	2.500	7.200	9.600
Hg	0.010	0.020	0.020	0.010	<D.L.	0.030	<D.L.
Mo	0.050	0.450	0.830	0.730	1.340	0.470	0.500
Ni	0.500	4.400	5.500	2.700	1.200	2.400	2.000
Pb	0.200	10.800	8.900	5.800	9.300	17.800	3.500
Sb	0.050	0.120	0.120	0.060	0.070	0.090	0.050
Se	1.000	<D.L.	<D.L.	<D.L.	<D.L.	<D.L.	<D.L.
Zn	1.000	27.000	34.000	34.000	11.000	20.000	40.000
Ce	0.100	75.400	147.000	106.200	74.400	65.900	78.900
Dy	0.050	3.160	6.600	4.210	3.590	4.240	3.650
Er	0.050	1.770	3.950	2.800	2.390	2.230	2.080
Eu	0.050	0.910	1.470	1.140	0.790	1.290	1.570
Gd	0.050	3.860	7.370	5.230	3.930	5.510	5.330
Ho	0.050	0.700	1.280	0.890	0.760	0.580	0.580
La	0.100	46.500	56.200	72.400	44.100	29.400	41.600
Lu	0.050	0.340	0.690	0.380	0.390	0.520	0.200
Nd	0.100	31.700	56.700	42.600	32.000	31.300	37.700
Pr	0.050	9.170	16.050	10.300	7.940	7.940	9.100
Sm	0.100	5.000	10.500	6.000	5.100	5.300	5.900
Tb	0.050	0.510	1.150	0.760	0.580	0.620	0.520
Tm	0.050	0.340	0.650	0.390	0.390	0.340	0.190
Yb	0.100	2.000	4.400	2.400	2.600	2.600	2.100
Eu/Eu*		0.630	0.510	0.620	0.540	0.730	0.860
LaN/YbN		15.680	8.610	20.340	11.440	7.620	13.360
Sum_REE		181.360	314.010	255.700	178.960	157.770	189.420

DL: Detection Limit
Major elements in wt. %; Trace elements in ppm

APPENDIX A5 – Major and trace element contents of intermediate to basic rocks from the Colíder Group.

Sample		MC-154C	TD-001	TD-182	TD-216A	TD-225	TD-157
Chemical Class.		Basalt	Andesite	L. Andesite	L. Andesite	Andesite	K. basalt
Latitude		-9.2269	-9.1136	-9.1451	-9.2156	-9.2374	-9.0424
Longitude		-58.655	-58.6203	-58.8637	-58.9509	-58.926	-58.8561
	D.L.						
SiO_2	0.100	48.640	59.340	57.600	55.700	53.200	47.200
Al_2O_3	0.100	17.670	16.440	17.000	16.500	16.500	18.100
Fe_2O_3	0.010	10.580	6.040	7.820	9.520	10.400	12.200
MgO	0.100	8.210	3.250	2.690	2.900	3.380	5.170
CaO	0.010	9.850	5.630	4.940	6.970	7.770	9.910
Na_2O	0.100	2.900	4.180	2.810	3.950	2.260	2.730
K_2O	0.010	1.480	1.870	3.380	1.570	1.370	1.160
MnO	0.010	0.270	0.090	0.120	0.140	0.200	0.210
TiO_2	0.010	0.800	0.530	0.860	1.210	1.180	1.500
P_2O_5	0.010	0.260	0.210	0.271	0.559	0.899	0.189
SUM		100.660	97.580	97.491	99.019	97.159	98.369
FeO	0.140	3.020	2.610	7.040	4.040	3.830	10.980
FeOt		12.540	8.040	14.070	12.610	13.190	21.960
FeOt/FeOt+MgO		0.600	0.710	0.840	0.810	0.800	0.810
K2O/Na2O		0.510	0.450	1.200	0.400	0.610	0.420
Na2O+K2O		4.380	6.050	6.190	5.520	3.630	3.890
A/NK		2.770	1.850	2.050	2.010	3.170	3.150
A/CNK		0.730	0.860	0.980	0.790	0.850	0.760
#mg		51.830	40.110	24.400	27.600	29.750	28.450
Ba	5.000	488.000	703.000	651.000	854.000	1202.000	465.000
Be	0.100	1.500	2.400	3.300	1.600	1.500	0.900
Cs	0.050	13.830	1.810	9.630	1.550	0.590	1.310
Ga	0.100	18.400	21.800	21.600	17.100	19.500	17.900
Hf	0.050	1.690	4.830	2.630	5.670	5.590	2.000
Nb	0.050	2.310	10.340	15.230	9.850	7.430	8.480
Rb	0.200	114.000	96.700	161.900	46.100	30.600	29.100
Sn	0.300	2.400	2.500	6.800	1.600	1.000	<D.L.
Sr	0.500	812.000	963.600	881.800	659.600	1131.000	767.400
Ta	0.050	0.140	1.060	0.980	0.510	0.230	0.260
Th	0.100	1.400	8.400	7.600	9.800	6.500	0.400
U	0.050	0.390	1.750	4.070	2.230	1.020	0.190
W	0.100	<D.L.	1.600	6.400	1.200	0.500	<D.L.
Zr	0.500	292.000	178.900	99.900	223.400	226.500	95.300
Ag	0.010	<D.L.	0.040	<D.L.	<D.L.	<D.L.	<D.L.
Au	0.100	<D.L.	<D.L.	<D.L.	<D.L.	<D.L.	<D.L.
As	1.000	3.000	7.000	<D.L.	2.000	<D.L.	2.000
Bi	0.020	0.130	<D.L.	0.170	<D.L.	0.360	<D.L.
Cd	0.010	0.060	0.030	0.100	0.020	0.020	0.150
Co	0.100	25.400	10.000	16.100	24.500	20.400	43.700
Cu	0.500	6.400	16.400	19.200	56.500	27.300	53.900
Hg	0.010	<D.L.	<D.L.	<D.L.	<D.L.	<D.L.	0.010
Mo	0.050	5.270	0.950	2.730	0.610	1.050	0.700
Ni	0.500	51.400	22.500	7.900	41.300	3.700	54.500
Pb	0.200	3.900	5.000	3.900	3.200	2.800	4.100
Sb	0.050	0.140	0.190	0.150	0.520	0.190	0.340
Se	1.000	<D.L.	<D.L.	<D.L.	<D.L.	<D.L.	<D.L.
Zn	1.000	55.000	36.000	74.000	82.000	75.000	55.000
Ce	0.100	31.600	64.000	64.000	103.600	99.600	36.400
Dy	0.050	3.040	2.150	10.950	5.360	6.150	3.140
Er	0.050	1.450	0.920	5.780	2.770	3.290	1.610
Eu	0.050	1.130	1.250	1.920	2.180	2.810	1.540
Gd	0.050	3.370	4.470	13.620	8.000	9.150	3.860
Ho	0.050	0.620	0.360	2.020	1.010	1.140	0.620
La	0.100	15.300	32.600	169.600	44.500	42.500	21.400
Lu	0.050	0.250	0.420	0.710	0.410	0.450	0.190
Nd	0.100	17.900	30.200	107.600	53.500	56.700	21.800
Pr	0.050	4.510	7.320	25.850	13.100	13.200	4.280
Sm	0.100	4.000	4.400	16.600	10.200	10.700	4.300
Tb	0.050	0.460	0.480	1.970	1.030	1.160	0.550
Tm	0.050	0.260	0.080	0.760	0.390	0.440	0.200
Yb	0.100	1.400	1.300	5.200	2.500	2.800	1.400
Sum REE		85.290	149.950	426.580	248.550	250.090	101.290
Eu/Eu*		0.940	0.860	0.390	0.740	0.870	1.160

DL: Detection Limit
Major elements in wt. %; Trace elements in ppm

APPENDIX B1 - U-Pb LA-ICP-MS data for microgranite GR-001 from the Paranaíta Intrusive Suite. (cont.)

				Apparent Ages													
Grain	**f^{206}(%)**	**Th/U**	**^{206}Pb / ^{204}Pb**	**^{207}Pb/ ^{206}Pb**	**Error (%) / 1σ**	**^{207}Pb / ^{235}U**	**Error (%) / 1σ**	**^{206}Pb / ^{238}U**	**Error (%) / 1σ**	**Rho**	**^{207}Pb / ^{206}Pb**	**1σ / (Ma)**	**^{207}Pb / ^{235}U**	**1σ (Ma)**	**^{206}Pb / ^{238}U**	**1σ (Ma)**	**Conc.(%)**
GR-001	**microgranite**																
Z01	0.010	0.277	151754	0.109489	0.42	4.436	0.91	0.293862	0.81	0.87	1791	8	1719	8	1661	12	92.73
Z02	0.009	0.266	167119	0.109479	0.44	4.681	0.81	0.310084	0.69	0.81	1791	8	1764	7	1741	10	97.23
Z03	0.008	0.261	198397	0.109559	0.39	4.690	0.90	0.310465	0.82	0.89	1792	7	1765	8	1743	12	97.26
Z04	0.013	0.377	118499	0.110030	0.82	4.750	1.12	0.313127	0.77	0.85	1800	15	1776	9	1756	12	97.56
Z05	0.024	0.358	64802	0.108744	0.67	4.463	2.38	0.297641	2.28	0.96	1778	12	1724	20	1680	34	94.44
Z06	0.010	0.266	160956	0.110507	0.40	4.627	0.70	0.303700	0.57	0.76	1808	7	1754	6	1710	8	94.57
Z07	0.01	0.37	175366	0.112240	0.38	4.788	0.71	0.309366	0.60	0.80	1836	7	1783	6	1738	9	94.64
Z08	0.006	0.271	275115	0.109193	0.81	4.787	1.36	0.317939	1.09	0.92	1786	15	1783	11	1780	17	99.65
Z09	0.006	0.256	253521	0.110159	0.48	4.619	0.89	0.304094	0.75	0.82	1802	9	1753	7	1712	11	94.98
Z10	0.004	0.349	368472	0.110155	0.40	4.572	0.76	0.301056	0.65	0.82	1802	7	1744	6	1697	10	94.15
Z11	0.01	0.54	180550	0.112906	0.33	4.992	0.69	0.320684	0.60	0.85	1847	6	1818	6	1793	9	97.10
Z12.1	0.003	0.331	528458	0.109230	0.85	4.682	1.13	0.310907	0.74	0.83	1787	15	1764	9	1745	11	97.68
Z12.2	0.008	0.339	205578	0.108839	0.46	4.631	0.74	0.308625	0.58	0.73	1780	8	1755	6	1734	9	97.41
Z13.1	0.015	0.406	107065	0.108846	0.54	4.738	0.96	0.315674	0.79	0.80	1780	10	1774	8	1769	12	99.35
Z13.2	0.015	0.295	105407	0.109842	0.62	4.444	1.07	0.293415	0.87	0.80	1797	11	1721	9	1659	13	92.31
Z14.1	0.011	0.331	139374	0.109274	0.97	4.584	1.19	0.304278	0.69	0.77	1787	18	1746	10	1712	10	95.81
Z14.2	0.010	0.322	156426	0.109355	0.52	4.767	0.87	0.316182	0.69	0.77	1789	9	1779	7	1771	11	99.01
Z15	0.009	0.305	178560	0.108994	0.51	4.642	0.84	0.308904	0.66	0.75	1783	9	1757	7	1735	10	97.34
Z16	0.012	0.268	127655	0.108962	0.61	4.625	0.93	0.307819	0.71	0.72	1782	11	1754	8	1730	11	97.07
Z17	0.009	0.323	165892	0.109872	0.95	4.725	1.18	0.311926	0.70	0.78	1797	17	1772	10	1750	11	97.38
Z18	0.01	0.29	115566	0.107741	0.66	4.613	1.11	0.310517	0.89	0.78	1762	12	1752	9	1743	14	98.96
Z19	0.030	0.294	53551	0.109442	0.76	4.326	1.95	0.286701	1.79	0.92	1790	14	1698	16	1625	26	90.78
Z20	0.019	0.272	82190	0.109845	0.72	4.809	1.19	0.317497	0.95	0.78	1797	13	1786	10	1777	15	98.92
Z22	0.002	0.432	674242	0.110971	0.34	4.598	0.63	0.300540	0.53	0.79	1815	6	1749	5	1694	8	93.31
Z23.1	0.009	0.261	181133	0.109036	0.39	4.555	0.78	0.303012	0.67	0.84	1783	7	1741	6	1706	10	95.67
Z23.2	0.008	0.275	189294	0.109111	0.38	4.529	0.99	0.301074	0.91	0.91	1785	7	1736	8	1697	14	95.07
Z24	0.01	0.31	173415	0.108529	1.13	4.848	1.51	0.323949	1.00	0.85	1775	20	1793	13	1809	16	101.92

Notes: The f206(%) column shows the percentage of ^{206}Pb that is common lead. Common lead is corrected using the $^{206}Pb/^{204}Pb$ ratio. Conc. (%) corresponds to the level of concordance of the analyses.

APPENDIX B2 – U-Pb LA-ICP-MS data for porphyry granite GR-001A from the Paranaíta Intrusive Suite. (cont.)

											Apparent Ages						
Grain	f^{206}(%)	Th/U	$^{206}Pb/^{204}Pb$	$^{207}Pb/^{206}Pb$	Error (%) / 1σ	$^{207}Pb/^{235}U$	Error (%) / 1σ	$^{206}Pb/^{238}U$	Error (%) / 1σ	Rho	$^{207}Pb/^{206}Pb$	1σ / (Ma)	$^{207}Pb/^{235}U$	1σ (Ma)	$^{206}Pb/^{238}U$	1σ (Ma)	Conc.(%)
GR-001A	porphyry granite																
Z01	0.009	0.540	168906	0.111002	0.60	4.628	1.59	0.302399	1.47	0.92	1816	11	1754	13	1703	22	93.79
Z02	0.008	0.659	186002	0.108998	0.71	5.449	1.47	0.362601	1.29	0.87	1783	13	1893	13	1994	22	111.88
Z03	0.012	0.742	137600	0.111838	0.68	4.043	1.24	0.262207	1.04	0.82	1830	12	1643	10	1501	14	82.05
Z04	0.021	0.480	72585	0.112119	2.51	5.234	3.19	0.338563	1.97	0.83	1834	45	1858	27	1880	32	102.49
Z-05	0.027	0.770	56027	0.107543	1.03	5.631	1.82	0.379721	1.51	0.82	1758	19	1921	16	2075	27	118.02
Z06	0.008	0.434	189271	0.110565	0.53	5.390	0.99	0.353543	0.84	0.83	1809	10	1883	8	1951	14	107.89
Z07	0.011	0.563	136178	0.111793	0.64	5.476	1.20	0.355270	1.01	0.83	1829	12	1897	10	1960	17	107.16
Z08	0.009	0.451	176737	0.110071	1.32	5.564	1.81	0.366634	1.24	0.85	1801	24	1911	16	2014	21	111.83
Z09	0.009	0.582	175763	0.110780	0.67	5.279	1.13	0.345641	0.92	0.79	1812	12	1866	10	1914	15	105.60
Z10	0.009	0.603	162328	0.111240	0.70	5.297	1.12	0.345352	0.87	0.76	1820	13	1868	10	1912	14	105.09
Z11	0.008	0.515	180488	0.111160	1.00	5.326	1.29	0.347514	0.81	0.60	1818	18	1873	11	1923	14	105.73
Z12	0.006	0.413	274298	0.109281	1.27	5.154	1.70	0.342059	1.12	0.84	1787	23	1845	14	1897	18	106.10
Z13	0.031	0.479	49510	0.112675	1.72	5.131	2.58	0.330303	1.93	0.74	1843	31	1841	22	1840	31	99.83
Z14	0.010	0.554	150711	0.110066	0.67	5.272	1.14	0.347422	0.92	0.79	1800	12	1864	10	1922	15	106.76
Z15	0.014	0.713	109656	0.108582	0.97	5.071	1.42	0.338688	1.03	0.71	1776	18	1831	12	1880	17	105.89
Z16	0.012	0.537	131159	0.110388	1.51	5.501	1.94	0.361429	1.21	0.82	1806	28	1901	17	1989	21	110.14
Z17	0.014	0.457	107163	0.109522	0.94	5.398	1.53	0.357489	1.21	0.78	1791	17	1885	13	1970	20	109.98
Z18	0.035	0.512	44219	0.109881	1.20	4.867	1.98	0.321243	1.58	0.79	1797	22	1797	17	1796	25	99.91
Z19	0.020	0.389	77194	0.108954	1.21	4.970	1.91	0.330831	1.48	0.77	1782	22	1814	16	1842	24	103.39
Z20	0.027	0.560	57762	0.110868	1.34	4.983	2.07	0.326005	1.58	0.76	1814	24	1817	18	1819	25	100.29
Z21	0.011	0.515	136267	0.110967	1.19	5.092	1.52	0.332804	0.95	0.81	1815	22	1835	13	1852	15	102.02
Z22	0.020	0.627	80690	0.111606	0.80	4.544	1.39	0.295295	1.13	0.80	1826	15	1739	12	1668	17	91.36
Z23	0.019	0.562	79732	0.109146	1.16	4.944	1.66	0.328498	1.19	0.70	1785	21	1810	14	1831	19	102.57
Z-24	0.060	0.479	25588	0.112635	3.89	5.261	4.39	0.338733	2.04	0.72	1842	70	1862	37	1881	33	102.07

Notes: The f206(%) column shows the percentage of ^{206}Pb that is common lead. Common lead corrected using the $^{206}Pb/^{204}Pb$ ratio. Conc. (%) corresponds to the level of concordance of the analyses.

APPENDIX B3 – U-Pb LA-ICP-MS data for porphyry granite TD-T-050S from the Paranaíta Intrusive Suite. (cont.)

				Apparent Ages													
Grain	f^{206}(%)	Th/U	^{206}Pb / ^{204}Pb	^{207}Pb/ ^{206}Pb	Error (%) / 1σ	^{207}Pb / ^{235}U	Error (%) / 1σ	^{206}Pb / ^{238}U	Error (%) / 1σ	Rho	^{207}Pb / ^{206}Pb	1σ / (Ma)	^{207}Pb / ^{235}U	1σ (Ma)	^{206}Pb / ^{238}U	1σ (Ma)	Conc.(%)
TD-T-050S	**porphyry granite**																
Z1	0.043	0.508	36735	0.111344	1.64	4.427	2.53	0.288381	1.93	0.76	1821	30	1717	21	1633	28	89.68
Z2	0.031	0.498	52533	0.110979	1.85	4.184	3.75	0.273418	3.26	0.87	1816	34	1671	31	1558	45	85.82
Z3	0.043	0.456	37573	0.111925	1.56	3.748	5.88	0.242865	5.67	0.96	1831	28	1582	47	1402	71	76.55
Z4	0.064	0.221	23924	0.114422	3.39	5.375	3.70	0.340725	1.47	0.64	1871	61	1881	32	1890	24	101.04
Z5	0.020	0.389	76900	0.108596	1.30	5.129	3.45	0.342536	3.19	0.93	1776	24	1841	29	1899	53	106.92
Z6	0.028	0.755	56342	0.111865	2.25	4.514	3.37	0.292678	2.51	0.74	1830	41	1734	28	1655	37	90.43
Z7	0.032	0.409	49766	0.110560	1.66	4.405	1.95	0.288966	1.02	0.51	1809	30	1713	16	1636	15	90.47
Z8	0.019	0.306	81766	0.110989	2.75	5.592	6.17	0.365402	5.53	0.97	1816	50	1915	53	2008	95	110.58
Z9	0.017	0.441	89950	0.108457	1.13	5.028	2.95	0.336223	2.73	0.92	1774	21	1824	25	1868	44	105.35
Z10	0.026	0.466	59842	0.109611	0.94	4.615	2.30	0.305377	2.10	0.91	1793	17	1752	19	1718	32	95.81
Z11	0.028	0.659	55038	0.110723	1.25	4.990	2.18	0.326887	1.79	0.82	1811	23	1818	18	1823	28	100.66
Z12	0.316	0.167	5537	0.115232	2.56	1.984	5.79	0.124841	5.20	0.97	1884	46	1110	39	758	37	40.26
Z13	0.114	0.244	14117	0.112737	0.82	4.266	4.00	0.274459	3.91	0.98	1844	15	1687	33	1563	54	84.78
Z14	0.046	0.520	33709	0.107705	0.89	4.981	2.54	0.335431	2.38	0.94	1761	16	1816	22	1865	39	105.89
Z15	0.022	0.357	75932	0.110476	0.76	3.184	3.03	0.209036	2.94	0.97	1807	14	1453	23	1224	33	67.71
Z16	0.005	0.567	318884	0.109559	1.51	4.949	4.25	0.327613	3.97	0.98	1792	27	1811	36	1827	63	101.94
Z17	0.102	0.216	16402	0.107995	1.97	3.029	2.85	0.203443	2.06	0.72	1766	36	1415	22	1194	22	67.60
Z18	0.012	0.388	133845	0.110854	0.73	4.592	2.84	0.300443	2.75	0.97	1813	13	1748	24	1694	41	93.39
Z19	0.048	0.210	35373	0.105448	1.58	2.689	4.69	0.184942	4.42	0.94	1722	29	1325	35	1094	44	63.52
Z20	0.047	0.381	33499	0.106958	2.94	4.503	3.87	0.305315	2.52	0.86	1748	54	1731	32	1718	38	98.25
Z21	0.023	0.341	64193	0.110509	1.10	5.709	4.10	0.374706	3.95	0.96	1808	20	1933	35	2052	69	113.48
Z22	0.104	0.451	14712	0.112078	11.56	5.371	14.02	0.347588	7.94	0.57	1833	209	1880	120	1923	132	104.89
Z23	0.017	0.439	91494	0.109969	0.99	4.773	1.88	0.314759	1.60	0.84	1799	18	1780	16	1764	25	98.07
Z24	0.074	0.206	21591	0.111079	2.14	4.440	3.62	0.289928	2.91	0.93	1817	39	1720	30	1641	42	90.32

Notes: The f206(%) column shows the percentage of ^{206}Pb that is common lead. Common lead is corrected using the measured ^{206}Pb/^{204}Pb ratio. Conc. (%) corresponds to the level of concordance of the analyses.

APPENDIX B4 – U-Pb LA-ICP-MS data for microgranite TD-T-050AM from the Paranaíta Intrusive Suite. (cont.)

										Apparent Ages							
Grain	f^{206}(%)	Th/U	$^{206}Pb/^{204}Pb$	$^{207}Pb/^{206}Pb$	Error (%) / 1σ	$^{207}Pb/^{235}U$	Error (%) / 1σ	$^{206}Pb/^{238}U$	Error (%) / 1σ	Rho	$^{207}Pb/^{206}Pb$	1σ / (Ma)	$^{207}Pb/^{235}U$	1σ (Ma)	$^{206}Pb/^{238}U$	1σ (Ma)	Conc.(%)
TD-T-050AM	microgranite																
03-Z1	0.004	0.327	356186	0.110067	1.12	5.220	1.79	0.343994	1.40	0.77	1801	20	1856	15	1906	23	105.85
04-Z2	0.013	0.233	122931	0.111772	0.74	5.115	1.65	0.331917	1.48	0.89	1828	13	1839	14	1848	24	101.05
06-Z4	0.034	0.349	45802	0.111000	2.18	5.047	2.48	0.329799	1.19	0.69	1816	40	1827	21	1837	19	101.19
07-Z5	0.016	0.381	98176	0.111177	0.86	4.670	1.44	0.304658	1.16	0.79	1819	16	1762	12	1714	17	94.26
08-Z6	0.014	0.496	113062	0.110994	0.73	4.756	1.55	0.310748	1.37	0.88	1816	13	1777	13	1744	21	96.07
09-Z7	0.123	0.323	13274	0.109557	2.63	3.679	4.07	0.243563	3.10	0.76	1792	48	1567	32	1405	39	78.41
10-Z8	0.003	0.664	564937	0.109851	1.44	4.534	1.87	0.299322	1.20	0.79	1797	26	1737	16	1688	18	93.93
13-Z9	0.587	0.483	2715	0.109765	2.73	4.261	3.10	0.281541	1.46	0.46	1796	49	1686	25	1599	21	89.06
14-Z10	0.569	0.423	2697	0.110321	1.03	5.204	1.72	0.342118	1.37	0.79	1805	19	1853	15	1897	23	105.11
15-Z11	0.009	0.424	178344	0.110537	0.64	4.946	1.11	0.324522	0.91	0.80	1808	12	1810	9	1812	14	100.19
16-Z12	0.463	0.438	3293	0.098191	11.71	4.771	11.94	0.352422	2.32	0.36	1590	204	1780	96	1946	39	122.40
17-Z13	0.023	0.239	76555	0.108609	0.65	2.205	2.86	0.147276	2.78	0.97	1776	12	1183	20	886	23	49.86
18-Z14	1.706	0.281	945	0.109158	1.78	3.916	2.36	0.260202	1.52	0.64	1785	32	1617	19	1491	21	83.50
19-Z15	0.018	0.357	87216	0.110531	0.60	4.916	1.21	0.322591	1.05	0.86	1808	11	1805	10	1802	16	99.68
20-Z16	0.015	0.362	107368	0.110987	1.19	4.226	1.71	0.276132	1.22	0.85	1816	22	1679	14	1572	17	86.57
23-Z17	0.018	0.466	87357	0.111793	1.33	4.208	1.84	0.272991	1.27	0.68	1829	24	1676	15	1556	18	85.08
24-Z18	0.026	0.630	59870	0.115043	2.58	4.693	2.88	0.295863	1.29	0.44	1881	46	1766	24	1671	19	88.84
25-Z19	0.309	0.486	5067	0.114385	1.09	4.934	1.59	0.312865	1.16	0.72	1870	20	1808	13	1755	18	93.83
26-Z20	0.325	0.372	4955	0.109595	1.12	4.040	2.68	0.267330	2.42	0.96	1793	20	1642	22	1527	33	85.19
27-Z21	0.031	0.333	53555	0.109706	0.63	3.618	2.23	0.239186	2.14	0.96	1795	11	1553	18	1382	27	77.04
28-Z22	0.198	0.468	8532	0.110966	1.35	2.841	4.85	0.185688	4.66	0.96	1815	25	1366	36	1098	47	60.48
29-Z23	0.012	0.413	128565	0.111132	0.70	4.373	1.34	0.285359	1.14	0.84	1818	13	1707	11	1618	16	89.01
30-Z24	1.335	0.363	1234	0.105938	3.06	3.294	3.47	0.225516	1.60	0.70	1731	55	1480	27	1311	19	75.75

Notes: The f206(%) column shows the percentage of ^{206}Pb that is common lead. Common lead is corrected using the measured $^{206}Pb/^{204}Pb$ ratio. Conc. (%) corresponds to the level of concordance of the analyses.

APPENDIX B5 – U-Pb LA-ICP-MS data for volcaniclastic TD-T-063K from the Colíder Group. (cont.)

				Apparent Ages													
Grain	f^{206}(%)	Th/U	$^{206}Pb/^{204}Pb$	$^{207}Pb/^{206}Pb$	Error (%) / 1σ	$^{207}Pb/^{235}U$	Error (%) / 1σ	$^{206}Pb/^{238}U$	Error (%) / 1σ	Rho	$^{207}Pb/^{206}Pb$	1s / (Ma)	$^{207}Pb/^{235}U$	1σ (Ma)	$^{206}Pb/^{238}U$	1σ (Ma)	Conc.(%)
TD-T-063K	volcaniclastic																
Z01	0.044	0.509	35491	0.111661	2.14	4.609	2.86	0.299365	1.902	0.659	1827	39	1751	24	1688	28	92.42
Z02	0.064	0.546	24762	0.108379	1.50	4.423	2.79	0.296006	2.352	0.841	1772	27	1717	23	1671	35	94.31
Z03	0.037	0.666	43417	0.109323	1.58	4.359	2.26	0.289214	1.615	0.707	1788	29	1705	19	1638	23	91.58
Z04	0.073	0.534	21718	0.106879	10.02	4.222	11.04	0.286533	4.636	0.677	1747	184	1678	91	1624	67	92.98
Z05	0.040	0.546	39833	0.110866	1.84	4.254	2.60	0.278272	1.840	0.701	1814	33	1684	21	1583	26	87.26
Z06	0.040	0.615	39079	0.108020	1.77	4.403	2.62	0.295599	1.935	0.734	1766	32	1713	22	1669	28	94.52
Z07	0.103	0.624	15575	0.109258	3.97	4.092	5.08	0.271624	3.166	0.621	1787	72	1653	41	1549	44	86.68
Z08	0.337	0.687	4856	0.116257	5.27	3.804	6.07	0.237286	3.007	0.745	1899	92	1594	48	1373	37	72.26
Z09	0.024	0.585	64475	0.110450	1.35	4.553	1.98	0.298945	1.456	0.726	1807	24	1741	17	1686	22	93.32
Z10	0.027	0.773	58966	0.111835	1.34	4.447	2.10	0.288408	1.626	0.767	1829	24	1721	17	1634	23	89.29
Z11	0.022	0.536	71923	0.111411	2.02	4.410	2.98	0.287062	2.189	0.732	1823	37	1714	25	1627	31	89.26
Z12	0.045	0.458	34806	0.111335	3.93	4.697	4.54	0.305946	2.274	0.745	1821	71	1767	38	1721	34	94.48
Z13	0.049	0.494	32121	0.110779	3.01	4.422	4.24	0.289537	2.983	0.702	1812	55	1717	35	1639	43	90.45
Z14	0.032	0.592	50433	0.110833	1.63	4.248	2.40	0.277954	1.764	0.730	1813	30	1683	20	1581	25	87.20
Z15	0.049	0.557	32525	0.111703	2.86	4.620	3.91	0.299961	2.666	0.680	1827	52	1753	33	1691	40	92.55
Z16	0.072	0.499	21732	0.112473	5.36	4.730	6.02	0.305037	2.748	0.707	1840	97	1773	50	1716	41	93.29
Z17	0.037	0.587	42557	0.110962	1.21	4.930	2.11	0.322210	1.730	0.814	1815	22	1807	18	1801	27	99.19
Z18	0.053	0.841	29160	0.117474	2.66	5.411	3.28	0.334056	1.914	0.578	1918	48	1887	28	1858	31	96.86
Z19	0.022	0.640	70626	0.110663	2.26	5.209	2.86	0.341376	1.747	0.605	1810	41	1854	24	1893	29	104.58
Z20	0.024	0.916	64401	0.110537	2.66	4.879	3.09	0.320123	1.577	0.737	1808	48	1799	26	1790	25	99.01
Z21	0.045	1.111	34706	0.112448	1.28	5.002	2.76	0.322647	2.446	0.884	1839	23	1820	23	1803	38	98.00
Z22	0.099	0.540	16062	0.120578	5.00	4.908	5.72	0.295209	2.781	0.484	1965	89	1804	48	1668	41	84.87
Z23	0.027	0.696	58019	0.111652	1.30	4.679	2.29	0.303906	1.888	0.821	1826	24	1763	19	1711	28	93.66
Z24	0.031	0.567	50988	0.111971	3.34	4.407	4.01	0.285422	2.209	0.777	1832	61	1714	33	1619	32	88.37

Notes: The f206(%) column shows the percentage of ^{206}Pb that is common lead. Common lead is corrected using the $^{206}Pb/^{204}Pb$ ratio. Conc. (%) corresponds to the level of concordance of the analyses.

APPENDIX B6 – U-Pb LA-ICP-MS data for granophyric rhyodacite TD-095 from the Colíder Group. (cont.)

				Apparent Ages													
Grain	f^{206}(%)	Th / U	^{206}Pb / ^{204}Pb	^{207}Pb / ^{206}Pb	Error (%) / 1σ	^{207}Pb / ^{235}U	Error (%) / 1σ	^{206}Pb / ^{238}U	Error (%) / 1σ	Rho	^{207}Pb / ^{206}Pb	1σ (Ma)	^{207}Pb / ^{235}U	1σ (Ma)	^{206}Pb / ^{238}U	1σ (Ma)	Conc.(%)
TD-095	**granophyric rhyodacite**																
Z01	0.018	1.167	84732	0.111205	2.19	5.002	2.59	0.326244	1.38	0.52	1819	39	1820	22	1820	21.77	100.0524827
Z02	0.167	1.172	9707	0.123878	3.49	4.312	7.45	0.252429	6.57	0.88	2013	61	1696	60	1451	85.00	72.08732293
Z03	0.022	0.577	70541	0.110777	0.61	4.666	1.10	0.305503	0.91	0.81	1812	11	1761	9	1719	13.79	94.83209112
Z04	0.024	0.418	64558	0.110127	1.26	4.664	1.66	0.307144	1.09	0.82	1802	23	1761	14	1727	16.44	95.84425886
Z05	0.026	0.843	59773	0.109041	1.15	4.667	1.66	0.310449	1.20	0.71	1783	21	1761	14	1743	18.32	97.726608
Z06	0.021	0.830	72749	0.109174	0.77	4.838	1.37	0.321375	1.13	0.81	1786	14	1791	11	1796	17.65	100.6029961
Z07	0.031	1.074	50204	0.109024	1.36	4.616	2.71	0.307104	2.35	0.86	1783	25	1752	22	1726	35.51	96.81891921
Z08	1.278	0.806	1256	0.109699	3.23	4.063	3.79	0.268590	1.96	0.76	1794	58	1647	30	1534	26.97	85.46704213
Z09	0.040	0.778	38828	0.111103	0.79	4.691	1.40	0.306256	1.16	0.82	1818	14	1766	12	1722	17.51	94.75788484
Z10	0.013	1.088	117529	0.109851	0.79	4.688	1.41	0.309516	1.16	0.82	1797	14	1765	12	1738	17.70	96.73785697
Z11	0.217	0.601	7450	0.113285	1.24	4.081	1.92	0.261298	1.47	0.76	1853	22	1651	16	1496	19.68	80.76963796
Z12	3.468	1.025	416	0.124044	91.13	7.226	91.16	0.422507	2.20	0.05	2015	1085	2140	597	2272	43.54	112.7360027
Z13	0.024	0.782	63607	0.111459	0.87	5.224	1.60	0.339934	1.35	0.83	1823	16	1857	14	1886	22.02	103.455762
Z14	0.035	1.085	43997	0.110002	0.83	4.894	1.23	0.322654	0.92	0.72	1799	15	1801	10	1803	14.39	100.1803475
Z15	0.212	0.904	7381	0.119499	3.18	5.184	3.70	0.314617	1.88	0.50	1949	56	1850	31	1763	29.03	90.4885218
Z16	0.012	0.835	132764	0.111049	1.34	5.011	1.71	0.327244	1.06	0.78	1817	24	1821	14	1825	16.89	100.4604777
Z17	0.019	0.772	84077	0.110399	0.87	4.880	2.07	0.320606	1.88	0.91	1806	16	1799	17	1793	29.37	99.26399621
Z18	0.035	0.574	44409	0.115536	1.87	5.028	2.32	0.315645	1.37	0.58	1888	33	1824	19	1768	21.19	93.65349594
Z19	0.050	0.598	33019	0.394232	27.10	12.480	39.84	0.229588	29.19	0.73	3887	357	2641	319	1332	342.24	34.27477672
Z20	0.009	0.602	165737	0.110026	1.29	4.679	1.72	0.308442	1.15	0.82	1800	23	1764	14	1733	17.40	96.28890695
Z21	0.057	0.809	27689	0.112047	2.05	4.632	3.08	0.299857	2.30	0.74	1833	37	1755	25	1691	34.15	92.23749633
Z22	0.038	0.861	40996	0.110576	1.48	4.747	2.31	0.311369	1.77	0.76	1809	27	1776	19	1747	27.07	96.60215669
Z23	0.756	0.553	2118	0.111856	2.09	4.210	2.85	0.272976	1.92	0.67	1830	37	1676	23	1556	26.67	85.03095054
Z24	1.021	1.226	1537	0.115436	12.78	4.858	12.87	0.305229	1.57	0.23	1887	214	1795	103	1717	23.79	91.01507011

Notes: The f206(%) column shows the percentage of ^{206}Pb that is common lead. Common lead is corrected using the measured $^{206}Pb/^{204}Pb$ ratio. Conc. (%) corresponds to the level of concordance of the analyses.

APPENDIX B7 – U-Pb LA-ICP-MS data for amphibolite TD-107 from the Colíder Group.

Grain	f^{206}(%)	Th / U	$^{206}Pb/^{204}Pb$	$^{207}Pb/^{206}Pb$	Error (%) / 1σ	$^{207}Pb/^{235}U$	Error (%) / 1σ	$^{206}Pb/^{238}U$	Error (%) / 1σ	Rho	Apparent Ages $^{207}Pb/^{206}Pb$	1σ (Ma)	$^{207}Pb/^{235}U$	1σ (Ma)	$^{206}Pb/^{238}U$	1s (Ma)	Conc.(%)
TD-107	**amphibolite**																
Z1	0.098	0.695	17400.2	0.112	2.975	2.489	6.494	0.161	5.773	0.889	1831	54	1269	47	964	52	53
Z2	0.028	0.731	55875.2	0.113	1.905	4.828	3.973	0.309	3.486	0.877	1852	34	1790	33	1737	53	94
Z3	0.027	0.482	53637.3	0.109	1.585	6.412	6.678	0.427	6.487	0.971	1781	29	2034	59	2293	125	129
Z4	0.033	0.648	46372.0	0.111	2.582	5.309	3.903	0.347	2.927	0.901	1815	47	1870	33	1921	49	106
Z5	0.405	0.474	3784.6	0.115	7.939	5.420	8.819	0.343	3.824	0.433	1872	137	1888	73	1902	63	102
Z6	0.027	0.669	56324.4	0.109	0.968	5.174	2.266	0.343	2.049	0.902	1789	18	1848	19	1902	34	106
Z7	0.063	0.571	25817.5	0.113	1.211	3.837	2.547	0.247	2.241	0.878	1841	22	1601	21	1425	29	77
Z8	0.215	0.474	7245.7	0.114	4.068	5.068	4.826	0.321	2.597	0.772	1871	73	1831	41	1796	41	96
Z9	0.041	0.682	37133.3	0.115	2.301	5.911	4.163	0.373	3.470	0.832	1879	41	1963	36	2044	61	109
Z10	0.174	0.717	8970.3	0.114	2.147	4.992	5.807	0.317	5.395	0.929	1866	39	1818	49	1776	84	95
Z11	0.021	0.462	72257.3	0.109	0.902	5.351	2.348	0.356	2.168	0.922	1782	16	1877	20	1964	37	110
Z12	0.010	0.484	160454.0	0.109	1.384	4.594	2.213	0.305	1.727	0.887	1789	25	1748	18	1714	26	96
Z13	0.019	0.429	81621.1	0.108	1.280	4.636	2.119	0.310	1.689	0.792	1772	23	1756	18	1742	26	98
Z14	0.009	0.399	177114.3	0.108	0.959	4.756	1.815	0.319	1.542	0.844	1768	18	1777	15	1785	24	101
Z15	0.836	0.571	1909.0	0.105	2.187	4.071	5.185	0.280	4.661	0.905	1720	40	1649	41	1593	66	93
Z16	0.030	0.704	52271.6	0.108	1.755	4.604	2.487	0.309	1.762	0.836	1770	32	1750	21	1734	27	98
Z17	0.468	0.622	2914.4	0.170	63.433	12.112	63.775	0.518	6.566	0.103	2555	793	2613	470	2689	143	105
Z18	0.761	0.519	1830.7	0.132	19.696	8.873	20.531	0.486	5.754	0.280	2130	309	2325	172	2553	121	120
Z19	0.969	0.232	1490.0	0.095	4.845	5.653	7.303	0.433	5.411	0.744	1520	89	1924	61	2321	106	153
Z20	1.112	0.500	1406.6	0.103	3.406	4.400	3.989	0.311	2.053	0.746	1673	62	1712	32	1745	32	104
Z21	0.665	0.182	2363.9	0.102	1.753	4.280	4.022	0.305	3.596	0.898	1655	32	1690	33	1718	54	104
Z22	0.549	0.973	2799.7	0.105	1.802	4.898	4.324	0.340	3.909	0.908	1707	33	1802	36	1885	64	110
Z23	0.073	0.642	21835.2	0.111	1.323	4.412	3.378	0.289	3.108	0.919	1811	24	1715	28	1637	45	90
Z24	0.020	0.403	76903.3	0.108	1.690	4.915	2.388	0.330	1.687	0.826	1765	31	1805	20	1840	27	104

Notes: The f206(%) column shows the percentage of ^{206}Pb that is common lead. Common lead is corrected using the measured $^{206}Pb/^{204}Pb$ ratio. Conc. (%) corresponds to the level of concordance of the analyses.